Graphene oxide (GO) coated metal-TiO_2 nanocomposites for photocatalytic applications

A Thesis
Submitted for the fulfillment of the requirement for the award of the degree of

Doctor of Philosophy

Submitted by:

Davinder Kaur

(Regn. No: 902009029)

THAPAR INSTITUTE
OF ENGINEERING & TECHNOLOGY
(Deemed to be University)

Under the supervision of

Dr. Bonamali Pal
Professor

Department of Chemistry & Biochemistry
Thapar Institute of Engineering and Technology
Patiala-147004, India

April, 2025

Certificate

This certifies that the research presented in the thesis titled **"Graphene oxide (GO) coated metal-TiO_2 nanocomposites for photocatalytic applications"** was conducted by Ms. Davinder Kaur under my supervision at the Department of Chemistry and Biochemistry, Thapar Institute of Engineering and Technology, Patiala. The candidate completed all the conditions required for the fulfillment of the award of the Degree of Philosophy.

I further confirm that the content of this thesis is entirely original and has not been previously submitted, in part or in full, for the conferral of any other degree at any other academic institution.

(Supervisor)

Dr. Bonamali Pal

Professor

Department of Chemistry and Biochemistry

Thapar Institute of Engineering and Technology

Patiala-147004, India

(Head)

Dr. Manmohan Chhibber

Professor

Department of Chemistry and Biochemistry

Thapar Institute of Engineering and Technology

Patiala-147004, India

Candidate's Declaration

I, hereby declare that the work presented in the thesis titled **"Graphene oxide (GO) coated metal-TiO_2 nanocomposites for photocatalytic applications"**, in fulfilment of the requirement for the award of the Degree of Philosophy to the Department of Chemistry and Biochemistry, Thapar Institute of Engineering and Technology, Patiala, is an authentic record of my work carried out under the supervision of Dr. Bonamali Pal (Professor), Department of Chemistry and Biochemistry, Thapar Institute of Engineering and Technology, Patiala, India. The matter embodied in this thesis has not been submitted in part or full to any other university or institute for the award of any degree in India or abroad.

Davinder Kaur

Dr. Bonamali Pal

(Professor and Supervisor)

Department of Chemistry and Biochemistry

Thapar Institute of Engineering and Technology

Patiala-147004, India

Dedicated

To

My Family

Acknowledgment

First and foremost, I wholeheartedly thank the Almighty God for giving me the courage, patience, vision, and endurance to accomplish this research work.

The completion of this thesis would not have been possible without the support and encouragement of several special people. Hence, I would like to take this opportunity to show my gratitude to those who have assisted me in several ways.

I want to express my heartfelt gratitude to my research supervisor, **Dr. Bonamali Pal**, Professor, for the privilege of working in his research group. His excellent guidance, priceless advice, insightful discussion, constant encouragement, profuse assistance, skillful suggestions, and continuous support throughout the experimental and thesis work are the basis for the success of this research. With deepest gratitude, I acknowledge my supervisor for picking me up as one of his research students and providing me with an excellent experimental atmosphere for completing the research work in time. The encouragement, support, and freedom rendered him provided me with a lot of opportunities to build my confidence in accomplishing the experimental work and persuaded me to act professionally. Without his persistent help, the goal of this research would not have been realized.

I sincerely acknowledge **Dr. Padmakumar Nair**, Honorable Director, **Dr. N. Tejo Prakash**, Dean of Research and Development Centre (DoRDC), and **Dr. Bhupendrakumar Chudasama**, Associate Dean RDC, TIET, Patiala, for providing all the necessary facilities that have been immensely helpful in carrying out this research.

My sincere appreciation to **Dr. Manmohan Chhibber**, Professor and Head, Department of Chemistry and Biochemistry, TIET, Patiala, for his ever-helping attitude and encouragement.

I extend my deep sense of gratitude to my doctoral committee members, **Dr. Banibrata Maity**, **Dr. Raj Kumar Das** and **Dr. Rajeev Mehta,** who were involved in the validation survey for this research project. Their valuable suggestions and scientific discussions help me represent my research work in a better way.

The kind help extended by all the faculty members of DCBC, TIET Patiala, is gratefully acknowledged. I am greatly appreciative of all the authorities, technical and office staff in the DCBC, especially Mr. Mayank Sharma and Mr. Chander Thakur, for their cooperation and support during the tenure of my work.

I sincerely acknowledge the **TIET-Virginia Tech Center of Excellence in Emerging Materials (CEEMS)** for providing financial support.

The help from all the analytical laboratories and institutes such as SAI labs, TIET, Patiala, SAIF lab, PU, Chandigarh and Sprint testing solutions is highly acknowledged.

I express my warm thanks to my lab senior, **Dr. Harpreet Kaur**, for her knowledgeable help, and also grateful to my colleagues **Ms. Priti, Ms. Kamya, Ms. Jemini**, **Ms. Sukhan**, **Ms. Ridhima, Ms. Shreya, Ms. Puneet,** for their support and cooperation during this period.

I would like to take a moment to express my deepest gratitude to my close friends, **Ms. Mehak, Ms. Jasmine, Ms. Anupriya, P.S. Rana** whose unwavering support and encouragement have been invaluable throughout my Ph.D journey. Your belief in me, especially during the challenging times, provided the motivation I needed to keep pushing forward. Thank you for the countless hours spent offering feedback and simply listening when I needed to vent. Whether it was sharing a laugh over coffee or providing a shoulder to lean on, you made this journey not only bearable but truly enjoyable. I am incredibly grateful for your friendship and support. This achievement is as much yours as it is mine.

I am indebted to my parents, **Mr. Darshan Singh** and **Mrs. Manjeet Kaur**. Your belief in my abilities and dreams has been a constant source of strength for me. Thank you for your sacrifices, love, and guidance, which have shaped who I am today. From long discussions to celebrating each milestone, you have been my biggest cheerleader. Your encouragement has inspired me to pursue my goals with passion and determination. This achievement is a testament to your love and support, and I am forever grateful to have you by my side. The most special “thank you” is to my loving brothers, **Mr. Sagar** and **Mr. Chetan** and my lovely sister, **Ms. Aditi**, for their unmatched affection, care, patience, and love.

I am thankful to my grandmother and late grandfather, who is watching me from above, I hope to honour his memory through my achievements. I would like to extend my heartfelt gratitude to my uncle, **Mr. Surjan Singh** and aunt, **Mrs. Amandeep Kaur,** for their support, love and care.

Besides this, I am eternally thankful to everyone who has been a part of my journey and knowingly and unknowingly helped me during the completion of this work.

My Ph.D. journey was an experience of a lifetime and, indeed, a huge learning process for me in every aspect, making me a much stronger person.

Davinder

Table of Contents

Chapter-1

Introduction and Literature Review

Chapter-2

Photocatalytic Degradation of Piroxicam-20 and Methanol Dehydrogenation using Graphene Oxide-modified Ag-TiO_2 under light irradiation

Chapter-3

Enhanced Photocatalytic Hydrogen Production with GO-modified Cu-TiO_2 for Alcohol Dehydrogenation under UV and Sunlight

Chapter-4

Graphene Oxide modified Ag-TiO_2 Hybrid Nanocomposites for Improved Photocatalytic Activity

List of abbreviations

a.u.	Arbitrary unit
CB	Conduction band
VB	Valence band
BET	Brunauer-Emmett-Teller
BJH	Barrett-Joyner-Halenda
DRS	Diffuse reflectance spectroscopy
SEM	Scanning electron microscopy
EDS	Energy dispersive X-ray spectroscopy
FESEM	Field emission scanning electron microscopy
EDS	Energy dispersive X-ray spectroscopy
HRTEM	High-resolution transmission electron microscopy
XPS	X-ray photoelectron spectroscopy
XRD	X-ray diffraction spectroscopy
GC	Gas chromatography
HRMS	High Resolution Mass spectroscopy
IPA	Isopropyl alcohol
JCPDS	Joint committee on powder diffraction standards
GO	Graphene oxide
NPs	Nanoparticles
UV	Ultraviolet
Vis	Visible

B.E.	Binding energy
nm	nanometer
DI	Deionized water
E_{CB}	Conduction band edge position
E_{VB}	Valence band edge position
E_g	Band gap
eV	Electron volt
Ar	Argon
wt%	Weight percentage
SPR	Surface plasmon resonance
ppm	Parts per million
H_2	Hydrogen
2D	Two-dimensional

List of symbols

e^-	Electron
h^+	Hole
$O_2^{\cdot -}$	Superoxide radical
·OH	Hydroxyl radical
Å	Angstrom
A	Absorbance
°	Degree
λ	Wavelength
%	Percentage
μ	Micro
θ	Theta
h	Hour
ν	Frequency
s	second
α	Absorbance coefficient
ml	Milli-litre
mM	Milli-molar
μL	Micro-litre
μmol	Micromol
mg	Milli-gram
C	Concentration

Abstracts

Chapter-1

This chapter provides a brief introduction to semiconductor-based photocatalysis, how TiO_2 acts as a photocatalyst, and its advantages and applications, such as photocatalyst for the degradation of hazardous water pollutants and photocatalytic hydrogen production, are discussed in this chapter. To overcome its drawbacks, the modification of TiO_2 with metal deposition and carbon-rich graphene oxide (GO) has been outlined. The related literature has been systematically reviewed, and a brief description of characterization techniques for assessing the properties of synthesized GO-modified metal- TiO_2 nanocomposites has been provided. In this regard, the realized research gaps were mentioned with the objective of the current research work.

Chapter-2

Graphene oxide (GO), an atomic sheet structure made of sp^2-bonded carbon atoms with superior optoelectronic, and catalytic properties, has attracted much interest. Incorporating a carbon-rich material, onto metal-loaded TiO_2 is reported to increase the photocatalytic properties of resultant composites. This research aimed at the deposition of different amounts (1-5 wt%) of GO using the ultrasonication method on bare TiO_2 and Ag (3wt%)-TiO_2 (AT3) and studied their influence on piroxicam-20 degradation under visible light and methanol dehydrogenation under UV light. The prepared composites' structural, optical, and morphological properties were characterized using XRD, DRS, HR-TEM, FE-SEM, and XPS. HRTEM analysis confirmed the existence of GO layers and spherical-shaped Ag nanoparticles deposited over the TiO_2 surface. GO(5wt%)@Ag(3wt%)-TiO_2 (G5@AT3) displayed better photodegradation efficiency (78%) ($k = 0.0082\ min^{-1}$) under 120 min, and GO(1wt%)@Ag(3wt%)-TiO_2 (G1@AT3) composite produced higher amount (427 mmol) of H_2 from photocatalytic dehydrogenation of CH_3OH under 5h relative to TiO_2 (2 mmol), AT3 (166 mmol) and GO(5wt%)@TiO_2 composite (GT5) (11 mmol). HRMS analysis was performed to identify the piroxicam-20 degradation intermediates. Thus, this research provides a proactive strategy highlighting the cooperative effect of Ag and GO loading to improve the photocatalytic efficiency of TiO_2 photocatalyst using both UV-visible light irradiation.

Chapter-3

The high efficiency of the production of hydrogen from alcohols is vital to the advancement of energy technology. This study thoroughly investigates the process of alcohol dehydrogenation utilising GO-modified Cu-TiO_2 photocatalyst under UV light and sunlight exposure. GO-modified Cu-TiO_2 photocatalyst was synthesised using the hydrothermal method. Various experimental techniques, including FESEM, HRTEM, XPS, and DRS, confirmed the formation of the ternary composite. The influence of different alcohols (methanol, ethanol, propanol) and their concentrations (same vol% and molarity) on the amount of hydrogen (H_2) production was examined in this study. The study thoroughly investigated the impact of various parameters, such as the influence of GO and Cu loading on TiO_2 and their combined effect, time course, nature of alcohol and the reaction conditions on the photocatalytic hydrogen production. The GO(0.5wt%)/Cu(3wt%)-TiO_2 ($G_{0.5}C_3T$) composite demonstrated the highest quantity of hydrogen production during methanol dehydrogenation when subjected to both UV and sunlight irradiation. The composite exhibited remarkably about three-fold higher hydrogen evolution in sunlight(881 mmol) than in UV light(294 mmol). The exceptional performance of this composite can be attributed to the efficient transfer of charge carriers and the delayed recombination of electron-holes, which is a result of the cooperative effect of GO and Cu deposited over the TiO_2 system. This approach offers a proactive strategy, signifying the synergetic effect of loading GO and Cu over TiO_2 to enhance the photocatalytic hydrogen production, which is regarded as a green fuel solution, and turns these materials into useful energy sources by using inexpensively synthesised photocatalysts.

Chapter-4

Graphene oxide (GO) has now emerged as one of the most promising materials in different areas such as photocatalysis, adsorption, and energy storage due to its high surface area, unique layered structure, etc. Among various types of precursors, anthracite coal has attracted a lot of attention nowadays as it affords GO a high concentration of sp^2 carbons, resulting in high conductivity and superior absorbance in the visible region. In this report, we have prepared GO-TiO_2 nanocomposites as it is supposed to possess high photocatalytic activity owing to facile electron transmission from the conduction band of TiO_2 to the GO surface, resulting in a much lower degree of electron-hole pair recombination. To boost the photocatalytic activity further, TiO_2 was coated with Ag nanoparticles also. These hybrid structures were

characterized by different analytical techniques, for example, XRD, HR-TEM, SEM, Raman spectroscopy, etc. The XRD pattern of these composites consists of characteristic peaks corresponding to GO, TiO_2 and Ag. The HR-TEM studies confirm the presence of GO layers, cube-shaped TiO_2 and spherical Ag nanoparticles. Phenol and 4-nitrophenol have been used as model pollutants to evaluate the photooxidation efficiencies under both UV and visible light irradiation. Under UV irradiation, the GO/Ag-TiO_2 ternary nanocomposite shows better photooxidation efficiency (62%) compared to Ag-TiO_2 (38%), GO-TiO_2 (9%), GO (17%), TiO_2 (8%) towards phenol degradation. The GO/Ag-TiO_2 also has the highest photocatalytic activity towards the removal of phenol under visible light irradiation (34%). The ternary heterostructure (85%) also possesses superior photooxidation activity compared to, Ag-TiO_2 (44%) and GO-TiO_2 (71%) towards the degradation of p-nitrophenol under UV light radiation for 60 minutes. The above observation reveals that the cooperative effect of Ag, TiO_2, and GO plays a crucial role in resulting in the high photooxidation activity of the GO/Ag-TiO_2 hetero-nanocomposites.

CHAPTER- 1

1.1 Introduction

1.1.1 TiO_2 as photocatalyst

In the present era, the world is facing two significant challenges: the need to protect and restore the environment and the requirement to manage, store, and convert energy in alternative ways. These challenges have arisen due to the substantial growth in global population, industrialization, and the consumption of natural resources. Therefore, it is imperative to discover an effective approach to address the issue of energy scarcity and the harm to the environment. "Semiconductor-based photocatalysis" is considered a promising approach for achieving a clean and sustainable future, considering its purity, inexhaustibility, effectiveness, and low-cost [1]. It mostly involves accelerating the chemical reaction by employing a light-activated SC(semiconductor) catalyst. In this context, the advanced oxidation process (AOP) is one of the most intriguing process that can achieve total oxidation of both organic and inorganic water pollutants. The term "heterogeneous photocatalysis" describes a process wherein a semiconductor material's surface is activated by light to produce reactive species, most notably hydroxyl radicals (•OH), that subsequently mineralize the pollutant of concern.

Among various photocatalysts, Titanium dioxide (TiO_2) is an established photocatalyst known for its robust photocatalytic oxidation, high room temperature activity, and excellent photostability. Titanium dioxide, or titania, is a naturally-found transition metal oxide represented by the scientific notation TiO_2. Furthermore, it is widely utilised throughout several industrial sectors like paints, varnishes, paper, printer inks, rubber, plastics, cosmetic items, and more[2–4]. As a result of its distinctive structural, optoelectrical, and photocatalytic characteristics, it is recognised as a promising semiconductor nanomaterial[5,6]. The physical-chemical stability, high refractive index, low toxicity, strong reactivity, ease of synthesis, low price, excellent catalytic activity, and excellent energy conversion efficiency of TiO_2 have been widely recognised (**Scheme- 1.1(a)**)[7,8]. For that reason, it is appropriate for a variety of critical technological applications, including the treatment of wastewater, the development of self-cleaning coatings[9], the production of disinfecting materials, the production of fuel cells [5,10], the development of solar cells[11,12], and sensors (**Scheme- 1.1(b)**).

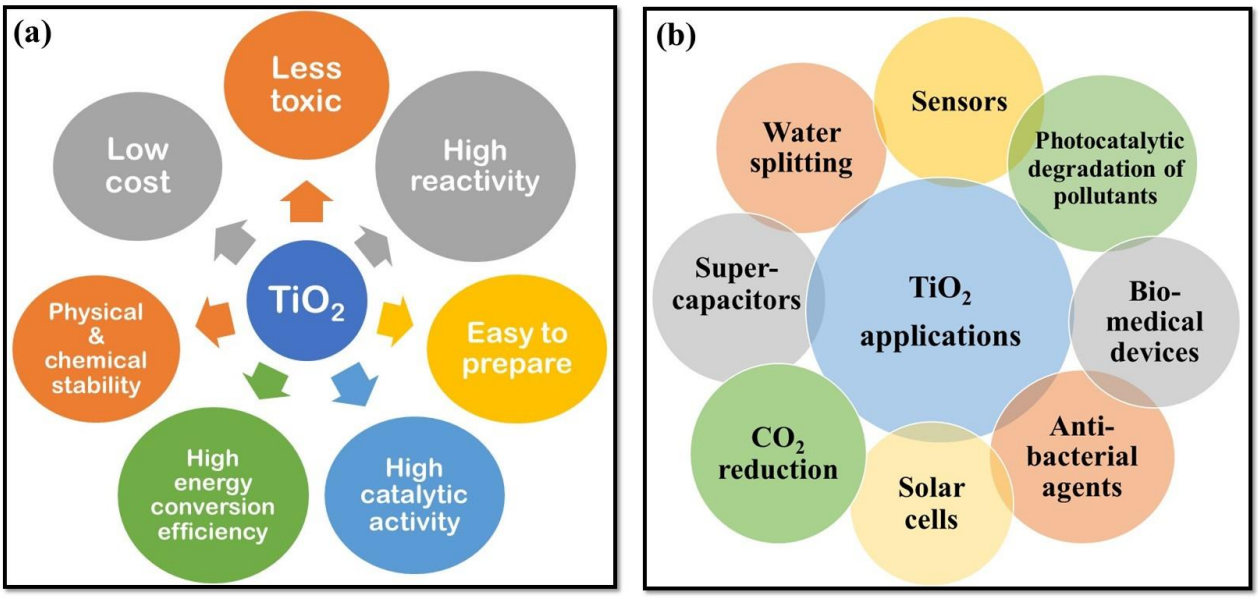

Scheme-1.1: (a) Various properties and (b) different applications of TiO_2 nanostructures.

It occurs naturally in the following three forms: anatase, rutile, and brookite. The states are defined by the interaction of TiO_6 octahedra while preserving the overall stoichiometry consistent with TiO_2[13–15]. This semiconductor photocatalyst demonstrates high efficiency, exhibiting band gaps of ~3.2 eV, ~3.02 eV, and ~2.96 eV across its anatase, rutile, and brookite phases, respectively. It demonstrates absorption in the ultraviolet (UV) region[2,16].

General mechanism of TiO_2 during photodegradation reaction on organic pollutant

Upon exposure to light irradiation, the photocatalyst (TiO_2) facilitates the transition of electrons (e^-) from the valence band (VB) to the conduction band (CB), allowing them to migrate to the surface of the catalyst, where they subsequently undergo reduction. The holes have the ability to undergo an oxidation process by directly reacting with the organic molecules or generating hydroxyl radicals ($^{\cdot}OH$), which then oxidise organic molecules and break them down into smaller products. Electrons also undergo reactions with organic molecules to produce reduction products. Dissolved O_2 can be reduced to $O_2^{\cdot -}$ radicals by the electrons in the conduction band (**Scheme-1.2**).

$$TiO_2 + hv \rightarrow h^+(VB) + e^- (CB)$$

$$h^+ + H_2O \rightarrow H^+ + OH^-$$

$$h^+ + OH^- \rightarrow OH^{\cdot}$$

$$e^- + O_2 \rightarrow {}^{\cdot}O_2^-$$

$$\cdot O_2^- + h^+ + OH^\cdot + organic\ pollutant \rightarrow CO_2 + H_2O + other\ mineralized\ products$$

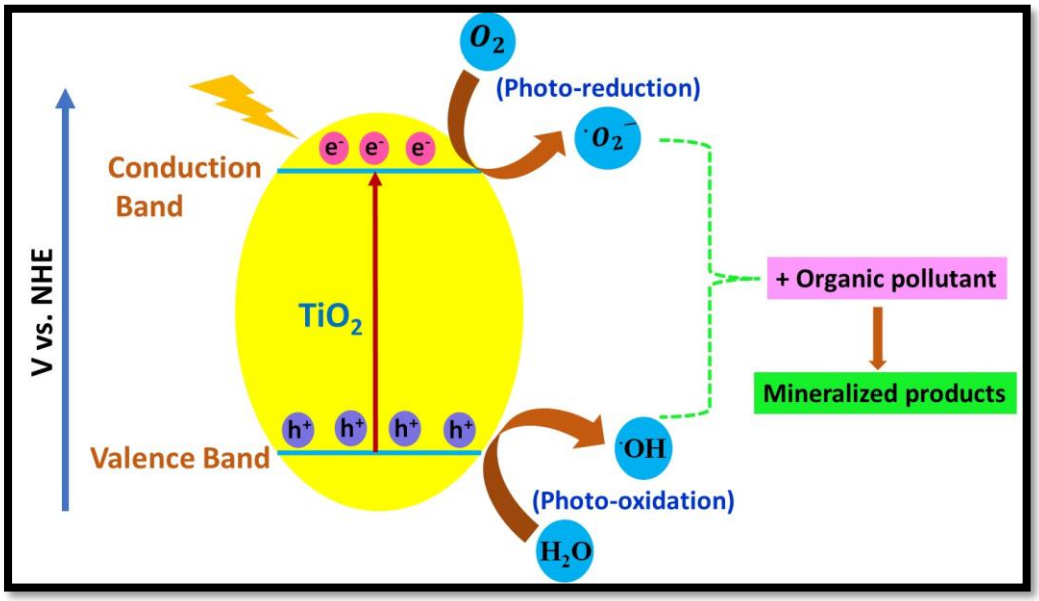

Scheme-1.2: A schematic representation of the photocatalysis process towards the degradation of organic pollutants.

Catalyst type	Organic pollutant	Source light	Result	Reference
Degussa P-25 TiO_2	Rhodamine B	UV light	Initial concentration is 0.2 g/L, at 120 min, 55% degradation	[17]
TiO_2 nanoribbons and carbon nanotubes	Methylene blue	UV light	Initial concentration is 0.2 g/L, at 180 min, 97.5% degradation	[18]
TiO_2 nanotube	Orange II	UV light	Initial concentration is 70 mg/L; at 2000 min, 89.46% degradation	[19]
Nano flower-like rutile TiO_2	Methylene blue	Solar light	Initial concentration is 5 mg/L; at 180 min; 98.95% degradation	[20]
TiO_2 Degussa P-25	Acridine Orange and ethidium bromide	Solar light	Highest efficiency of degradation was achieved using P-25 under alkaline conditions (pH ¼ 10)	[21]
TiO_2 Degussa P-25	Malachite Green	UV light	99.9% of Malachite Green was degraded at 6 h.	[22]
TiO_2 Degussa P-25	Acridine Orange and ethidium bromide	UV light	Degussa P25 showed better performance than other TiO_2.	[21]

Table 1.1: Summary of the photocatalytic efficiency of the TiO_2 form and structure on organic pollutants.

Various other shapes and structures of the TiO_2 photocatalysts have been assessed for their effects on wastewater treatment **(Table 1.1)**. Degussa P-25 TiO_2 exhibited substantially greater photocatalytic activity than that of other forms of TiO_2 photocatalysts, including UV100 (100% anatase; Hombikat) and PC500 (100% anatase; Millennium inorganic chemicals), among these various forms. References investigated the impact of these three versions of TiO_2 on the degradation of Ethidium Bromide, Triphenylmethane dye and Acridine Orange. It determined that Degussa P-25 TiO_2 exhibited the maximum degradation rate[23]. The reason for this is that the Degussa P-25 is composed of microscopic nano-crystallites of the rutile (18%) which are dispersed inside the anatase matrix (73%). During the photocatalytic activity, these two forms of TiO_2 exhibit a synergistic effect in DegussaP-25 TiO_2.

1.1.2 Limitations of TiO_2 as photocatalyst

Although TiO_2 have significant potential for photocatalytic applications, its effectiveness is hindered by its rather small specific surface area, rapid recombination of photogenerated charge carriers, and limited efficiency in utilising solar or visible light due to the wide band gap. The limitations greatly constrain the widespread application of the material. A significant amount of effort has been directed towards the modification of TiO_2 in order to enhance the lifetime of the charge carrier and the light absorption features.

1.1.3 Modification over TiO_2

1.1.3.1 Metal deposition

On the contrary, the primary challenge to optimising TiO_2's photocatalytic efficiency is the broadband gap (approximately 3.0–3.2 eV), which restricts its activity solely to the UV light region, thereby preventing the effective utilisation of the entire solar spectrum, along with a rapid electron-hole recombination rate. Currently, numerous potential approaches are being considered, including stimulating using noble or transition metals and combining them with other semiconductors or carbon-based substances[24]. The enhancement of photocatalytic processes by modifying semiconductor materials with noble metals is ascribed to more efficient e^--h^+ separation, the expansion of photoactivity to the visible range, and the surface plasmon resonance (SPR) exhibited by the metal nanoparticles[25]. Noble metal nanoparticles (Au, Pt, Ag) exhibit a significant absorption of visible light as a result of their surface plasmon

resonance (SPR). This phenomenon is characterised by the collective oscillation of their conducting electrons, which is triggered by the electric field of incoming visible light[26]. When the Fermi level of the metal is positioned between its VB and CB, photoinduced electrons transfer from the semiconductor's CB directly to the metal nanoparticles. These metal nanoparticles function as electron sinks owing to the Schottky barriers that are established at the metal-semiconductor contact. Metal nanoparticles' photoinduced electrons are captured by appropriate reactive species. Thus, by depositing metal on the semiconductor surface, the charge transfer distance is reduced, the electron-hole pairs are suppressed from reuniting, and the photocatalyst's response in the visible region is improved.

The absorption and scattering properties of metallic nanoparticles can be optimised by tailoring their morphology and dielectric environment. Noble metals are photoactive to a limited extent when present in bulk. However, when deposited over the semiconductor surface, such as TiO_2, they exhibit electron storage properties, which result in enhanced charge separation. The noble metal nanoparticles exhibit unique optical and catalytic properties that are not typically observed in bulk metal. Deposition of a nano-noble metal over the TiO_2 surface can improve photocatalytic efficiency by facilitating faster electron transfer between semiconductor and metal deposits, as opposed to the surface trapping states caused by bulk modification. The presence of localised surface plasmon resonance (SPR) in gold (Au) and silver (Ag) nanoparticles often results in the appearance of intense and broad absorption bands within the visible light spectrum. Furthermore, this phenomenon is employed to produce photocatalysts that are stimulated by visible light. In this regard, the metal nanoparticle size, synthesis method, and weight loading play a crucial role.

The strong SPR effect and intriguing electrical conductivities of coinage metals (such as Cu, Ag, and Au) have been a subject of considerable attention[27]. In this regard, these materials have been employed in a variety of sizes, forms, and shapes to alter the optical and surface characteristics of TiO_2 photocatalysts[28,29]. Due to their appropriate redox potentials (Cu=0.337eV, Ag=0.799eV, and Au=1eV), these metals have been photo-deposited on the surface of TiO_2 and examined for a variety of environmental photocatalytic applications. For example, mesoporous RuO_2-TiO_2 has been photo-deposited with Au, Pd, and Pt metals for CH_3OH oxidation. RuO_2-TiO_2 composites containing Au exhibited a significant photocatalytic activity in visible light in comparison to Pd, Pt-deposited catalysts[30]. Likewise, TiO_2 nanoparticles modified with Ag and CuO have been identified as effective electron scavengers for the photooxidation of acetic acid and phenol[27]. Moreover, several Ag, Cu, Pt, and Au -

modified TiO_2 nanocomposites have been documented in the literature to investigate the efficient oxidation-reduction pathways[31,32].

1.1.3.2 Modification with Graphene oxide (GO)

In an alternative method, the photocatalytic properties of TiO_2 can be improved by immobilising TiO_2 on carbonaceous materials, including carbon nanotubes and graphene[33–36]. The 2D carbon nanostructure graphene exhibits exceptional charge transfer capabilities, chemical stability, and optical characteristics. Graphene is an exceptional material characterized by its atomic sheets consisting of sp^2-bonded carbon atoms. It has garnered significant interest due to its remarkable properties, such as an extensive surface area, high chemical and thermal stability, excellent interfacial contact with adsorbents, and outstanding charge carrier mobility. Combining TiO_2 with materials composed of graphene can reduce e^--h^+ recombination, shifting TiO_2's sensitivity from UV to visible range. The primary drawback of graphene, however, is its extremely limited solubility in ordinary organic solvents[37]. Conversely, graphene oxide (GO) is a perfect substitute for producing solution-processable graphene since it easily produces stable dispersion in a range of solvents[38].

It can be synthesised chemically through a chemical exfoliation process to produce GO. This produces a multilayered-graphene-sheet containing functional groups, including epoxy, hydroxyl, and carboxyl. The functional groups react with metal precursors, which causes metal ions to accumulate and, in the end, immobilises metal nanoparticles onto the GO sheet. The TiO_2/graphene composite exhibits superior photocatalytic performance that possesses improved light absorption as well as high surface activity. Additionally, it creates interfaces between TiO_2 and carbon nanostructures, functioning as p-n heterojunctions[39]. The heterojunctions facilitate the separation of photoinduced electrons and holes, which enhance the photocatalytic activity of such composites. The TiO_2/graphene composites synthesis has been accomplished using several methods, such as the sol-gel[40,41], solvothermal[42–44], and hydrothermal processes[45–48]. The hybrid composites comprising nanoparticulate metals and graphene oxide (GO) can display superior characteristics, including high adsorption capacity for organic dyes, reduced recombination rate of the photo-generated charge transporters, and excellent π-π stacking with dye chromophores.

Khalid and his colleagues[49] employed the sol-gel method for fabricating Cu-TiO_2 nanoparticles and then used a hydrothermal approach to combine Cu-TiO_2 with graphene. The composites had a broad spectrum of light absorption encompassing both ultraviolet and visible

light wavelengths and exhibited superior photoactivity compared to the Cu−TiO_2 and TiO_2/graphene composites. A Pd−TiO_2/graphene composite was synthesised by Song and his team[50] by the incorporation of TiO_2 nanoballs onto the graphene utilising a poly (diallyl dimethyl ammonium chloride) as a linker. The composite was added to a solution of palladium chloride and ammonia and then placed inside a hydrothermal reactor, continuing heating. Katsarakis[38]synthesised an Ag−TiO_2 powder by coupling P25-TiO_2 with an $AgNO_3$ precursor and dimethylamine borane as a reducing agent. The obtained powder was added to an ethanol-water mixture, followed by the addition of GO and introduced into a hydrothermal reactor. The Ag TiO_2/GO composite exhibited exceptional photoactivity in the photodegradation of methylene blue dye.

1.1.4 Photocatalytic applications

1.1.4.1 Water pollutant remediation

In recent years, water contamination has emerged as a significant concern. Numerous hazardous substances, such as pesticides, personal care products, industrial dyes, fertilizers, disinfectants, prescription medications, and inorganic pollutants (specifically heavy metals), are being released into water bodies on a daily basis without undergoing any chemical treatment. The continual presence of these hazardous to-health pollutants in water sources poses dangers to both human and aquatic life. Industrial development is linked to the presence of toxic contaminants, including phenolic compounds, which are harmful to humans, harmful to the environment, and difficult to eliminate through natural means.

Phenolic compounds are aromatic compounds that have one or more hydroxyl groups bonded to the aromatic ring. The subject matter of phenols and their derivatives has garnered an increasing amount of global attention. This category of pollutants is predominantly present in industrial effluents. Phenols, when exposed to the environment in effluent, directly pose a threat to humans due to their rapid absorption by the lungs in a brief period. Because of their corrosive properties, all forms of phenols and their derivatives can induce irritation in the respiratory tract, eyes, and skin. These chemicals have wide-ranging applications in the textile, pharmaceutical, and agrochemical sectors.

Pharmaceutical pollutants, including antibiotics, analgesics, and disinfectants, have been found in surface water at concentrations ranging from ng/L to g/L. Approximately 70-90% of antibiotics are excreted in either chemically unmodified or active metabolite form by humans

and animals. The poor metabolic rate, excessive intake, and insufficient absorption of these compounds make environmental resources vulnerable to contamination. According to reports, these substances are not removed altogether at sewage treatment plants. As a result of the severe repercussions of water pollution caused by pharmaceutical and dye contaminants, researchers have made numerous efforts to remove these potentially harmful substances from the effluent.

Recent studies have investigated and evaluated several environmental strategies for the removal of persistent contaminants from polluted wastewater[51]. These include integrated Fenton oxidation, sonochemical degradation[52], electrochemical treatment[53], adsorption[54,55], ion exchange[56],and biological treatment[57]. Nevertheless, those methods have disadvantages, including high operational costs as a result of their substantial energy consumption. In recent times, photocatalytic degradation has become increasingly attractive as a highly promising approach for eliminating refractory contaminants such as dyes, pharmaceutical drugs, other organic pollutants, etc. This advanced oxidation process provides multiple advantages ranging from minimal operational costs, reusability, ability to utilize solar energy, and contaminant removal from different media.

In recent years, heterogeneous photocatalysis has shown considerable significance as a viable solution for treating wastewater generated by various sectors. The photocatalytic process is predicated on the production of hydroxyl radicals ((˙OH), which possess a high degree of oxidative power and can efficiently oxidise organic pollutants, as well as disinfect microorganisms. Barakat et al.[58] synthesized $Ni(OH)_2$/graphene oxide/ TiO_2 nanocomposite and employed it for wastewater treatment, including toxic organic compounds, microbes, and lipids in dairy effluent. It was examined for both the degradation of 2-chlorophenol (2-CP) and the pre-treatment of dairy effluent to enhance digestibility and remove microbial pollutants through anaerobic digestion. The composite efficiently removed 80% of the 2-CP in 4h under solar light with 25mg/l concentration (pH= 6.0). The organic solubilisation of dairy effluent is enhanced by the pretreatment process, resulting in an increase in soluble chemical oxygen demand (sCOD) content from 272 to 631 mg/l within six hours of photocatalysis. A study conducted by Moonrisi et al.[59] documented an increased rate of degradation of 4-chlorophenol (4-CP) while employing Pt-deposited (1 mol%) P25 under experimental circumstances, including nitrogen bubbling. Their observation revealed a reduction in the rate of degradation when dissolved oxygen was present. Qi et al.[60] synthesized the Ag-modified GO- TiO_2 (Ag/GO-TMCs) composite using photoreduction deposition method. The study aimed to explore the photocatalytic characteristics of the catalyst for the degradation of

Rhodamine B dye (RhB) and dinitro butyl-phenol (DNBP) when exposed to visible light. From the prepared composites, Ag/GO-TMCs-7.5% composite, where 7.5% Ag deposited over GO-TMCs exhibited the highest amount of degrading efficiency for RhB and DNBP when evaluated under visible light illumination for 3h. The enhanced photocatalytic efficiency of Ag/GO-TMCs can be ascribed to the increased affinity of Ag nanoparticles and GO for visible light and the surface plasmon resonance (SPR) effect.

1.1.4.2 Photocatalytic hydrogen production

In the forthcoming decades, the primary obstacles will be the energy crisis and environmental contamination issues. Among the diverse alternative energy sources, hydrogen energy is a critical element of the renewable energy strategy of the developed world due to its immediate availability and high fuel efficiency. Researchers have devoted significant focus to the use of hydrogen as an environmentally friendly energy carrier and to the establishment of novel methods for its generation without relying on fossil fuels. Presently, the majority of the energy used by humankind is generated through the combustion of fossil fuels, which are a finite natural resource. According to statistical data, there has been a prevailing tendency in recent years towards economic expansion worldwide, resulting in a rise in energy consumption per unit of gross domestic product[61,62]. Among renewable energy sources include solar and photovoltaic energy, biomass, hydropower, tidal energy, ocean thermal energy[63]. In this instance, solar energy is a strategically significant resource, as it is the major form of renewable energy. Consequently, the direct conversion of light energy into the energy of chemical bonds is one of the most promising areas for the development of solar energy. The ultimate objective may be the photocatalytic production of hydrogen[64,65].

Sodium borohydride, ammonia, borane, methanol, ethanol, formaldehyde, and hydrazine have been assessed as initial substrates in catalytic and photocatalytic reactions for hydrogen generation[66,67]. Benzyl alcohol, glucose, alkanes, and ethanol have recently gained significant interest as potential precursors in photocatalytic hydrogen production systems[68,69]. CdS, TiO_2, $Cd_{1-x}Zn_xS$, and g-C_3N_4-based heterogeneous catalysts have been widely preferred in photocatalytic hydrogen production[70,71]. Although there is a wide range of suggested novel photocatalyst materials, titanium dioxide remains one of the most frequently used photocatalysts because of its abundant availability, very low toxicity, and exceptional durability. The photocatalytic efficiency of pure TiO_2 is well-documented to be somewhat poor,

given the rapid recombination of electron-hole pairs. Deposition of noble metal co-catalysts onto the surface of TiO_2 is a generally used method to enhance activity. Metal nanoparticles function as electron traps due to the creation of the Schottky barrier at the metal-semiconductor interface, thereby extending the lifespan of electron-hole pairs. A recent study by Zhu et al. revealed that plasmonic Au/TiO_2 displayed exceptional HCHO oxidation activity when exposed to visible light. This high performance is due to the combined effects of plasmonically excited electrons on the Au and active oxygen species on the surface[72]. Bamwenda and colleagues[73] conducted an experiment to examine the catalytic activity of two catalysts, Au/TiO_2 and Pt/TiO_2, for the generation of H_2. The findings indicated that the performance activity of the Pt sample was 30% greater than that of the Au sample. A high production of hydrogen was observed when both Au and Pt samples were calcined in air at 573K.

Additionally, carbon-based materials such as graphene oxide, reduced graphene oxide, or graphitic nitride on TiO_2 can be highly beneficial due to their high conductive properties and extensive surface area for electron transfer and delocalisation, which results in a reduced recombination rate of the e^-/h^+ pair. Zhang et al.[74] synthesized a ternary graphene-like photocatalyst using Mo and GO over a SiC semiconductor catalyst. The experimental results indicated that the ternary photocatalyst exhibited robust photocatalytic hydrogen production activity in comparison to pure SiC. The maximum quantum yield of 21.69% was observed at the 400–700 nm wavelength when the catalyst was loaded with 2.5 wt% of GO weight. Rayees et al.[75] prepared a Cu-mpTiO_2 photocatalyst for hydrogen production from water under sunlight. Cu-mpTiO_2 generated 1000 μmol of H_2 (AQE = 11.39%) when exposed to sunlight, a significant increase from the amount of H_2 produced by Cu impregnated on commercial P25-TiO_2. In another study[76], they synthesized a GO-coated Au-TiO_2 nanocatalyst that exhibited improved photocatalytic hydrogen production from water due to its core-shell morphology. The structural framework of Au-TiO_2@GO exhibited a thin layer (about 2.5 nm) of graphene oxide shell on top of the Au-TiO_2 core, which had a greater specific surface area (about 100 m^2g^{-1}). The Au-TiO_2@GO nanocomposite exhibited the highest rate of H_2 evolution, which increased over a period of 3 hours (110μmol). In comparison to TiO_2 and Au-TiO_2, the lower reduction potential of GO enables a reduction in the recombination rate of charge carriers. Conversely, the presence of Au loading enhances the sensitivity of TiO_2 to visible light, leading to an improvement in the efficiency of solar to hydrogen-conversion.

These investigations consistently demonstrate a synergistic effect between graphene oxide and metal, resulting in an enhanced photocatalytic activity of the composite material.

1.2 Research Gaps

Through the literature review, we discovered that the photocatalytic activity of bare TiO_2 has been extensively studied for the photocatalytic degradation of organic pollutants and photocatalytic hydrogen generation from water splitting. Various reports have been published on metal-TiO_2 hybrids for enhancing the photocatalytic properties of TiO_2. At the same time, there is still plenty of scope to enhance the photocatalytic capabilities of metal-TiO_2. Several transition metals have been found to suffer oxidation/corrosion processes that effectively decrease the semiconductor's photo-efficiency. By combining it with a carbonaceous material, the stability of metal-TiO_2 can be enhanced. It can be deduced that graphene with unpaired π electrons could be used to change the TiO_2 surface to produce a visible-light-responsive photocatalyst by means of the interaction between unpaired π electrons of graphene and Ti atoms. Thus, the band edge and the significant reduction of the band gap of graphene-TiO_2 can be obtained. The lower reduction potential of GO compared to TiO_2 enables a rapid reduction in the recombination rate of charge carriers. On the other hand, the presence of metal loading enhances the sensitivity of TiO_2 to visible light, leading to a higher efficiency of converting solar energy into hydrogen compared to TiO_2 and metal-TiO_2.

Recent research has demonstrated that the photocatalytic activity of the SC photocatalyst can be significantly enhanced by the combined use of graphene oxide and metals. Exploring the benefits of GO/M-TiO_2 nanocomposites, which include excellent electron conductivity, the specific Schottky barrier of the metal, enhanced light-absorption properties, and a large specific surface area, will greatly enhance the performance of TiO_2 for the various photocatalytic applications.

There are numerous reports on hydrogen production from water splitting, but there are only a handful of studies that have been reported on the generation of hydrogen from alcohols using such GO-modified/metal-TiO_2 catalysts. Moreover, it would be significant to explore both oxidative and reductive photocatalytic properties in the same prepared GO/M-TiO_2 composite. The objective of this research is to optimise the photocatalytic oxidative and reductive activity of TiO_2 by modulating its band gap and surface-structural properties through the addition of GO and metal. This would result in the development of various ternary (GO/M-TiO_2) heterostructure composites. Furthermore, the several hybrid interfaces formed (M-TiO_2, GO-TiO_2) in the structure would lead to enhancement of the efficiency of separating photo-excited charges, thereby leading to improved photocatalytic efficiency of the ternary composite.

1.3 Objectives

1. Preparation of Graphene oxide (GO) from coal /graphite and its coating over TiO_2 for improved surface structural, physical and chemical properties.
2. Preparation of different metal M-TiO_2 (M= Ag, Fe, Cu, Co, Ni, etc.) nanocomposites and GO-coated M-TiO_2 composites.
3. Study of surface structural, optical properties and photocatalytic degradation with GO-TiO_2, M-TiO_2, GO@M-TiO_2 nanocomposites.
4. To investigate the H_2 production from photocatalytic dehydrogenation of waste alcoholic solvents by as prepared nanocatalysts under visible light/sunlight irradiation.

1.4 Methodology

1.4.1 Synthesis of metal deposited TiO_2 (M- TiO_2)

The photo-deposition method was applied to deposit metal over the TiO_2 surface. In a standard procedure, about 100 mg of the P25-TiO_2 catalyst was dispersed in a 50-vol% aqueous solution of the sacrificial agent in a test tube. For preparing different wt% metal composites, a calculated amount of metal salt solution was added to the above test tube. Afterwards, the test tube was purged with argon gas to remove excess oxygen and prevent oxidation. It was sealed with a rubber septum and placed and stirred under UV light for 2-4h. The obtained solution was centrifuged, washed and dried.

1.4.2 Synthesis of Graphene oxide (GO)

The GO was synthesised using the modified Hummer's method. An initial mixture of 1 g each of graphite and $NaNO_3$ powder in a 1:1 ratio was combined in a conical flask. This was then followed by the addition of 23 ml of H_2SO_4 and magnetically stirred for 3 h, maintaining the temperature at around 20 °C. The mixture solution was stirred continuously at ~20 °C for 2 h after $KMnO_4$ (3 g) addition. Distilled water (46 ml) was added slowly to the above-mentioned solution and further stirred for 2 h, maintaining the temperature at ~98 °C. Afterwards, another 100ml of distilled water was added, followed by H_2O_2 (10 ml) after 5 min. The resultant mixture was centrifuged and washed with DI water and HCl 3-4 times, and the sample was dried at 55 °C overnight.

1.4.3 Synthesis of GO-TiO_2 and GO/M-TiO_2

For different wt% GO loadings, the pre-calculated amount of GO (1-5 wt% wrt to TiO_2) was added in (2:1) ethanol: water solution and sonicated for over 2h to exfoliate the solution. To

create a homogeneous suspension, 200 mg of P25 TiO_2 powder (for GO-TiO_2 composite) and 200 mg of M-TiO_2 (for GO/M-TiO_2 composite) were added in the sonicated GO solution and subjected to magnetic stirring at room temperature for 2h followed by transferring it to Teflon autoclave and heated at 180 °C for 5h. The resultant mixture was centrifuged and washed with DI water and ethanol, and dried.

1.5 Characterization techniques

The synthesis of M- TiO_2, GO-TiO_2, and GO/M-TiO_2 nanocomposites involved the use of various modified synthetic methods (specific experimental information can be found in the corresponding chapters). The surface, structural, and physicochemical properties of the as-prepared catalysts were further investigated using a variety of characterisation techniques.

1.5.1 X-ray powder diffraction (XRD):

The X-ray diffraction (XRD) technique was employed to quantify the diffraction pattern, crystallinity, and lattice plane of a catalyst that has been synthesised using an X-ray diffractometer (BRUKER) with Cu Kα (1.54 Å) and an angle range of 10°–90° at a rate of 5° per minute.

1.5.2 Morphological analysis:

The as-prepared nanocatalysts were analysed for their structural characteristics, including shape and particle size, using electron microscopy techniques such as Field Emission Scanning Electron Microscope (FE-SEM, JEOL JSM-7600F) and High-Resolution Transmission electron microscopy (HRTEM, JEOL JEM-2100 model). The elemental composition was determined through an Energy dispersive X-ray spectrometer (EDS) (Bruker, QUANTAX 200) connected to the above-mentioned FE-SEM scanning module.

1.5.3 Raman analysis:

Raman spectroscopy studies were conducted using a Labram HR 124 Evolution Raman microscope with a 532 nm excitation laser.

1.5.4 Optical studies:

The UV-visible diffuse reflectance spectra (DRS) were recorded for the optical absorption properties of catalysts using a diffuse reflectance spectrophotometer (Avantes) with $BaSO_4$ serving as the reference. The PL emission spectrum was measured at room temperature to

investigate the separation of photoinduced e^--h^+ pairs. Samples were dispersed in distilled water, and data was recorded using a spectrofluorometer (SHIMADZU, RF-6000) for the analysis.

1.5.5 Surface area and porosity determination:

The Quanta Chrome Nova 2200 Surface Area & Pore Size Analyser was employed to analyse the surface area and pore size distribution of the samples using the BET (Brunauer-Emmett-Teller) and BJH (Barrett-Joyner-Halenda) methods, respectively(Analysis gas: Nitrogen, Bath Temp: 77.3 K, Outgas Time: 6 h, Outgas temperature: 200 °C).

1.5.6 X-ray photoelectron spectroscopy(XPS):

The XPS analysis was employed to determine the elemental composition and oxidation states present in the composite. Using a monochromatic Al K Alpha X-ray source (1486 eV), the XPS data was recorded on a Thermo Fisher ESCALAB Xi+ spectrometer.

1.5.7 Gas-chromatography (GC):

The hydrogen production during the photocatalytic dehydrogenation of alcohol was quantified using a NUCON, a gas chromatograph using argon as a carrier gas, and a molecular sieve (5X A column) with a thermal conductivity detector (TCD). The temperatures of the oven, injector, and detector were set according to the experimental conditions required. The hydrogen produced was quantified against a standard (505 ppm H_2 and 503 ppm CO_2, balanced with Argon).

1.5.8 High-resolution mass spectroscopy (HRMS):

The intermediates and degradation products were analysed using the HRMS (High-resolution mass spectroscopy) on Waters, QTOF mass spectrometer with UPLC (XEVO G2 XS).

1.6 Photocatalytic activity

The photocatalytic efficiency of synthesized GO-TiO_2, M-TiO_2, GO/M-TiO_2 nanocomposites was measured by examining the following two photocatalytic reactions:

1.6.1 Photocatalytic degradation of organic pollutants

The photocatalytic degradation efficiency of all composites was investigated for the degradation of various organic pollutants. In the course of photodegradation experiments, a

certain quantity of catalyst was introduced into a test tube containing an aqueous solution of a particular pollutant. The test tube was firstly exposed to dark for a certain time period in order to attain adsorption-desorption equilibrium and then light illumination under two sources: UV lamp (125W Hg arc, 104 mW/cm^2) and visible light (50W LED lamp, Wipro Garnet B22, with an intensity ~100W/m^2, $\lambda > 360$ nm) for distinct durations. At regular intervals, the test tube was taken out, the catalyst was separated from the pollutant solution by centrifugation, and the change in the concentration of the solution at different time intervals was measured using a UV-visible spectrophotometer (Shimadzu UV-2600 spectrophotometer). An analysis of the degradation products and intermediates was conducted using HRMS.

1.6.2 Photocatalytic dehydrogenation of alcohols

The photocatalytic production of hydrogen by the dehydrogenation of different alcohols was investigated using synthesised composites. A test tube containing 10 mL of an aqueous alcoholic solution (50 vol%) was used along with the desired amount of catalyst. The test was sealed with rubber septum to establish an inert atmosphere after being purged with argon gas for 20 minutes. Afterwards, the test tube was placed under light illumination with continuous stirring for a certain time period. A syringe was used to extract 1 ml of the sample gas produced in the test tube, which was then injected into the injector port of the GC and analysed for hydrogen production. The GC chromatogram was subsequently compared to a standard hydrogen chromatogram.

References

1. Zhang X, Yuan X, Jiang L, Zhang J, Yu H, Wang H, et al. Powerful combination of 2D g-C3N4 and 2D nanomaterials for photocatalysis: recent advances. Chem Eng J. 2020;390:124475.

2. Prakash J, Sun S, Swart HC, Gupta RK. Noble metals-TiO2 nanocomposites: from fundamental mechanisms to photocatalysis, surface enhanced Raman scattering and antibacterial applications. Appl Mater Today. 2018;11:82–135.

3. Ge M, Cao C, Huang J, Li S, Chen Z, Zhang K-Q, et al. A review of one-dimensional TiO 2 nanostructured materials for environmental and energy applications. J Mater Chem A. 2016;4:6772–801.

4. Haider AJ, Jameel ZN, Al-Hussaini IHM. Review on: titanium dioxide applications. Energy Procedia. 2019;157:17–29.

5. Wang J, Chen S, Liu D, Chen C, Li R, Peng T. Fabrication of PbS nanocrystal-sensitized ultrafine TiO2 nanotubes for efficient and unusual broadband-light-driven hydrogen production. Mater Today Chem. 2020;17:100310.

6. Ravishankar TN, Vaz M de O, Ramakrishnappa T, Teixeira SR, Dupont J. Ionic liquid–assisted hydrothermal synthesis of Nb/TiO2 nanocomposites for efficient photocatalytic hydrogen production and photodecolorization of Rhodamine B under UV-visible and visible light illuminations. Mater Today Chem. 2019;12:373–85.

7. Singh N, Prakash J, Misra M, Sharma A, Gupta RK. Dual functional Ta-doped electrospun TiO2 nanofibers with enhanced photocatalysis and SERS detection for organic compounds. ACS Appl Mater Interfaces. 2017;9:28495–507.

8. Niu B, Wang X, Wu K, He X, Zhang R. Mesoporous titanium dioxide: Synthesis and applications in photocatalysis, energy and biology. Materials (Basel). 2018;11:1910.

9. Ren Y, Li W, Cao Z, Jiao Y, Xu J, Liu P, et al. Robust TiO2 nanorods-SiO2 core-shell coating with high-performance self-cleaning properties under visible light. Appl Surf Sci. 2020;509:145377.

10. Dong W, Tong Y, Zhu B, Xiao H, Wei L, Huang C, et al. Semiconductor TiO 2 thin film as an electrolyte for fuel cells. J Mater Chem A. 2019;7:16728–34.

11. Buapuean T, Jarudilokkul S. Synthesis of mesoporous TiO2 with colloidal gas aphrons, colloidal liquid aphrons, and colloidal emulsion aphrons for dye-sensitized solar cells. Mater Today Chem. 2020;16:100235.

12. Prakash J, Singh A, Sathiyan G, Ranjan R, Singh A, Garg A, et al. Progress in tailoring perovskite based solar cells through compositional engineering: Materials properties, photovoltaic performance and critical issues. Mater today energy. 2018;9:440–86.

13. Verma R, Gangwar J, Srivastava AK. Multiphase TiO 2 nanostructures: A review of efficient synthesis, growth mechanism, probing capabilities, and applications in bio-safety and health. RSC Adv. 2017;7:44199–224.

14. Paul KK, Giri PK. Shape Tailored TiO 2 Nanostructures and Their Hybrids for Advanced Energy and Environmental Applications: A Review . J Nanosci Nanotechnol. 2018;19:307–31.

15. Rath H, Dash P, Som T, Prakash J, Tripathi A, Avasthi DK, et al. Surface evolution of titanium oxide thin film with swift heavy ion irradiation. Radiat Eff Defects Solids [Internet]. 2011;166:571–7. Available from: https://doi.org/10.1080/10420150.2011.559239

16. Gupta SM, Tripathi M. A review of TiO2 nanoparticles. Chinese Sci Bull [Internet]. 2011;56:1639–57. Available from: https://doi.org/10.1007/s11434-011-4476-1

17. Bagbi Y, Sarswat A, Mohan D, Pandey A, Solanki PR. Lead and chromium adsorption from water using L-cysteine functionalized magnetite (Fe3O4) nanoparticles. Sci Rep. 2017;7:7672.

18. Shaban M, Ashraf AM, Abukhadra MR. TiO2 nanoribbons/carbon nanotubes composite with enhanced photocatalytic activity; fabrication, characterization, and application. Sci Rep. 2018;8:1–17.

19. Zulfiqar M, Chowdhury S, Sufian S, Omar AA. Enhanced photocatalytic activity of Orange II in aqueous solution using solvent-based TiO2 nanotubes: kinetic, equilibrium and thermodynamic studies. J Clean Prod. 2018;203:848–59.

20. Alias SS, Harun Z, Azhar FH, Ibrahim SA, Johar B. Comparison between commercial and synthesised nano flower-like rutile TiO2 immobilised on green super adsorbent towards dye wastewater treatment. J Clean Prod. 2020;251:119448.

21. Faisal M, Tariq MA, Muneer M. Photocatalysed degradation of two selected dyes in UV-irradiated aqueous suspensions of titania. Dye Pigment. 2007;72:233–9.

22. Chen CC, Lu CS, Chung YC, Jan JL. UV light induced photodegradation of malachite green on TiO2 nanoparticles. J Hazard Mater. 2007;141:520–8.

23. Saquib M, Muneer M. Titanium dioxide mediated photocatalyzed degradation of a textile dye derivative, acid orange 8, in aqueous suspensions. Desalination. 2003;155:255–63.

24. Woan K, Pyrgiotakis G, Sigmund W. Photocatalytic carbon-nanotube–TiO2 composites. Adv Mater. 2009;21:2233–9.

25. Zang L, Macyk W, Lange C, Maier WF, Antonius C, Meissner D, et al. Visible-light detoxification and charge generation by transition metal chloride modified titania. Chem Eur J. 2000;6:379–84.

26. Kelly KL, Coronado E, Zhao LL, Schatz GC. The optical properties of metal nanoparticles: the influence of size, shape, and dielectric environment. J. Phys. Chem. B. ACS Publications; 2003. p. 668–77.

27. Méndez-Medrano MG, Kowalska E, Lehoux A, Herissan A, Ohtani B, Bahena D, et al. Surface modification of TiO2 with Ag nanoparticles and CuO nanoclusters for application in photocatalysis. J Phys Chem C. 2016;120:5143–54.

28. Sato Y, Naya S, Tada H. A new bimetallic plasmonic photocatalyst consisting of gold (core)-copper (shell) nanoparticle and titanium (IV) oxide support. APL Mater. 2015;3.

29. Wongwisate P, Chavadej S, Gulari E, Sreethawong T, Rangsunvigit P. Effects of monometallic and bimetallic Au–Ag supported on sol–gel TiO2 on photocatalytic degradation of 4-chlorophenol and its intermediates. Desalination. 2011;272:154–63.

30. Ismail AA, Bahnemann DW, Al-Sayari SA. Synthesis and photocatalytic properties of nanocrystalline Au, Pd and Pt photodeposited onto mesoporous RuO2-TiO2 nanocomposites. Appl Catal A Gen [Internet]. 2012;431–432:62–8. Available from: https://www.sciencedirect.com/science/article/pii/S0926860X12002256

31. Pascucci B, Otero GS, Belelli PG, Illas F, Branda MM. Comparative density functional theory based study of the reactivity of Cu, Ag, and Au nanoparticles and of (111) surfaces toward CO oxidation and NO 2 reduction. J Mol Model. 2014;20:1–11.

32. Chen J-J, Wang W-K, Li W-W, Pei D-N, Yu H-Q. Roles of crystal surface in Pt-loaded titania for photocatalytic conversion of organic pollutants: a first-principle theoretical calculation. ACS Appl Mater Interfaces. 2015;7:12671–8.

33. Khan SA, Arshad Z, Shahid S, Arshad I, Rizwan K, Sher M, et al. Synthesis of TiO2/Graphene oxide nanocomposites for their enhanced photocatalytic activity against methylene blue dye and ciprofloxacin. Compos Part B Eng. 2019;175:107120.

34. Gonçalves BS, Palhares HG, Souza TCC de, Castro VG de, Silva GG, Silva BC, et al. Effect of the carbon loading on the structural and photocatalytic properties of reduced graphene oxide-TiO2 nanocomposites prepared by hydrothermal synthesis. J Mater Res Technol [Internet]. 2019;8:6262–74. Available from: https://www.sciencedirect.com/science/article/pii/S2238785419302613

35. Jain P, Kumar A, Verma N, Gupta RK. In-situ synthesis of TiO2 nanoparticles in ACF: Photocatalytic degradation under continuous flow. Sol Energy [Internet]. 2019;189:35–44.

Available from: https://www.sciencedirect.com/science/article/pii/S0038092X19307042

36. Zhou Y, Cheng X, Tynan B, Sha Z, Huang F, Islam MS, et al. High-performance hierarchical MnO2/CNT electrode for multifunctional supercapacitors. Carbon N Y [Internet]. 2021;184:504–13. Available from: https://www.sciencedirect.com/science/article/pii/S0008622321008435

37. Ali S, Razzaq A, Kim H, In S-I. Activity, selectivity, and stability of earth-abundant CuO/Cu2O/Cu0-based photocatalysts toward CO2 reduction. Chem Eng J. 2022;429:131579.

38. Vasilaki E, Georgaki I, Vernardou D, Vamvakaki M, Katsarakis N. Ag-loaded TiO 2 /reduced graphene oxide nanocomposites for enhanced visible-light photocatalytic activity. Appl Surf Sci [Internet]. 2015;353:865–72. Available from: http://dx.doi.org/10.1016/j.apsusc.2015.07.056

39. Yang H. A short review on heterojunction photocatalysts: Carrier transfer behavior and photocatalytic mechanisms. Mater Res Bull. 2021;142:111406.

40. Saleem H, Habib A. Study of band gap reduction of TiO2 thin films with variation in GO contents and use of TiO2/Graphene composite in hybrid solar cell. J Alloys Compd. 2016;679:177–83.

41. Zou F, Hu J, Miao W, Shen Y, Ding J, Jing X. Synthesis and characterization of enhanced photocatalytic activity with Li+-doping nanosized TiO2 catalyst. ACS omega. 2020;5:28510–6.

42. Zhang Z, Yang W, Zou X, Xu F, Wang X, Zhang B, et al. One-pot, solvothermal synthesis of TiO2–graphene composite nanosheets. J Colloid Interface Sci. 2012;386:198–204.

43. Yadav HM, Kim J-S. Solvothermal synthesis of anatase TiO2-graphene oxide nanocomposites and their photocatalytic performance. J Alloys Compd. 2016;688:123–9.

44. Li G, Huang J, Chen J, Deng Z, Huang Q, Liu Z, et al. Highly active photocatalyst of Cu2O/TiO2 octahedron for hydrogen generation. ACS omega. 2019;4:3392–7.

45. Fan Y, Lu H-T, Liu J-H, Yang C-P, Jing Q-S, Zhang Y-X, et al. Hydrothermal preparation and electrochemical sensing properties of TiO2–graphene nanocomposite. Colloids Surfaces B Biointerfaces. 2011;83:78–82.

46. Najafi M, Kermanpur A, Rahimipour MR, Najafizadeh A. Effect of TiO2 morphology on structure of TiO2-graphene oxide nanocomposite synthesized via a one-step hydrothermal method. J Alloys Compd. 2017;722:272–7.

47. Zhang D, Pu X, Ding G, Shao X, Gao Y, Liu J, et al. Two-phase hydrothermal synthesis of TiO2–graphene hybrids with improved photocatalytic activity. J Alloys Compd. 2013;572:199–204.

48. Li W, Liang R, Zhou NY, Pan Z. Carbon black-doped anatase TiO2 nanorods for solar light-induced photocatalytic degradation of methylene blue. ACS omega. 2020;5:10042–51.

49. Khalid NR, Ahmed E, Hong Z, Ahmad M, Zhang Y, Khalid S. Cu-doped TiO2 nanoparticles/graphene composites for efficient visible-light photocatalysis. Ceram Int. 2013;39:7107–13.

50. Ren Y, Sun C, Li K, Wang L, Song M. Preparation of TiO2–reduced graphene oxide–Pd nanocomposites for phenol photocatalytic degradation. Ceram Int. 2016;42:1339–44.

51. Krithiga T, Sathish S, Renita AA, Prabu D, Lokesh S, Geetha R, et al. Persistent organic pollutants in water resources: Fate, occurrence, characterization and risk analysis. Sci Total Environ. 2022;831:154808.

52. Nagata Y, Nakagawa M, Okuno H, Mizukoshi Y, Yim B, Maeda Y. Sonochemical degradation of chlorophenols in water. Ultrason Sonochem. 2000;7:115–20.

53. Song S, Fan J, He Z, Zhan L, Liu Z, Chen J, et al. Electrochemical degradation of azo dye CI Reactive Red 195 by anodic oxidation on Ti/SnO2–Sb/PbO2 electrodes. Electrochim Acta. 2010;55:3606–13.

54. Kurniawan TA, Lo WH, Sillanpää MET. Treatment of contaminated water laden with 4-chlorophenol using coconut shell waste-based activated carbon modified with chemical agents. Sep Sci Technol. 2011;46:460–72.

55. Yanyan L, Kurniawan TA, Zhu M, Ouyang T, Avtar R, Othman MHD, et al. Removal of acetaminophen from synthetic wastewater in a fixed-bed column adsorption using low-cost coconut shell waste pretreated with NaOH, HNO3, ozone, and/or chitosan. J Environ Manage. 2018;226:365–76.

56. Wu J-S, Liu C-H, Chu KH, Suen S-Y. Removal of cationic dye methyl violet 2B from water by cation exchange membranes. J Memb Sci. 2008;309:239–45.

57. Eskelinen K, Särkkä H, Kurniawan TA, Sillanpää MET. Removal of recalcitrant contaminants from bleaching effluents in pulp and paper mills using ultrasonic irradiation and Fenton-like oxidation, electrochemical treatment, and/or chemical precipitation: a comparative study. Desalination. 2010;255:179–87.

58. Barakat MA, Anjum M, Kumar R, Alafif ZO, Oves M, Ansari MO. Design of ternary Ni(OH)2/graphene oxide/TiO2 nanocomposite for enhanced photocatalytic degradation of organic, microbial contaminants, and aerobic digestion of dairy wastewater. J Clean Prod. 2020;258.

59. Moonsiri M, Rangsunvigit P, Chavadej S, Gulari E. Effects of Pt and Ag on the photocatalytic degradation of 4-chlorophenol and its by-products. Chem Eng J. 2004;97:241–8.

60. Qi HP, Wang HL, Zhao DY, Jiang WF. Preparation and photocatalytic activity of Ag-modified GO-TiO 2 mesocrystals under visible light irradiation [Internet]. Appl. Surf. Sci. Elsevier B.V; 2019. Available from: https://doi.org/10.1016/j.apsusc.2019.02.194

61. Barber J. Photosynthetic energy conversion: natural and artificial. Chem Soc Rev. 2009;38:185–96.

62. Armaroli N, Balzani V. The future of energy supply: challenges and opportunities. Angew Chemie Int Ed. 2007;46:52–66.

63. Hussain A, Arif SM, Aslam M. Emerging renewable and sustainable energy technologies: State of the art. Renew Sustain energy Rev. 2017;71:12–28.

64. Kozlova EA, Parmon VN. Heterogeneous semiconductor photocatalysts for hydrogen production from aqueous solutions of electron donors. Russ Chem Rev. 2017;86:870.

65. Nikolaidis P, Poullikkas A. A comparative overview of hydrogen production processes. Renew Sustain energy Rev. 2017;67:597–611.

66. Zhou P, Zhang Q, Chao Y, Wang L, Li Y, Chen H, et al. Partially reduced Pd single atoms on CdS nanorods enable photocatalytic reforming of ethanol into high value-added multicarbon compound. Chem. 2021;7:1033–49.

67. Yang L, Fan C, Zhang J, Zhang F, Li R, Yi S, et al. Poly (acrylic acid)-modified silica nanoparticles as a nonmetal catalyst for NaBH4 methanolysis. Int J Hydrogen Energy. 2021;46:23236–44.

68. Zhang L, Jiang D, Irfan RM, Tang S, Chen X, Du P. Highly efficient and selective photocatalytic dehydrogenation of benzyl alcohol for simultaneous hydrogen and benzaldehyde production over Ni-decorated Zn0.5Cd0.5S solid solution. J Energy Chem [Internet]. 2019;30:71–7. Available from: https://www.sciencedirect.com/science/article/pii/S2095495618301591

69. Tkachenko P, Volchek V, Kurenkova A, Gerasimov E, Popovetskiy P, Asanov I, et al. Photocatalytic H2 generation from ethanol and glucose aqueous solutions by PtOx/TiO2 composites. Int J Hydrogen Energy [Internet]. 2023;48:22366–78. Available from: https://www.sciencedirect.com/science/article/pii/S0360319922055835

70. Liu J, Wan J, Liu L, Yang W, Low J, Gao X, et al. Synergistic effect of oxygen defect and doping engineering on S-scheme O-ZnIn2S4/TiO2-x heterojunction for effective photocatalytic hydrogen production by water reduction coupled with oxidative dehydrogenation. Chem Eng J [Internet]. 2022;430:133125. Available from: https://www.sciencedirect.com/science/article/pii/S138589472104701X

71. Zou J, Zhou W, Huang L, Guo B, Yang C, Hou Y, et al. Photocatalytic H2 evolution integrated with selective amines oxidation promoted by NiS2 decorated CdS nanosheets. J Catal. 2021;400:347–54.

72. Zhu X, Jin C, Li X-S, Liu J-L, Sun Z-G, Shi C, et al. Photocatalytic formaldehyde oxidation over plasmonic Au/TiO2 under visible light: moisture indispensability and light enhancement. ACS Catal. 2017;7:6514–24.

73. Bamwenda GR, Tsubota S, Nakamura T, Haruta M. Photoassisted hydrogen production from a water-ethanol solution: a comparison of activities of Au□ TiO2 and Pt□ TiO2. J Photochem Photobiol A Chem. 1995;89:177–89.

74. Zhang Y, Zhang Y, Li X, Zhao X, Anning C, Crittenden J, et al. Photocatalytic water splitting of ternary graphene-like photocatalyst for the photocatalytic hydrogen production. Front Environ Sci Eng. 2020;14:1–13.

75. Rather RA, Singh S, Pal B. A Cu+1/Cu0-TiO2 mesoporous nanocomposite exhibits improved H2 production from H2O under direct solar irradiation. J Catal [Internet]. 2017;346:1–9. Available from: https://www.sciencedirect.com/science/article/pii/S0021951716302755

76. Rather RA, Singh S, Pal B. Core–shell morphology of Au-TiO2@ graphene oxide nanocomposite exhibiting enhanced hydrogen production from water. J Ind Eng Chem. 2016;37:288–94.

CHAPTER- 2

Photocatalytic Degradation of Piroxicam-20 and Methanol Dehydrogenation using Graphene Oxide-modified Ag-TiO_2 under light irradiation

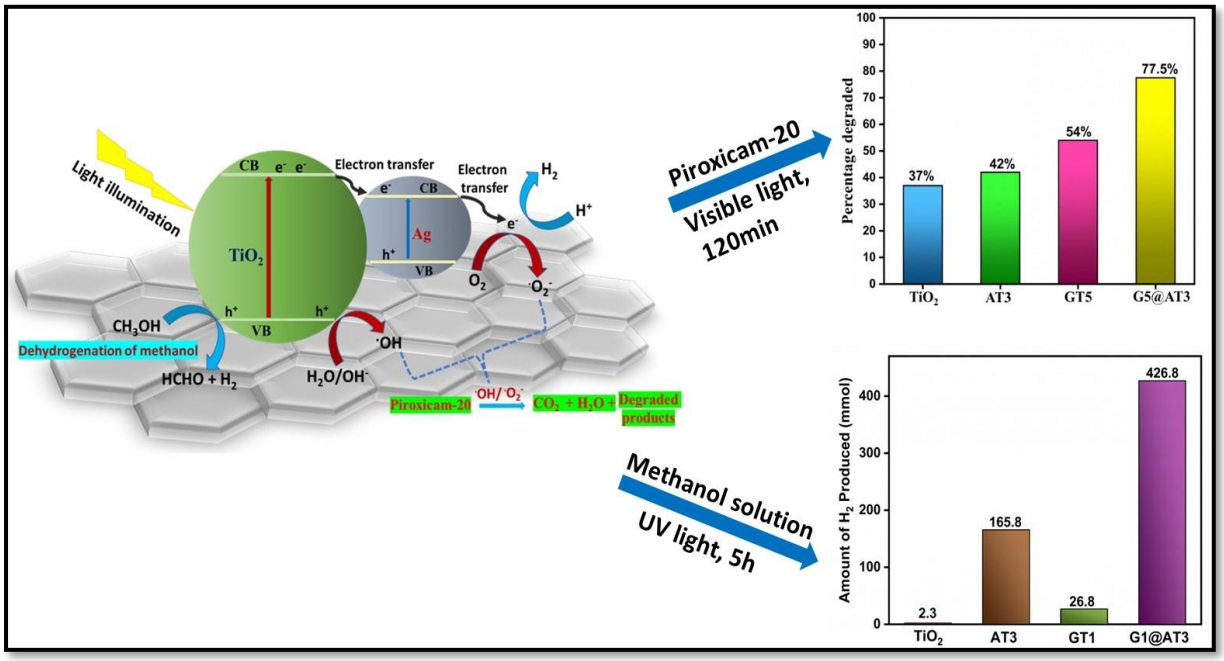

Schematic outline:

This study investigated the impact of graphene oxide (GO) at varying amounts (1-5 wt%) on TiO_2 and Ag (3 wt%)-doped TiO_2 (AT3) photocatalysts for piroxicam-20 degradation and methanol dehydrogenation. The GO(5wt%)@Ag(3wt%)-TiO_2 (G5@AT3) composite achieved the highest photodegradation efficiency (78%) under visible light. Conversely, GO(1wt%)@Ag(3wt%)-TiO_2 (G1@AT3) produced the most hydrogen (427 mmol) from methanol dehydrogenation under UV light, outperforming other composites and pure TiO_2. HRMS analysis was used to identify degradation intermediates. The results highlight the enhanced photocatalytic performance of TiO_2 with combined Ag and GO loading under both UV and visible light.

2.1 Introduction

Graphene oxide (GO), a widely used graphitic substance, has received significant attention during the past few years. It is a graphene aromatic lattice containing alcohols, epoxides, carboxylic groups, and ketone carbonyls. Functional groups containing oxygen on their surface make them hydrophilic and a good option for supporting metal oxide-based semiconductors [1,2]. For a variety of applications, GO displayed superior optical, electronic, and catalytic properties[3,4]; hence, GO-based materials have been widely reported for the photodegradation of various organic pollutants present in waste effluent[5–8]. Different antibiotic residue levels with associated harmful effects on aquatic and terrestrial organisms have been found in pharmaceutical and agricultural effluents[9]. Medications including piroxicam, diclofenac, naproxen, and ibuprofen fall under Nonsteroidal anti-inflammatory medicines (NSAIDs)[10–12]. NSAIDs are of particular importance among the different pharmacological families due to their enormous consumption as they are given for numerous diseases. Numerous NSAIDs have been found in surface and subsurface water, wastewater effluents, and biological sludge[13,14]. The wastewater containing drug residues must be treated to prevent pharmaceuticals from entering the environment. Derikvandi et al. photo-catalytically degraded Metronidazole, one such water pollutant drug, with the help of clinoptilolite nanoparticles supported ZnO and NiO photocatalysts[15].

Another major growing issue is the massive amounts of alcoholic solvents that are often drained away after usage since they are a combination of several solvents. Various alcoholic solvents such as glycol, methanol, butanol, cyclohexanol, higher chain alcohols, and cyclic alcohols are used in chemical labs and various food, cosmetic, and fertilizer industries. The photocatalytic dehydrogenation of alcohols is a promising method for the conversion of alcoholic solvents into hydrogen, along with some useful organic products[16]. In this occurrence, there appears to be an ongoing research effort to develop effective visible-light photocatalysts with versatile properties achieved through various methods and material combinations, like loading semiconductors[17–20] with noble metals or carbon-based materials. Photocatalysis has emerged as a safe and affordable method to remove pollutants from water bodies[21–25]. In this process, a semiconductor material is exposed to light by a photon with an energy greater than the semiconductor's band gap energy. This produces electron-hole pairs on the surface of the catalyst, which can be used to reduce or oxidize organic molecules in aqueous solutions. The produced electrons and holes can also combine with water and dissolved oxygen to produce hydroxyl and superoxide radicals, respectively, which are

potent oxidizing agents capable of attacking contaminants and converting them to smaller fragments and, eventually, to CO_2 and H_2O[26]. Rather et al. coated a thin GO shell over the Au-TiO_2 core, and it displayed better H_2 productivity from water than from a bare metal-TiO_2 catalyst[27]. Hunge et al. investigated the photocatalytic activity of GO/TiO_2 composite for salicylic acid degradation under sunlight, which showed higher photodecomposition activity (57%) than bare TiO_2[28]. Jing et al. synthesized different TiO_2/graphene oxide composites and compared the degradation of quinoline under visible light illumination and found that in many instances, the TiO_2/graphene oxide composite exhibited a 6.17 times higher photodegradation rate than bare P25-TiO_2[29]. Ghattavi et al. synthesised AgBr/g-C_3N_4 catalyst to photocatalytically degraded methyl orange (MO) dye. The carbon-based g-C_3N_4 increased the charge transfer between the composite, which significantly decreased the electron-hole recombination rate, suggesting the importance of g-C_3N_4 in photocatalytic degradation of the MO[30].

To make metal oxide-based semiconductors like TiO_2, ZnO, WO_3, SnO_2, etc., visible light active, many potential approaches are being investigated, which include loading with noble or transition metals[31–33], coupling it with other semiconductors[34,35] or carbon-based materials[36] or making ternary heterojunction composites[37,38] for enhancing their photocatalytic activity under visible/ sunlight. Noble metal nanoparticles (Au, Ag, Pt) absorb visible light strongly due to their surface plasmon resonance (SPR), whereby the electric field of visible light causes a collective oscillation in their conducting electrons, which helps in the separation of photoinduced e^-/h^+ pairs generated on the semiconductor surface and to make semiconductor as visible light active photocatalyst[39–42]. It was observed that many transition metals undergo oxidation/corrosion process, which retards the photo-efficiency of the semiconductor. Metal-TiO_2 stability can be improved by introducing noble metals, and its photocatalytic capabilities can be further improved by loading it with carbon-rich material.

In the past, many studies have been done using Ag-TiO_2, GO-TiO_2, and GO@Ag-TiO_2 for the photocatalytic degradation of pollutants under UV/visible /sunlight. However, very rare studies have been reported for hydrogen production from alcohols using these catalysts and showing both the photocatalytic properties together i.e. oxidative (photodegradation) and reductive (alcohol dehydrogenation) using the same catalyst. In this article, we have synthesized a ternary heterojunction composite to study both the photocatalytic properties under different light sources. The research aimed to tune the photocatalytic oxidative and reductive activity of TiO_2 by modifying its band energetics and surface structural property with GO & Ag loading to make

different ternary (GO@Ag-TiO_2) heterostructure composites. Secondly, the formation of different hybrid interfaces (Ag-TiO_2, GO-TiO_2)in this structure led to an improvement in the photoexcited charge separation efficiency resulting in better photocatalytic activity of this ternary composite. This work demonstrated the influence of different amounts (1-5 wt%) of GO loading and 3 wt% Ag photo deposition over the TiO_2 surface on the photocatalytic properties of GO@TiO_2, Ag@TiO_2, and GO@Ag-TiO_2 hybrid nanocomposite under light irradiation. Modifying the surface of Ag-TiO_2 with GO induced light-responsive photocatalytic activity which helped in the photodegradation of piroxicam-20 drug under visible light and methanol dehydrogenation under UV light.

2.2 Experimental Section

2.2.1 Materials and reagents

Silver nitrate, Graphite powder, potassium permanganate, and sodium nitrate were obtained from Sigma Aldrich, India. Piroxicam-20 drug tablet (Kivonyx Healthcare Pvt. Ltd.) was purchased from the local drugstore. The distillation unit present in our department (Milli-Q, Millipore) provided the distilled water (DI). Degussa Corporation from Germany provided commercial TiO_2 (P25) as a token of gift. All chemicals were utilised without any additional purification.

2.2.2 Synthesis of Graphene oxide (GO)

The GO from graphite powder was prepared using a modified Hummer's method[28]. Firstly, 1g mixture of $NaNO_3$ and graphite powder (1:1) was mixed in the conical flask, followed by the addition of H_2SO_4 (23 ml) and stirred for 3h (~20 $^{\circ}$C). After that, $KMnO_4$ (3g) was added gently, and the mixture solution was constantly agitated around ~20 $^{\circ}$C for 2h. Distilled water (46ml) was slowly poured into the above-mentioned solution and further stirred at 98° C for 2 h. 100 ml water was added to the above solution, and H_2O_2 (10 ml) was added after 5 mins. The resultant black-brown coloured mixture was centrifuged @7500rpm, 10 mins with HCl and DI water three to four times, and the obtained product was dried for 12 h at 55 $^{\circ}$C.

2.2.3 Synthesis of Ag(3wt%)-TiO_2

The photodeposition method was applied to deposit Ag (3wt%) over TiO_2[43]. In a typical procedure, 100 mg TiO_2 powder was dispersed in 50 vol% (5 ml isopropyl alcohol: 5 ml DI water), after which $AgNO_3$ solution (0.01M, 2790µL) was added into the test tube. After that,

the above-mentioned test tube was purged by Argon gas, sealed using rubber septa, and placed under UV light (mercury arc lamp) with constant stirring for 2h. The resultant solution was washed with DI water and ethanol after centrifuging at @6000 rpm and dried at 70 ˚C for 4-5 h. The resultant sample has been abbreviated as AT3.

2.2.4 Synthesis of GO-TiO_2 / GO@Ag-TiO_2

The GT/ G@AT3 composite was synthesized using the ultrasonication method with slight modification. Different amount of GO (2,6,10 mg for 1,3,5wt% respectively) was dispersed in a 2:1 mixture solution of (DI water (20 ml) and ethanol (10 ml), and ultrasonication was used to exfoliate the mixture for 2h. P25 TiO_2 powder (200 mg) was taken (for GO-TiO_2 composite) / 200 mg Ag-TiO_2 (for GO@Ag-TiO_2 composite) to the sonicated GO solution and magnetically stirred at room temperature for 6h to achieve a uniform suspension. The final composite was obtained, recovered by filtering, washed three to four times with DI water, and then dried for 12 h at 70 °C. GO(1,3,5wt%) deposition over TiO_2 has been abbreviated as GT1, GT3,GT5 respectively. Similarly for GO(1,3,5wt%) deposition over Ag (3wt%)-TiO_2 has been abbreviated as G1@AT3, G3@AT3, G5@AT3 respectively.

2.2.5 Characterization

X-ray Diffraction (XRD) pattern was analyzed with the help of Panalytical X'Pert PRO with Cu Kα (λ=1.540Å) scan rate of 10 min^{-1}. The surface morphology was studied with the help of Field Emission Scanning Electron Microscopy (FE-SEM, JEOLJSM-7600F) and furthermore, analysis was conducted using High-Resolution Transmission Electron Microscopy (HRTEM, JEOL JEM-2100 model). Raman spectroscopy was characterised by LabRam HR 124 Evolution Raman microscope with 532 nm excitation wavelength. Shimadzu UV-2600 spectrophotometer was used for measuring the change in concentration value of piroxicam-20 at an absorbance of 355nm. The oxidation state of different elements present was determined using XPS (X-ray photoelectron spectroscopy). The optical absorption of prepared composites was examined with Avantes, Diffuse reflectance spectrophotometer (DRS). Using a PL-spectrophotometer (RF-5301), photoluminescence investigations were carried out at an excitation wavelength of 320 nm. The intermediates and degradation products were analysed using the HRMS (High-resolution mass spectroscopy) on Waters, QTOF mass spectrometer with UPLC (XEVO G2 XS). The hydrogen produced during the photocatalytic dehydrogenation of methanol was measured with the help of NUCON, Gas chromatograph with argon gas as a carrier, and a molecular sieve (5X A column) with thermal conductivity

detector (TCD). The column, detector, and injector temperatures were set at 40 °C, 50 °C, and 40 °C, respectively.

2.2.6 Photocatalytic study

2.2.6.1 Photocatalytic degradation of piroxicam-20

The photocatalytic activity of all composites was studied for the degradation of piroxicam-20 drug (2 mM) under visible light (50W LED lamp). For preparing a stock solution of 2 mM piroxicam-20, firstly, the tablet was crushed using a mortar pestle and 33 mg of drug powder was added into the 50 ml DI water and shaken a few times to dissolve it and filtered in a volumetric flask. Briefly, 5mg of catalyst was added in 10 ml piroxicam-20 solution in a test tube. Before light illumination, the reaction mixture was placed and stirred under the dark for 30 min to attain adsorption-desorption equilibrium. The visible (LED) lamp was then turned on to study the photodegradation over different time intervals. Supernatants of the suspension were periodically collected from the test tube, the photocatalyst was removed using centrifugation, and the sample's absorbance spectrum was measured by a UV-visible spectrophotometer at 355 nm to assess the change in absorbance. The photocatalytic degradation efficiency(%) of drug removal was calculated by using the following equation:

$$\eta = \left(\frac{C_0 - C_t}{C_0}\right) \times \mathbf{100}(\%) \qquad \text{(equation no. 2.1)}$$

where η is the photocatalytic efficiency, C_0 is the initial concentration of piroxicam, and C_t is the concentration of piroxicam after 't' minutes under visible light irradiation.

2.2.6.2 Photocatalytic dehydrogenation of methanol

Further, the prepared GO and Ag-loaded TiO_2 nanocomposites were studied for the photocatalytic dehydrogenation of methanol. 50 mg of the catalyst was taken in 10 ml of methanol solution (50 vol%) in argon purged sealed test tube and placed under a UV lamp for 5h. A gas-confined syringe was used to inject 1 ml of gas produced into the injector port. Gas chromatography was used to determine the amount of H_2 produced during the process. The GC chromatograms were measured against a standard of 500 PPM Hydrogen.

2.3 Results and Discussion

2.3.1 Crystallographic, structural and surface morphological studies

The XRD pattern of the prepared composites is shown in **Fig.2.1(a)**. The high-intensity peak was observed at 2θ =10.5°, corresponding to the characteristic lattice plane (002) for graphene oxide (GO) and another peak at 42.1° with lattice plane (101) confirming the formation of GO(as shown in **Fig.2.1(b)**). The lattice plane (101), (004), (200), (105), (211), (204), (116), (220), (215) were crystalline plane of anatase TiO_2 (JCPDS card no. 21-1272) and lattice plane (110), (101), (111) corresponds to rutile form of TiO_2 (JCPDS Card No. 21- 154 1276). Upon loading of GO on TiO_2 (GT5) and Ag-TiO_2(G5@AT3), the diffraction peak corresponding to GO becomes significantly weaker or negligible due to the fact that both Ag and TiO_2 have a greater X-ray scattering coefficient compared to GO because of their higher atomic numbers. The existence of (111) and (200) in G5@AT3 indicates the presence of Ag NPs. For estimating the size of the G5@AT3 crystallites, the subsequent Scherer equation was applied[44,45]. The crystallite size of TiO_2, GT5, and G5@AT3 composite was calculated with an average size of 19.06, 19.23, and 19.45nm, respectively.

$$\mathbf{D = K .\lambda / \beta.\cos \theta} \qquad \text{(equation no. 2.2)}$$

Where D = crystallite size (nm), K = 0.9 (Scherrer constant), λ = 0.15406 nm (wavelength of the X-ray source Cu-Kα), β = FWHM (Full-width at half maximum), θ = the diffraction angle.

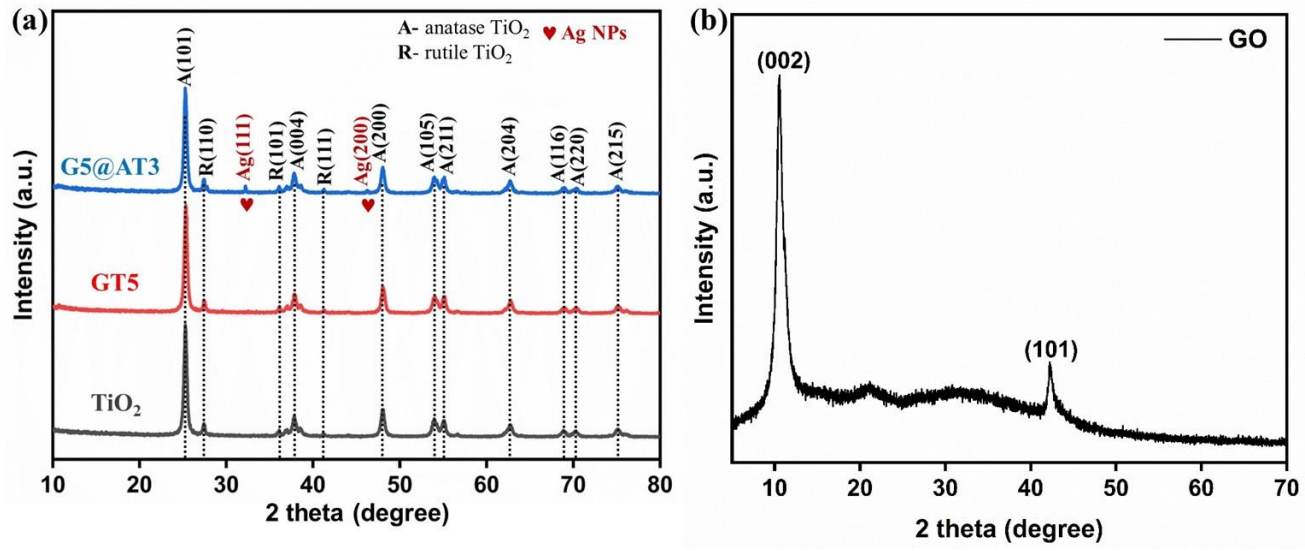

Fig.2.1: XRD diffraction patterns of (a) TiO_2, GT5, and G5@AT3 composites, (b) graphene oxide (GO).

FE-SEM was used to determine the morphology of prepared AT3, and G5@AT3 composites. It was seen in **Fig.2.2(a-b)** that GO exhibits wrinkled layered morphology with several stacked layers. In **Fig.2.2(c-d),** due to the low wt% deposition of Ag present in the AT3 composite, the

deposition of Ag on the TiO_2 surface was not visible. In **Fig.2.2(e-f)**, the Ag-TiO_2 was non-uniformly dispersed on the surface of GO layers. **Fig.2.3(a,b)** depicts the HRTEM analysis of the AT3 composite. The dark grey-coloured small spherical particles of Ag (highlighted by the red circle) were deposited on the light grey-coloured spheres of TiO_2 (circled in yellow) in **Fig.2.3(b)**. **Fig.2.3(c-e)** showed the non-uniform dispersion of Ag-TiO_2 onto the GO sheets in the G5@AT3 composite. The plane (111) was ascribed to a lattice fringe with a d-spacing of 0.23nm to Ag nanoparticles and a fringe with a lattice spacing of 0.349 nm assigned to the (101) crystal plane of TiO_2 deposited on the GO sheet.

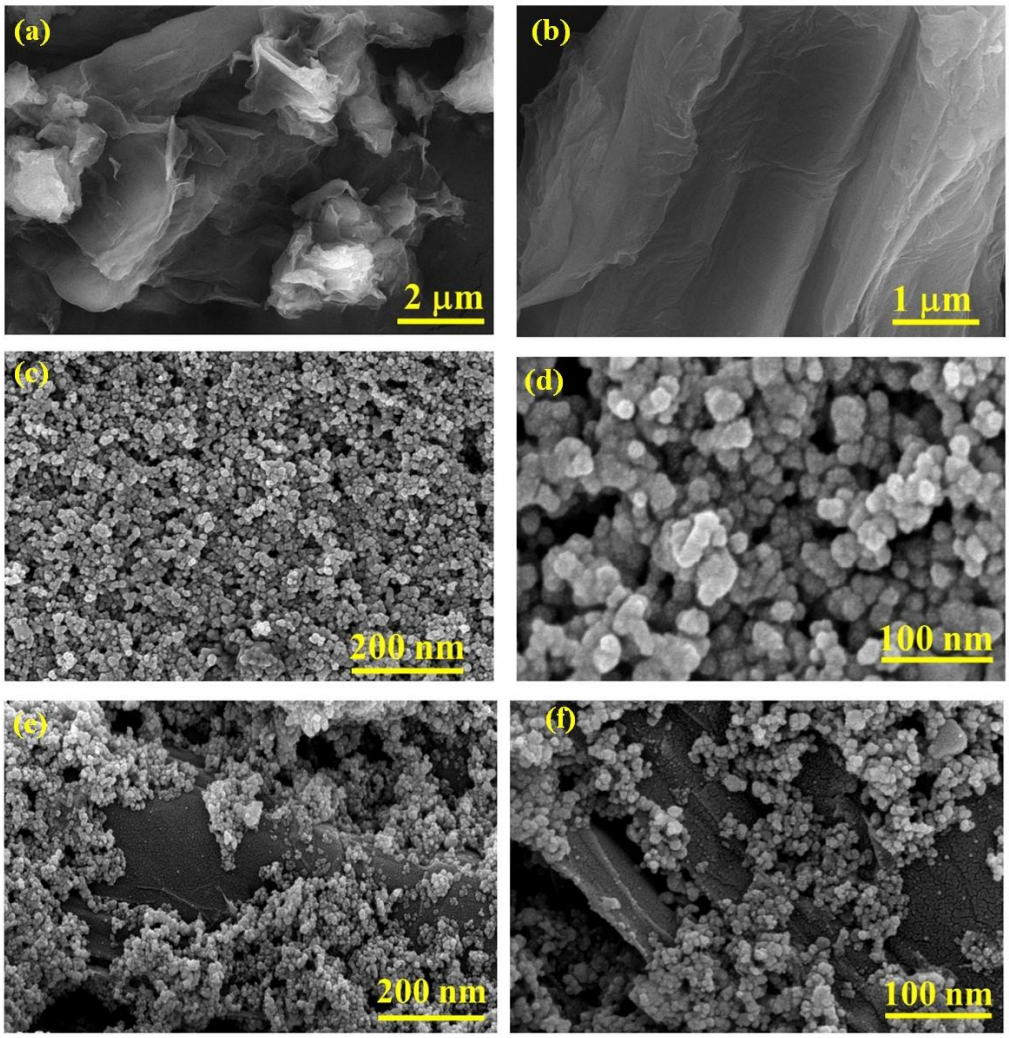

Fig.2.2: FE-SEM images of (a-b) GO sheets, (c-d) Ag(3wt%)-TiO_2 (AT3) and (e-f) GO(5wt%)loaded over Ag-TiO_2 (G5@AT3) composite.

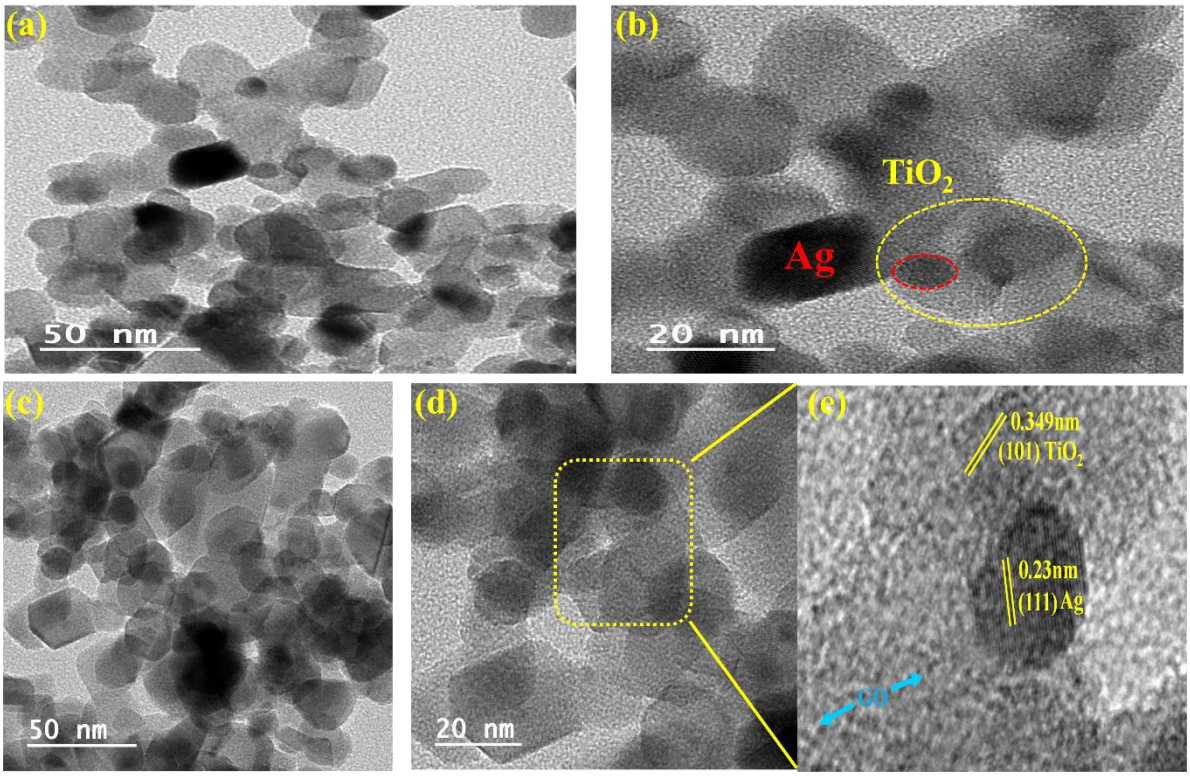

Fig.2.3: HRTEM images of (a-b) AT3 composite, (c-e) G5@AT3 composite at different nm scale; 50nm, 20 nm. In Fig.2.3(e), the inset corresponding lattice fringes are shown.

Raman spectra were collected and displayed to further understand the structure of the prepared samples. In **Fig.2.4**, prepared GT5 and G5@AT3 composites both displayed two peaks at 1347 and 1595 cm^{-1} owing to D & G bands of GO, respectively, which confirms the deposition of GO onto the TiO_2, Ag-TiO_2 surface[46]. The D band is found in disordered sp^2 carbon, whereas the G band, also known as the E_{2g} mode, is found due to the stretching of sp^2-hybridized C-C bonds. All the prepared samples displayed peaks at 146, 394, 515, and 635 cm^{-1} corresponding to E_g (O-Ti-O symmetric stretching), A_{1g} and E_g (O-Ti-O asymmetric stretching), B_{1g} (O-Ti-O wag), modes which were in accord with anatase TiO_2[47]. The GO peaks associated with the D and G bands appeared in the spectra which supports the deposition of GO over Ag-TiO_2 as seen in HRTEM images of G5@AT3 composite (figure 3). The D&G bands of GO and E_g, A_{1g}, B_{1g} modes of anatase TiO_2 were found in the Raman spectra, confirming the formation of GT5, and G5@AT3 composites.

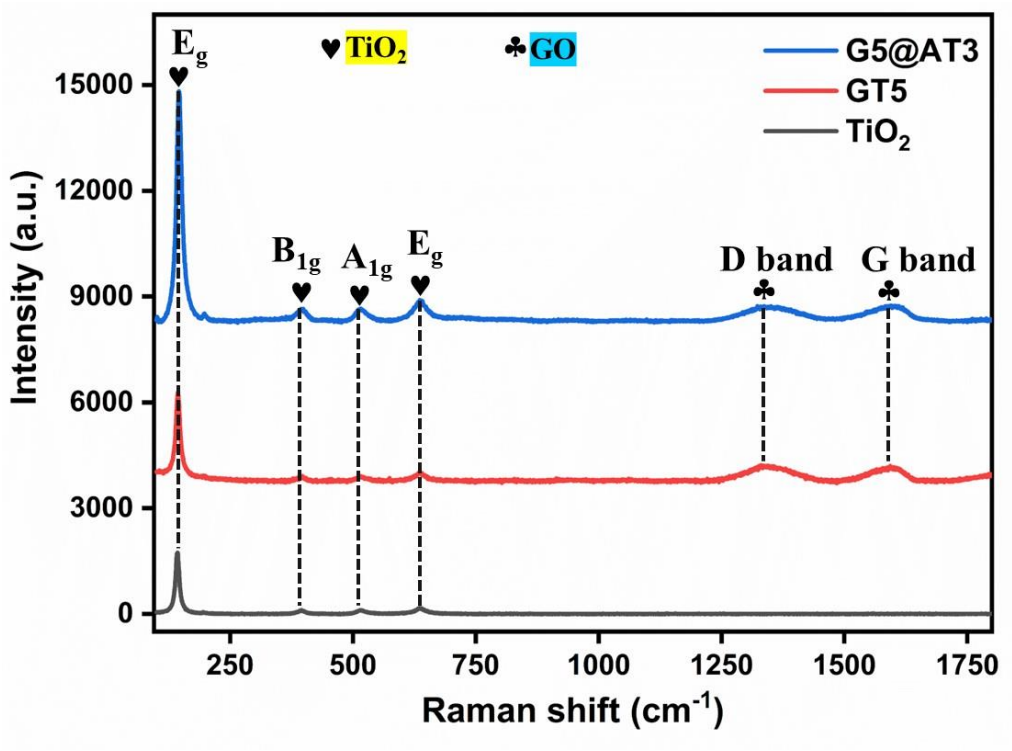

Fig.2.4: Raman Spectra of TiO_2, GT5, and G5@AT3 composites showing characteristic D and G bands for GO-loaded samples.

2.3.2 Optical studies

Photoluminescence (PL) is an efficient method for evaluating the charge transfer effect. To determine the recombination process of electron (e^-)-hole (h^+) pair, photoluminescence spectra were recorded. As shown in **Fig.2.5(a)**, all the GO(1,3,5) wt% loaded TiO_2 composites showed less intensity as compared to the bare TiO_2. Likewise, all GO loaded onto Ag-TiO_2 (different wt%)composites **Fig.2.5(b)** was also observed to have lower intensity than AT3, suggesting that the charge transfer effect of GO loaded@AT3 composite was faster than that of AT3. The reduced PL signal intensity could be associated with improved electrical conductivity due to GO and the induced SPR effect of plasmonic Ag NPs.

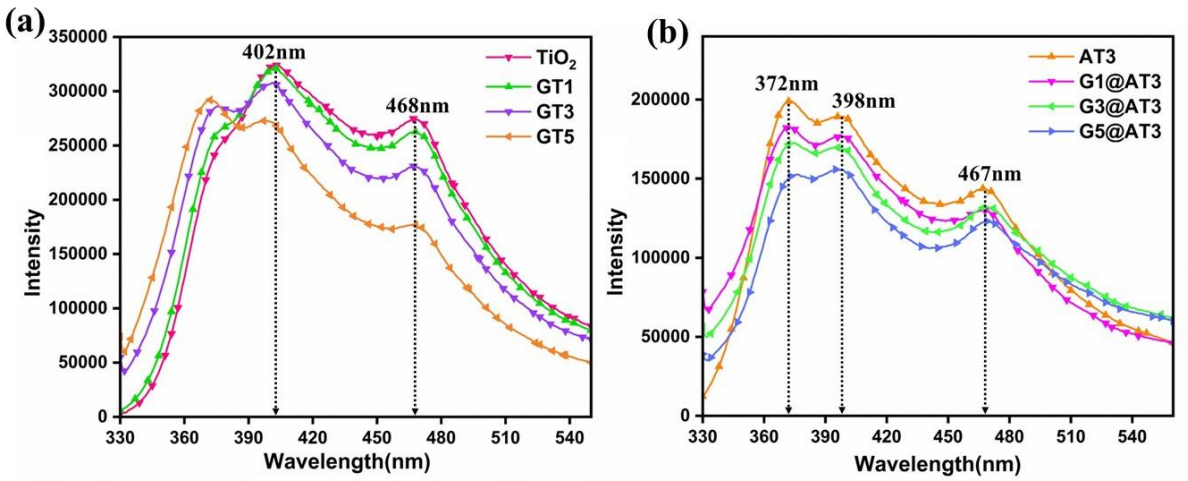

Fig.2.5: Photoluminescence spectra of (a) bare TiO_2, GO(x=1,3,5wt%) over TiO_2 and (b) AT3, GO(x=1,3,5wt%)@AT3 composites.

Fig.2.6(a) shows the UV-vis absorbance spectra of TiO_2 and different wt% loaded GO composites with TiO_2. Due to the interaction between GO and TiO_2, GT(1,3,5) wt% showed improved light absorption ability in the 400-800 nm region than bare TiO_2. In the case of AT3 and different wt% GO loaded Ag-TiO_2 composites **Fig.2.6(b)**, a broad absorption band around 400-600nm in the visible domain is observed which attributes the presence of Ag NPs in the composites. The Kubelka-Munk equation was applied to the DRS spectra using the following equation[48–50] and Tauc's plot ($(\alpha h\nu)^n$ *vs* $h\nu$) were drawn by extrapolating the linear part of the curve crossing the x-axis to calculate the bandgap energy of the synthesised composites:

$$\alpha h\nu = A(h\nu - E_g)^n \qquad \text{(equation no. 2.3)}$$

where α denotes the coefficient of absorption, h is Planck's constant, υ is light's frequency, A = constant, n= ½ , 2 (for allowed direct and indirect electronic transitions, respectively), and E_g denotes the energy of the bandgap. As shown in **Fig.2.7**, the E_g values were calculated for n= ½ (allowed direct transition) for bare TiO_2, GT5, and G5@AT3 and were found to be 3.2eV, 2.86 eV, and 2.67 eV, respectively. It is clear that the band gap value decreases for G5@AT3 significantly from 3.2 to 2.67 eV when Ag and GO are simultaneously added to TiO_2.

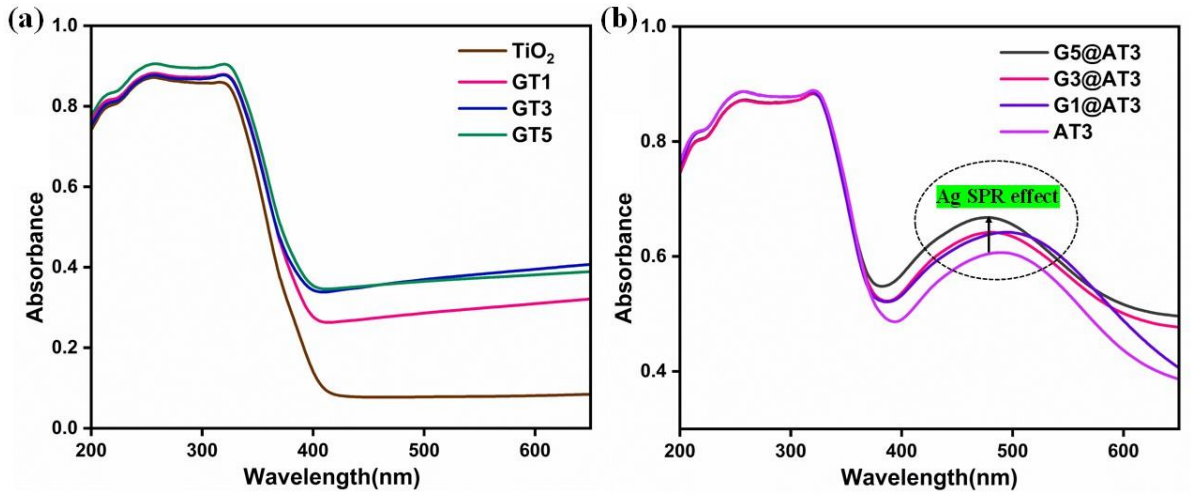

Fig.2.6: Diffuse reflectance spectra of (a) TiO_2, GO(x=1,3,5wt%) over TiO_2 and (b) AT3, GO(x=1,3,5wt%)@AT3 composites.

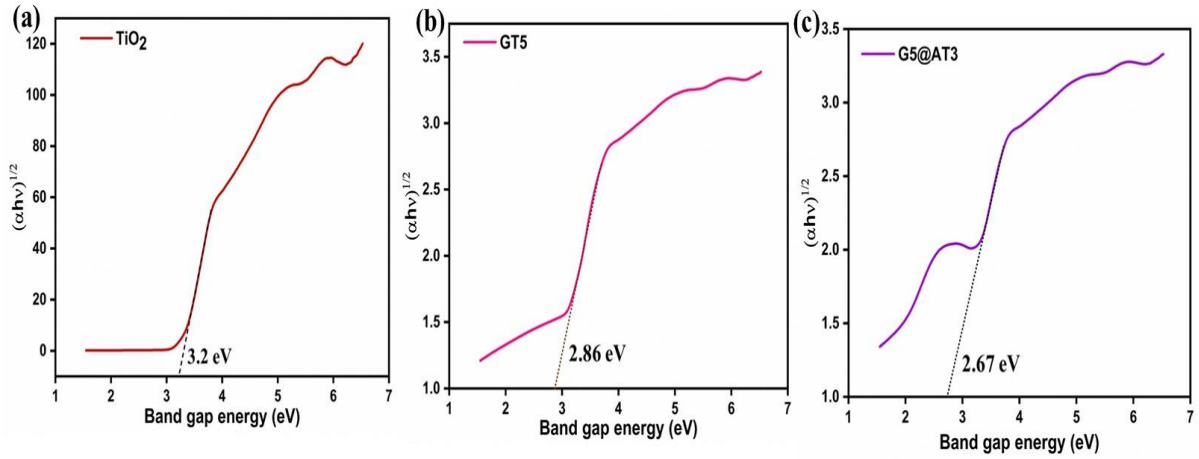

Fig.2.7: Tauc plots for allowed direct transition of prepared samples (a) TiO_2, (b) GT5 and (c) G5@AT3 composites.

XPS spectra were analyzed to determine the prepared composites' surface composition and elemental states. The XPS spectra **Fig.2.8(a)**, for Ag 3d of G5@AT3 composite, showed two binding energy peaks at 367.5eV($3d_{5/2}$) and 373.5eV ($3d_{3/2}$), and the difference in their peaks is 6eV which is characteristic for Ag in (0) oxidation state. The XPS spectra in **Fig.2.8(b)** for Ti 2p displayed peaks at 458.3 eV ($2p_{3/2}$) and 464eV ($2p_{1/2}$). It indicates the presence of Ti in (+4) because it agrees well with the typical binding energy of Ti in pure TiO_2. In O 1s spectra **Fig.2.8(c)**, the 529.6eV and 531eV peaks could be attributed to O^{2-}, C-O in TiO_2 lattice[47,51].

In **Fig.2.8(d)** XPS spectra of C 1s, the peaks at 284eV, 286eV, and 288eV were in perfect accord with C-C, C-O, and C=O, respectively.

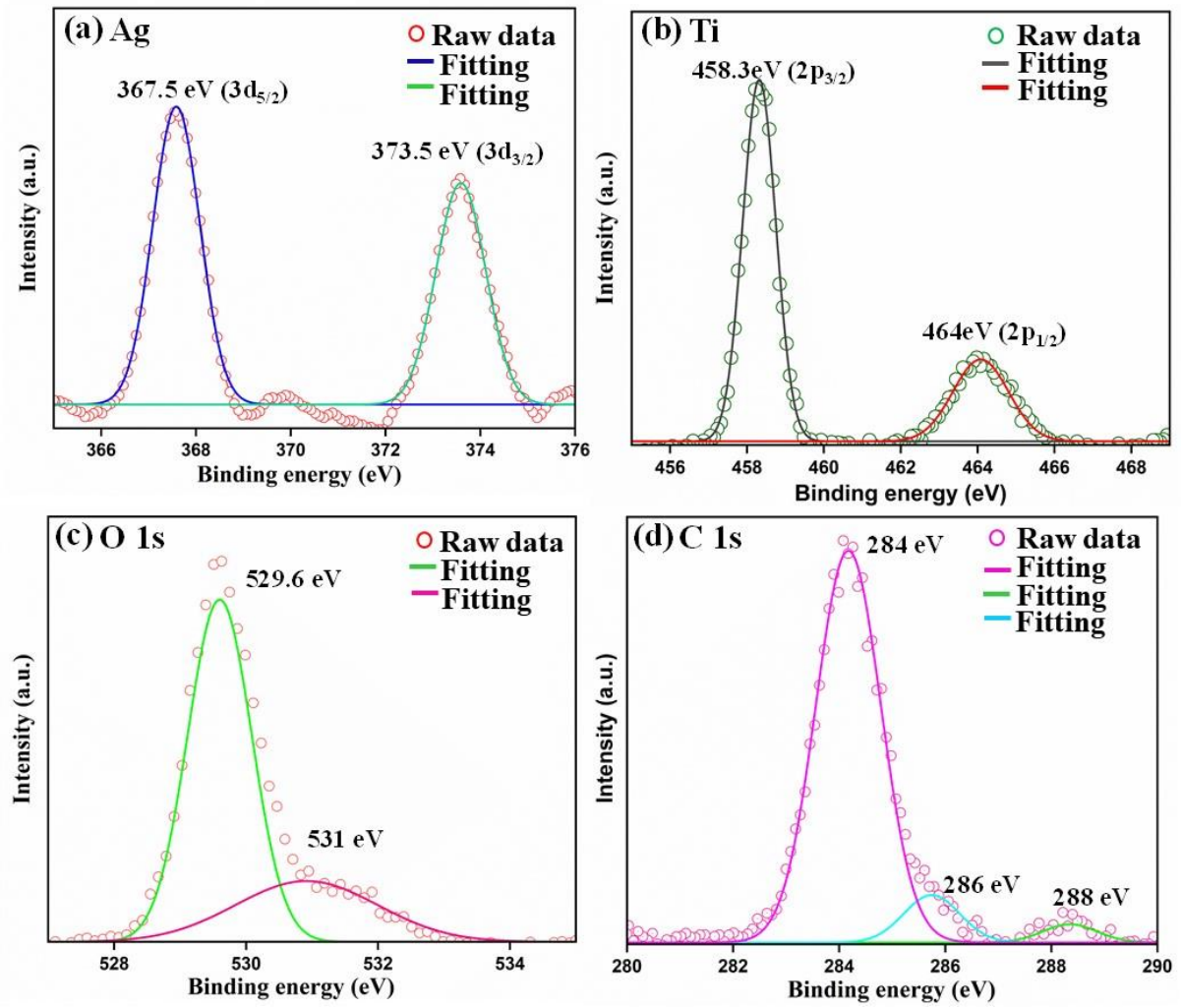

Fig.2.8: XPS spectra of prepared G5@AT3 composite: (a) Ag 3d, (b)Ti 2p, (c)O 1s, and (d) C 1s.

2.3.3 Photocatalytic activity

2.3.3.1 Photodegradation of piroxicam-20 drug

The photoactivity of the prepared composites was evaluated by monitoring the change in the absorbance peak intensity at λ_{max} = 355nm of piroxicam-20 drug under visible light. Under visible light, TiO_2 showed less photocatalytic activity (37%) (as shown in **Fig.2.9**) because of the wide band gap, however after photo-deposition of Ag(3wt%) nanoparticles onto TiO_2, owing to the SPR effect and sensitization of Ag, the AT3 composite showed its increased degradation efficiency (42%). After the addition of GO(5wt%) onto TiO_2, due to GO serving as an electron reservoir and transmission source, the prepared GT5 composite showed higher photoactivity (54%). The G5@AT3 catalyst showed the highest degradation efficiency (78%)

as compared to other catalysts (as shown in Table 2.1). The recorded absorbance spectra for the same can be seen in **Fig.2.10(a)** for 120 min. The possible reason for higher degradation efficiency could be due to the cooperative effect of Ag NPs, GO, and TiO_2 which played an important role in maximizing the photocatalytic activity. Under the same experimental conditions, the synthesized catalysts were placed in dark and visible light for 2h, and the percentage adsorbed (in dark) and removed (in light) were calculated in **Fig.2.10(b)& (c)**.

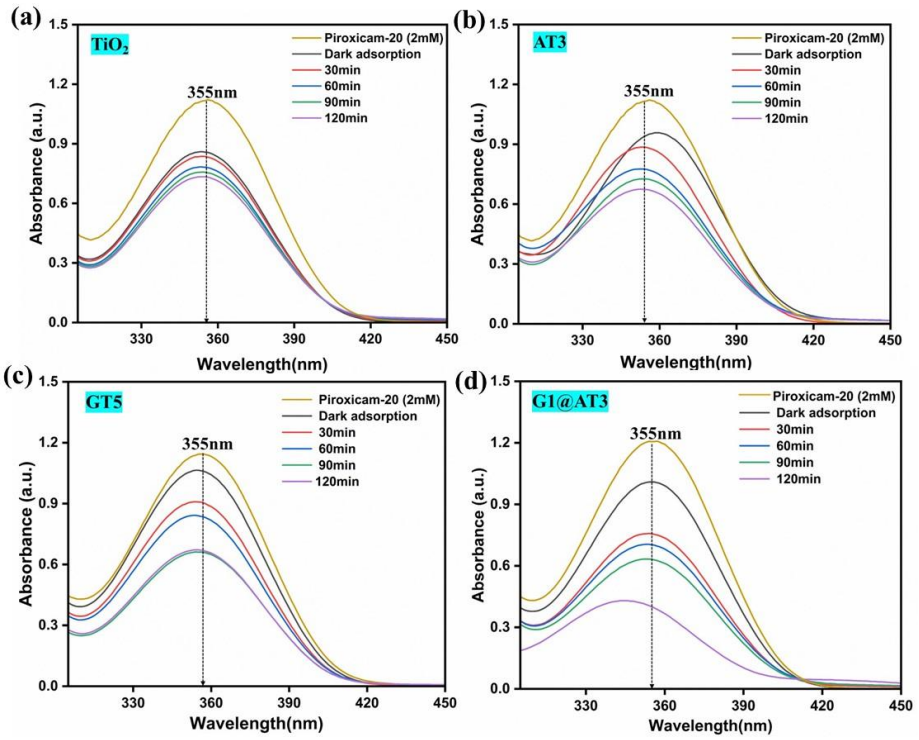

Fig.2.9: Changes in absorbance spectra of (2 mM) piroxicam-20 in the presence of different photocatalysts under visible light for 2 h.

The piroxicam-20 photocatalytic degradation rate was described using the pseudo-first-order reaction shown below:

$$\ln \frac{C_0}{C_t} = kt \qquad \text{(equation no. 2.4)}$$

where C_0 is the initial concentration of piroxicam-20 solution before light irradiation; C_t is the concentration of piroxicam-20 solution at time t, k = pseudo-first-order rate constant, and t is the experimental time. According to the Langmuir–Hinshelwood model, the photodegradation of pollutants occurred via pseudo-first-order kinetics; therefore, the rate constants of reactions (k) can be determined by analysing the slopes of the straight-line segment in the plots of $\ln(C_0/C_t)$ versus t, where t is a function of the experimental parameters that were

utilised[52,53]. As shown in **Fig.2.10(d)**, the linear graphs fit best in the pseudo-first-order kinetics equation with the rate constant values of 0.0034, 0.0041, 0.0048, 0.0082 min^{-1} for TiO_2, AT3, GT5, G5@AT3 respectively.

The electrical energy per order (E_{EO}) as a measure of the energy consumption efficiency for the photocatalytic process for the G5@AT3 system was calculated using the following equation[54]:

$$E_{EO} = \frac{P_E \times 0.0384}{V \times K_{app}} \qquad \text{(equation no. 2.5)}$$

Where P_E = electric power (in kW), V = reactor volume (in m^3), K_{app} = kinetic constant (in min^{-1}).

The E_{EO} for the photocatalytic system was calculated out to be 4.98 $kWh.L^{-1}$. $order^{-1}$. The lower the value of this metric indicates a more efficient method as pollutant removal would require less energy.

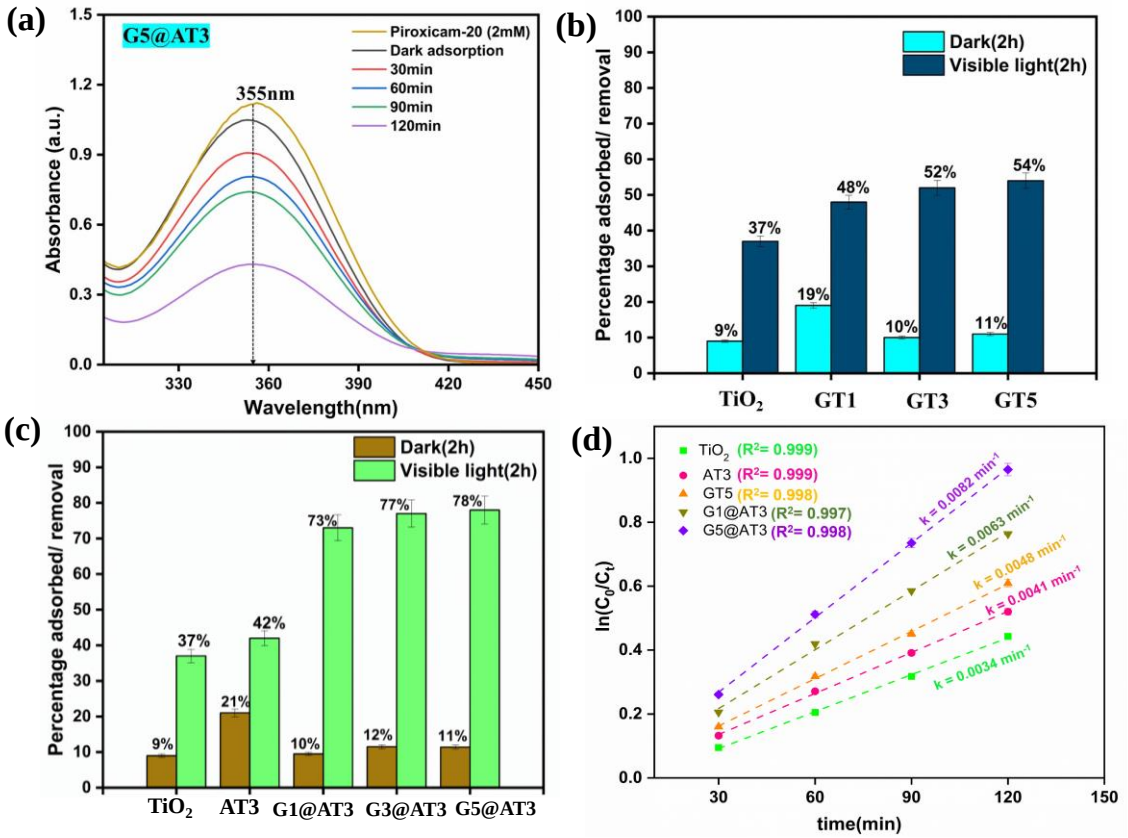

Fig.2.10: The absorbance spectra of piroxicam-20 (2mM) solution at different time intervals under visible light for 2h by: a) G5@AT3, (b,c) percentage adsorbed (under dark) and degradation removal (under visible light) of piroxicam-20 using different catalysts (d) linear fitting of pseudo-first-order reaction kinetic plot.

Sr. no.	Catalyst	% Degradation
1.	TiO_2	37
2.	AT3	42
3.	GT5	54
4.	G5@AT3	78

Table 2.1: Comparison of the different synthesized photocatalysts for photodegradation removal of piroxicam-20.

2.3.3.2 Scavenger studies:

The scavenging experiments were conducted in order to find out the active species playing major role in the photodegradation process. Scavengers such as $K_2Cr_2O_7$, methanol and iso-propyl alcohol (IPA) were used to test for $O_2^{\cdot-}$, $^{\cdot}OH$, h^+ radical species respectively. For the scavenging experiment, the same reaction conditions as mentioned above were followed for the degradation of piroxicam-20 under visible light. The degradation efficiency of G5@AT3 was found to be considerably diminished upon adding $K_2Cr_2O_7$, as shown in **Fig.2.11(a)**. The results suggested that the $O_2^{\cdot-}$ radical species were crucial in facilitating the degradation process. However, methanol and isopropanol also inhibited the degradation process, suggesting that the $^{\cdot}OH$, h^+ species also played essential role in the photodegradation process.

2.3.3.3 Reusability and stability study:

The reusability of the G5@AT3 catalyst was studied by five cycles for the photodegradation of piroxicam-20 under above mentioned experimental conditions. The catalyst was recovered from the degraded solution via centrifugation, washed with distilled water, dried and reused for the second run and so on. As shown in **Fig.2.11(b)**, after five cycles, the catalyst efficiency only decreased by about 4% compared to the initial run.

To determine the stability[55,56] of the G5@AT3 catalyst, the XRD spectra were recorded before and after the photodegradation process. **Fig.2.11(c)** depicts that there is no change in the crystal lattice structure of the photocatalyst before and after the degradation, which proves the high stability of the catalyst.

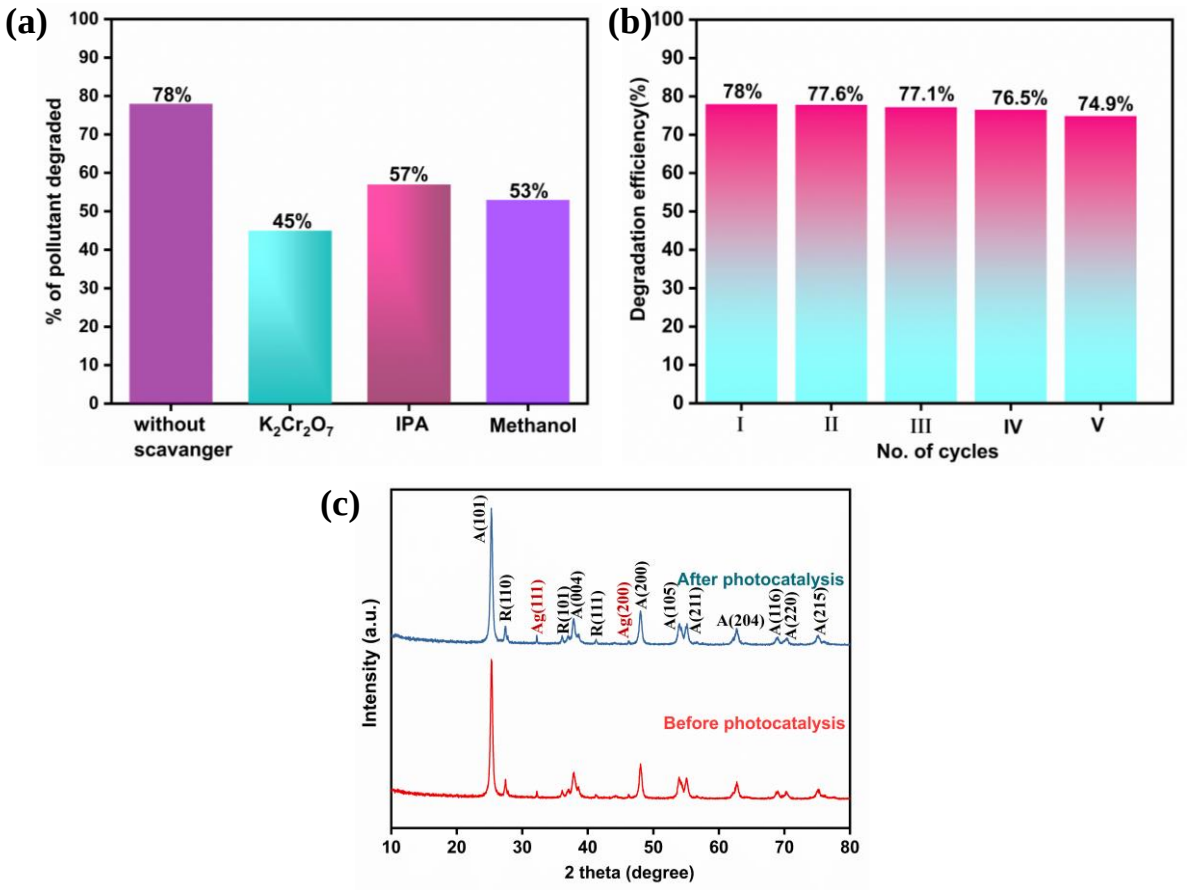

Fig.2.11: (a) Effect of various scavengers on the degradation of piroxicam-20 with G5@AT3 photocatalyst, (b) Recyclability study of the G5@AT3 composite for the degradation of piroxicam-20 solution under visible light and (c) XRD spectra of G5@AT3 before and after the degradation of piroxicam-20.

2.3.3.4 Proposed photodegradation mechanism:

The E_g values calculated above from DRS were used to determine the valence band (VB) and conduction band (CB) potential positions at the zero-point charge [57,58] using the following equations:

$$E_{VB} = \chi - E^e + 0.5E_g \qquad \text{(equation no. 2.6)}$$

$$E_{CB} = E_{VB} - E_g \qquad \text{(equation no. 2.7)}$$

Where E_{VB} = valence band edge, E_{CB} = conduction band edge, χ = absolute electronegativity of photocatalyst (5.90 vs NHE for TiO_2), E^e = free electron energy (4.5 eV vs NHE), E_g = energy of the bandgap.

The possible explanation for the higher photodegradation can be explained with the proposed mechanism **Scheme 2.1**. When the catalyst is exposed to light, the electrons get excited and move from the valence band to the conduction band. They then migrate to the surface of the catalyst and undergo reduction. Oxidation processes occur through the direct participation of the holes left in the valence band. Following this, the organic pollutant molecules are attacked by the present free radicals, which degrade them into smaller products. From the above equation no. 2.6 & 2.7, the VB and CB band edge positions for TiO_2 were calculated to be +3.0eV and -0.20eV respectively. As the CB value was less negative for E_{O2}/ $E_{O2^{\cdot-}}$ (-0.046 eV versus NHE), the electrons present in the conduction band might reduce dissolved O_2 to $O_2^{\cdot-}$ radicals. The E_{VB} value being more positive than that of $E_{OH^{\cdot}/H_2O}$ (+2.68 eV versus NHE), the valence band holes could easily oxidise H_2O to $^{\cdot}OH$ radicals. Due to the large band gap, TiO_2 cannot be excited by visible light. The Ag loading increased the sensitization of TiO_2 because of its SPR effect in visible light, the electric field of visible light caused a collective oscillation in their conducting electrons, which helped in the separation of photoinduced e^-/h^+ pairs generated on the semiconductor TiO_2 surface and helped it in making as a visible light active photocatalyst which is consistent with DRS and PL results. GO has a lower reduction potential (-0.08 eV) than TiO_2 which results in the decrease in the recombination rate of charge carriers and it has high conduction which fastens the mobility of the transferred e^-s. The photoexcited e^-s react with oxygen molecules to produce ($O_2^{\cdot-}$) radical anions and the holes present in the valence band of TiO_2 oxidize the H_2O molecules to generate hydroxyl ($^{\cdot}OH$) radicals. Finally, the hydroxyl($^{\cdot}OH$) radicals / ($O_2^{\cdot-}$) radical anions interact with the piroxicam-20 to produce H_2O, CO_2, and other small organic products. This pathway suggests the increased photocatalytic efficiency of prepared G5@AT3 composite.

2.3.3.5 Degradation mechanism study using HRMS analysis:

To further investigate the photodegradation mechanism, HR-MS test was performed to identify the piroxicam-20 degradation intermediates. The investigations were studied with the positive mode of electrospray ionization. Using the above-mentioned photodegradation conditions, piroxicam-20 solution photodegradation was carried out with G5@AT3 catalyst under visible light for 2h. Following collection and centrifugation of the degraded solution, the absorbance spectra were recorded with a UV-visible spectrophotometer. The degradation efficiency for the G5@AT3 catalyst was found to be 78%. The collected degraded solution sample was used for HRMS analysis to predict the intermediates formed. Possible piroxicam-20 breakdown

pathways are constructed, shown in **Fig.2.12**, according to the intermediate products identified in the HRMS spectra (**Fig.2.13**). The degradation of piroxicam-20 was initiated by the different reactive species attack via ring-opening reactions, functional group cleavage, etc. In the first degradation pathway(I), there is the removal of a benzene ring and SO_2 group, resulting in an intermediate product of m/z = 217, which further got oxidized by h^+, and via the loss of amine, produced fragment at m/z = 202 which was not recorded in the spectra. The resulting fragment further generated m/z = 172 with the loss of the (CH_2=NH) group. In pathway (II), the m/z = 217 fragment underwent loss of methylamine (CH_3NH_2) to form m/z = 186, which further went for removal of HCN, leading to a fragment of m/z = 162, which after decarboxylation led to m/z = 158 and ultimately deteriorated into smaller products [59]. For the third and fourth pathways, the $OH^{\cdot}$ radical from the water molecule attacked the C-N bond, leading to the loss of 2-Aminopyridine, resulting in m/z = 256 for pathway (III) and m/z = 274 for pathway (IV) through the ring-opening process. On further degradation, it led to smaller fragments of m/z = 121 and m/z = 136 [60]. Finally, all degradation pathways resulted in the mineralization of small-molecule inorganic compounds such as CO_2 and H_2O from the remaining organic molecules. As a result, HR-MS analysis showed that h^+ and $OH^{\cdot}$ were involved in the photodegradation of piroxicam-20 molecules.

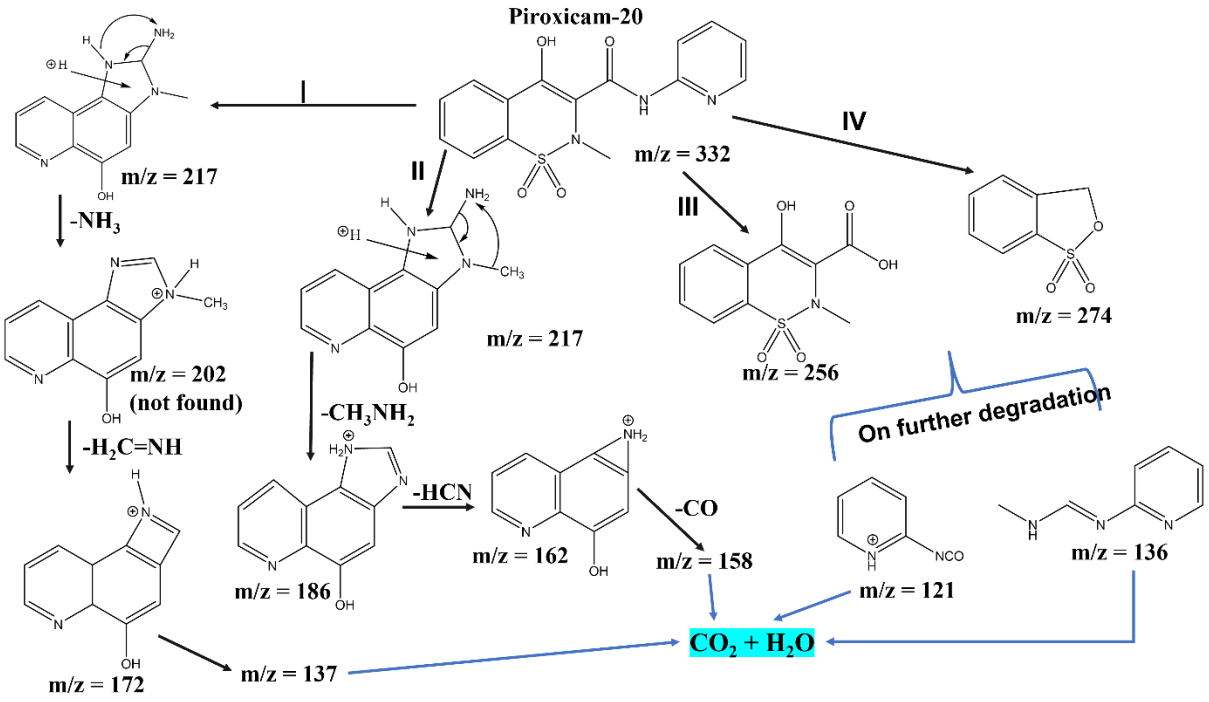

Fig.2.12: The proposed pathway of piroxicam-20 degradation in the G5@AT3 photocatalytic reaction system.

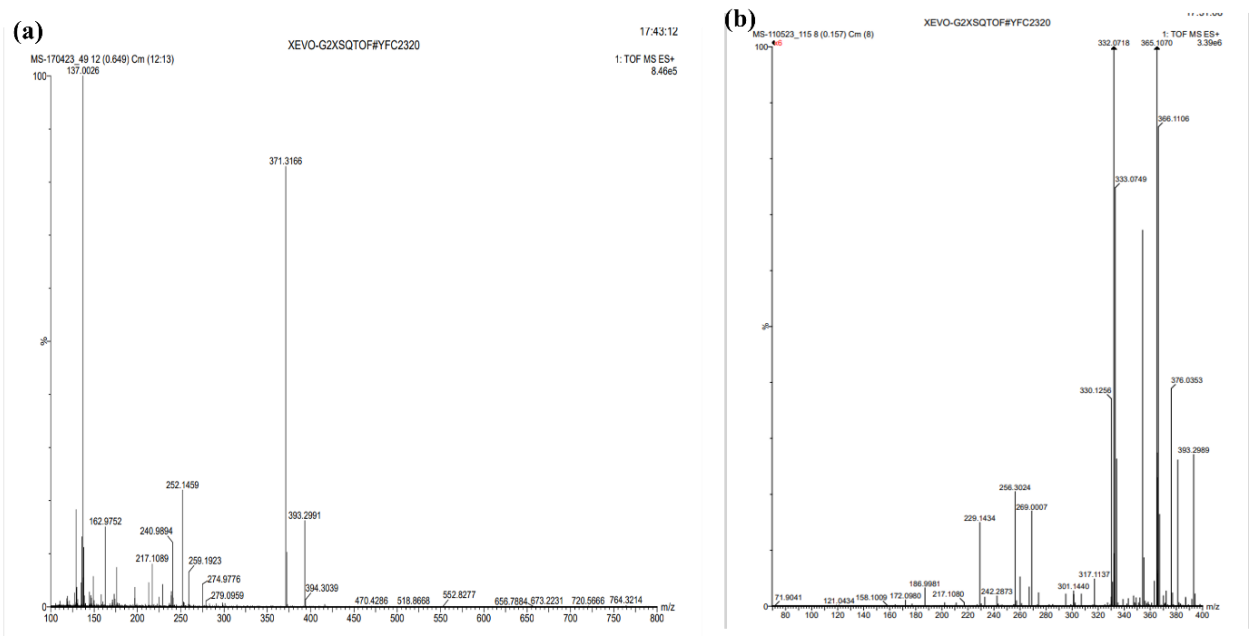

Fig.2.13: HRMS spectra of piroxicam-20 degradation in G5@AT3 photocatalytic reaction system at different m/z range (a)100-800 (b)0-400.

2.3.3.6 Dehydrogenation of methanol

The photocatalytic activity of the different prepared GO and Ag-loaded nanocomposites was assessed under UV light. The photocatalyst's hydrogen production results after 5 h are shown in **Fig.2.14.** The amount of hydrogen produced followed the order: bare TiO_2 < GT1< GT5< AT3 < G5@AT3< G1@AT3 respectively. The photocatalytic dehydrogenation activity of all the photocatalysts was clearly superior to those of bare TiO_2. In particular, the 1 wt% GO loading onto the AT3 composite could achieve the highest H_2 evolution amount. The results show that GO can significantly improve photocatalytic activity and that the loading weight of GO is indeed significant for photocatalytic hydrogen production[61]. The results indicated that with the addition of higher wt% of GO (i.e. 3,5 wt%), the photocatalytic hydrogen production performance became poor because the extra GO will induce more photon absorption and scattering during the photocatalytic process. The outcome suggests that optimum GO loading increased the photocatalytic hydrogen production activity.

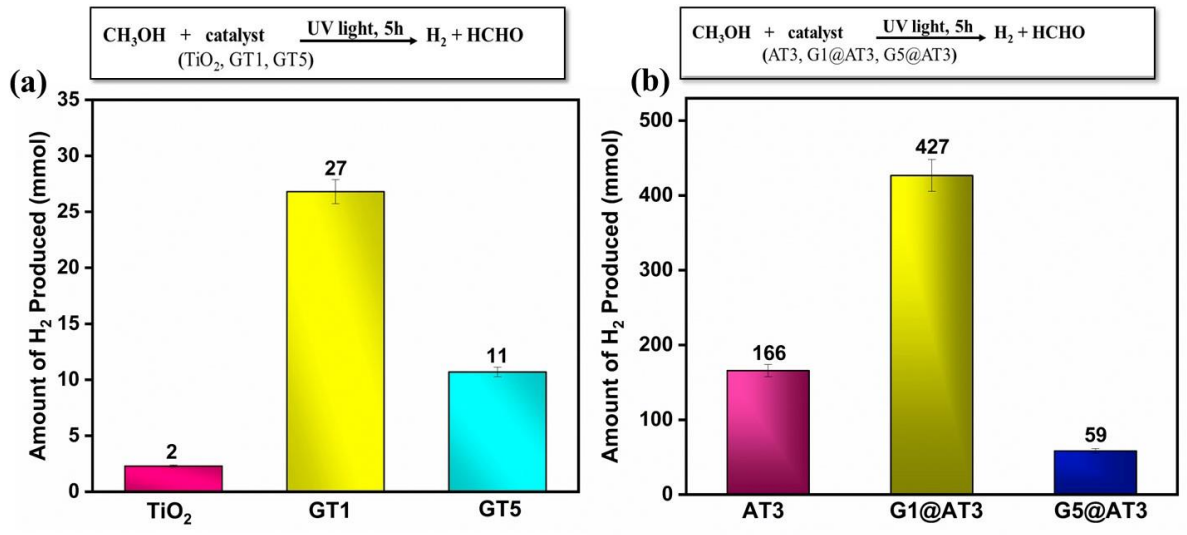

Fig.2.14: Amount of hydrogen gas produced by different prepared catalysts in 50 vol% of 10ml methanol solution irradiated in UV light for 5h.

Based on the preceding research, **Scheme 2.1** confirms that the mechanism behind the production of photocatalytic hydrogen in the G5@AT3 system with GO and Ag loading over TiO_2 can be attributed to the cooperative effect of Ag NPs, GO, and TiO_2. The possible explanation for the photocatalytic dehydrogenation can be explained with the help of the above-proposed **Scheme 2.1**: When the photocatalyst (TiO_2) is exposed to UV light, electrons from the valence band (VB) of TiO_2 are stimulated to their corresponding conduction band (CB). Ag loading over TiO_2 serves as a heterojunction for the stimulated electrons. These e^-s are further transferred from CB of Ag-TiO_2 to GO surface, which possesses excellent conduction, which boosts the transferred e^-s' mobility and reduces H^+ to H_2. The holes present in the VB of TiO_2 oxidize methanol molecules to formaldehyde and hydrogen molecules. This approach shows that the prepared G1@AT3 composite has a higher hydrogen photocatalytic dehydrogenation efficiency.

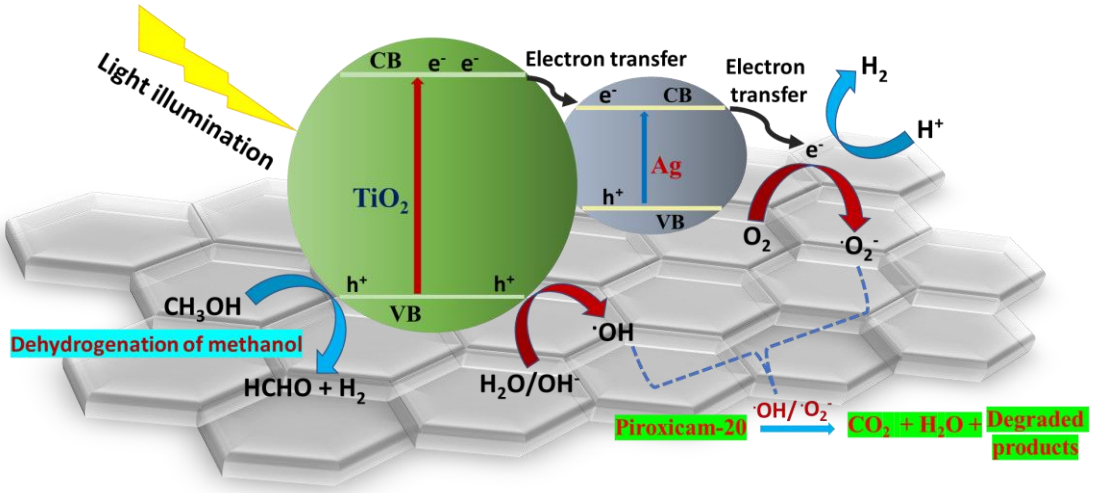

Scheme 2.1: The plausible reaction mechanism of piroxicam-20 degradation and photocatalytic dehydrogenation of methanol over G5@AT3 composite under light irradiation.

2.4 Conclusion

In this work, we have efficiently synthesized the photocatalyst which improved the photocatalytic properties of TiO_2 by depositing Ag and GO and investigated their relative impact on the surface structural, optical, and physicochemical properties. The GO-loaded Ag-TiO_2 composite provided a strong optical response in the visible range, improved charge separation, superior photodegradation of piroxicam-20 and methanol dehydrogenation. The piroxicam-20 degradation reaction under visible light followed pseudo-first-order kinetics with a rate constant value of 0.0082 min^{-1} for G5@AT3 which is ~2.5 times higher than of bare TiO_2. G1@AT3 composite produced (427 mmol) of H_2 ~214 times higher than bare TiO_2 under UV light. Based on photodegradation and reaction intermediates, a plausible mechanism has been proposed suggesting the cooperative effect of Ag NPs, GO, and TiO_2 which played an important role in enhancing the photocatalytic activity of GO-loaded Ag-TiO_2. The developed GO-loaded Ag-TiO_2 composite materials are anticipated to exhibit noticeably improved photocatalytic activity after the synthesis process is further controlled (by determining the ideal mass ratio of GO-titania/ GO- Ag-TiO_2).

References

1. Gilje S, Han S, Wang M, Wang KL, Kaner RB. A chemical route to graphene for device applications. Nano Lett. 2007;7:3394–8.

2. Boukhvalov DW, Katsnelson MI. Modeling of graphite oxide. J Am Chem Soc.

2008;130:10697–701.

3. Geim AK, Novoselov KS. The rise of graphene. Nanosci Technol A Collect Rev from Nat Journals. 2009;11–9.

4. Allen MJ, Tung VC, Kaner RB. Honeycomb carbon: a review of graphene. Chem Rev. 2010;110:132–45.

5. Jing J, Zhang Y, Li W, Yu WW. Visible light driven photodegradation of quinoline over TiO 2/graphene oxide nanocomposites. J Catal [Internet]. 2014;316:174–81. Available from: http://dx.doi.org/10.1016/j.jcat.2014.05.009

6. Qi HP, Wang HL, Zhao DY, Jiang WF. Preparation and photocatalytic activity of Ag-modified GO-TiO 2 mesocrystals under visible light irradiation [Internet]. Appl. Surf. Sci. Elsevier B.V; 2019. Available from: https://doi.org/10.1016/j.apsusc.2019.02.194

7. Vasilaki E, Georgaki I, Vernardou D, Vamvakaki M, Katsarakis N. Ag-loaded TiO2/reduced graphene oxide nanocomposites for enhanced visible-light photocatalytic activity. Appl Surf Sci. 2015;353:865–72.

8. Rout DR, Jena HM. Facile synthesis of novel Z-scheme GO-modified ternary composite as photocatalyst for enhanced degradation of bisphenol-A under sunlight. J Taiwan Inst Chem Eng [Internet]. 2023;147:104914. Available from: https://www.sciencedirect.com/science/article/pii/S1876107023002420

9. Huang J-F, Zhang H-J, Feng Y-Q. Chloramphenicol extraction from honey, milk, and eggs using polymer monolith microextraction followed by liquid chromatography− mass spectrometry determination. J Agric Food Chem. 2006;54:9279–86.

10. Madikizela LM, Chimuka L. Occurrence of naproxen, ibuprofen, and diclofenac residues in wastewater and river water of KwaZulu-Natal Province in South Africa. Environ Monit Assess. 2017;189:1–12.

11. de Jesus Gaffney V, Cardoso VV, Cardoso E, Teixeira AP, Martins J, Benoliel MJ, et al. Occurrence and behaviour of pharmaceutical compounds in a Portuguese wastewater treatment plant: Removal efficiency through conventional treatment processes. Environ Sci Pollut Res. 2017;24:14717–34.

12. Chen Z, Ning B, Cai Y, Liu M, Xu P, Zhang P, et al. Rapid degradation of levofloxacin by p-n heterojunction AgFeO2/Ag3VO4 photocatalyst: Mechanism study and degradation pathway. J Taiwan Inst Chem Eng [Internet]. 2023;151:105126. Available from: https://www.sciencedirect.com/science/article/pii/S1876107023004558

13. Archer E, Petrie B, Kasprzyk-Hordern B, Wolfaardt GM. The fate of pharmaceuticals and personal care products (PPCPs), endocrine disrupting contaminants (EDCs), metabolites and illicit drugs in a WWTW and environmental waters. Chemosphere. 2017;174:437–46.

14. Thiebault T, Boussafir M, Le Milbeau C. Occurrence and removal efficiency of pharmaceuticals in an urban wastewater treatment plant: mass balance, fate and consumption assessment. J Environ Chem Eng. 2017;5:2894–902.

15. Derikvandi H, Nezamzadeh-Ejhieh A. Increased photocatalytic activity of NiO and ZnO in photodegradation of a model drug aqueous solution: Effect of coupling, supporting, particles size and calcination temperature [Internet]. J. Hazard. Mater. Elsevier B.V.; 2017. Available from: http://dx.doi.org/10.1016/j.jhazmat.2016.09.056

16. Navarro RM, Pena MA, Fierro JLG. Hydrogen production reactions from carbon feedstocks: fossil fuels and biomass. Chem Rev. 2007;107:3952–91.

17. Ni M, Leung MKH, Leung DYC, Sumathy K. A review and recent developments in photocatalytic water-splitting using TiO2 for hydrogen production. Renew Sustain Energy Rev. 2007;11:401–25.

18. Matsuoka M, Kitano M, Takeuchi M, Tsujimaru K, Anpo M, Thomas JM. Photocatalysis for new energy production: Recent advances in photocatalytic water splitting reactions for hydrogen production. Catal Today. 2007;122:51–61.

19. Shimura K, Yoshida H. Heterogeneous photocatalytic hydrogen production from water and biomass derivatives. Energy Environ Sci. 2011;4:2467–81.

20. Pougin A, Dodekatos G, Dilla M, Tüysüz H, Strunk J. Au@ TiO2 core–shell composites for the photocatalytic reduction of CO2. Chem Eur J. 2018;24:12416–25.

21. Gholami P, Khataee A, Soltani RDC, Dinpazhoh L, Bhatnagar A. Photocatalytic degradation of gemifloxacin antibiotic using Zn-Co-LDH@ biochar nanocomposite. J Hazard Mater. 2020;382:121070.

22. Jo W-K, Kim Y-G, Tonda S. Hierarchical flower-like NiAl-layered double hydroxide microspheres encapsulated with black Cu-doped TiO2 nanoparticles: Highly efficient visible-light-driven composite photocatalysts for environmental remediation. J Hazard Mater. 2018;357:19–29.

23. Ayanda OS, Aremu OH, Akintayo CO, Sodeinde KO, Igboama WN, Oseghe EO, et al. Sonocatalytic degradation of amoxicillin from aquaculture effluent by zinc oxide nanoparticles. Environ Nanotechnology, Monit Manag. 2021;16:100513.

24. Abbasi S, Ahmadpoor F, Imani M, Ekrami-Kakhki M-S. Synthesis of magnetic Fe3O4@ ZnO@ graphene oxide nanocomposite for photodegradation of organic dye pollutant. Int J Environ Anal Chem. 2020;100:225–40.

25. Diksha, Kaur M, Yempally V, Kaur H. Sustainable magnetically recoverable Iridium-coated Fe3O4 nanoparticles for enhanced catalytic reduction of organic pollutants in water. Environ Sci Pollut Res. 2023;30:56464–83.

26. Pourtaheri A, Nezamzadeh-Ejhieh A. Photocatalytic properties of incorporated NiO onto clinoptilolite nano-particles in the photodegradation process of aqueous solution of cefixime pharmaceutical capsule [Internet]. Chem. Eng. Res. Des. Institution of Chemical Engineers; 2015. Available from: http://dx.doi.org/10.1016/j.cherd.2015.10.031

27. Rather RA, Singh S, Pal B. Core-shell morphology of Au-TiO2@graphene oxide nanocomposite exhibiting enhanced hydrogen production from water. J Ind Eng Chem [Internet]. 2016;37:288–94. Available from: http://dx.doi.org/10.1016/j.jiec.2016.03.039

28. Hunge YM, Yadav AA, Dhodamani AG, Suzuki N, Terashima C, Fujishima A, et al. Enhanced photocatalytic performance of ultrasound treated GO/TiO2 composite for photocatalytic degradation of salicylic acid under sunlight illumination. Ultrason Sonochem. 2020;61:104849.

29. Jing J, Zhang Y, Li W, William WY. Visible light driven photodegradation of quinoline over TiO2/graphene oxide nanocomposites. J Catal. 2014;316:174–81.

30. Ghattavi S, Nezamzadeh-Ejhieh A. GC-MASS detection of methyl orange degradation

intermediates by AgBr/g-C3N4: Experimental design, bandgap study, and characterization of the catalyst. Int J Hydrogen Energy [Internet]. 2020;45:24636–56. Available from: https://doi.org/10.1016/j.ijhydene.2020.06.207

31. Bhardwaj S, Sharma D, Kumari P, Pal B. Influence of photodeposition time and loading amount of Ag co-catalyst on growth, distribution and photocatalytic properties of Ag@TiO2 nanocatalysts. Opt Mater (Amst) [Internet]. 2020;106:109975. Available from: https://doi.org/10.1016/j.optmat.2020.109975

32. Grover IS, Prajapat RC, Singh S, Pal B. Highly photoactive Au-TiO2 nanowires for improved photo-degradation of propiconazole fungicide under UV/sunlight irradiation. Sol Energy. 2017;144:612–8.

33. Kaur R, Pal B. Plasmonic coinage metal–TiO 2 hybrid nanocatalysts for highly efficient photocatalytic oxidation under sunlight irradiation. New J Chem. 2015;39:5966–76.

34. Mirsalari SA, Nezamzadeh-Ejhieh A, Massah AR. A designed experiment for CdS-AgBr photocatalyst toward methylene blue. Environ Sci Pollut Res [Internet]. 2022;29:33013–32. Available from: https://doi.org/10.1007/s11356-021-17569-1

35. Nezamzadeh-Ejhieh A, Zabihi-Mobarakeh H. Heterogeneous photodecolorization of mixture of methylene blue and bromophenol blue using CuO-nano-clinoptilolite. J Ind Eng Chem [Internet]. 2014;20:1421–31. Available from: http://dx.doi.org/10.1016/j.jiec.2013.07.027

36. Woan K, Pyrgiotakis G, Sigmund W. Photocatalytic carbon-nanotube–TiO2 composites. Adv Mater. 2009;21:2233–9.

37. Ghattavi S, Nezamzadeh-Ejhieh A. A double-Z-scheme ZnO/AgI/WO3 photocatalyst with high visible light activity: Experimental design and mechanism pathway in the degradation of methylene blue. J Mol Liq [Internet]. 2021;322:114563. Available from: https://doi.org/10.1016/j.molliq.2020.114563

38. Derikvandi H, Nezamzadeh-Ejhieh A. A comprehensive study on electrochemical and photocatalytic activity of SnO 2 -ZnO/clinoptilolite nanoparticles. J Mol Catal A Chem [Internet]. 2017;426:158–69. Available from: http://dx.doi.org/10.1016/j.molcata.2016.11.011

39. Kelly KL, Coronado E, Zhao LL, Schatz GC. The optical properties of metal nanoparticles: the influence of size, shape, and dielectric environment. J. Phys. Chem. B. ACS Publications; 2003. p. 668–77.

40. Subramanian P, Szunerits S, Boukherroub R. Plasmon-induced photocatalytic transformations. Nanostructured Photocatal. Elsevier; 2020. p. 249–75.

41. Dinari M, Dadkhah F. Visible light photodegradation of 4-nitrophenol by new high-performance and easy recoverable Fe3O4/Ag2O-LDH hybrid photocatalysts. Appl Organomet Chem. 2021;35:e6355.

42. Yousefi A, Nezamzadeh-Ejhieh A. Preparation and characterization of SnO2-BiVO4-CuO catalyst and kinetics of phenazopyridine photodegradation. Iran J Catal. 2021;11:247–59.

43. Bhardwaj S, Dogra D, Pal B, Singh S. Photodeposition time dependant growth, size and photoactivity of Ag and Cu deposited TiO2 nanocatalyst under solar irradiation. Sol Energy. 2019;194:618–27.

44. Norouzi A, Nezamzadeh-Ejhieh A. α-Fe2O3/Cu2O heterostructure: Brief characterization

and kinetic aspect of degradation of methylene blue. Phys B Condens Matter. 2020;599.

45. Tamiji T, Nezamzadeh-Ejhieh A. Electrocatalytic behavior of AgBr NPs as modifier of carbon past electrode in the presence of methanol and ethanol in aqueous solution: A kinetic study. J Taiwan Inst Chem Eng [Internet]. 2019;104:130–8. Available from: https://doi.org/10.1016/j.jtice.2019.08.021

46. Spanakis E, Pervolaraki M, Katsarakis N, Koudoumas E, Vernardou D. Effect of gold and silver nanoislands on the electrochemical properties of carbon nanofoam. Electrochim Acta. 2013;111:305–13.

47. Palmisano G, Loddo V, El Nazer HH, Yurdakal S, Augugliaro V, Ciriminna R, et al. Graphite-supported TiO2 for 4-nitrophenol degradation in a photoelectrocatalytic reactor. Chem Eng J. 2009;155:339–46.

48. Senobari S, Nezamzadeh-Ejhieh A. A novel ternary nano-composite with a high photocatalyitic activity: Characterization, effect of calcination temperature and designing the experiments. J Photochem Photobiol A Chem [Internet]. 2020;394:112455. Available from: https://doi.org/10.1016/j.jphotochem.2020.112455

49. Rahmani-Aliabadi A, Nezamzadeh-Ejhieh A. A visible light FeS/Fe2S3/zeolite photocatalyst towards photodegradation of ciprofloxacin. J Photochem Photobiol A Chem [Internet]. 2018;357:1–10. Available from: https://doi.org/10.1016/j.jphotochem.2018.02.006

50. Mehrabanpour N, Nezamzadeh-Ejhieh A, Ghattavi S, Ershadi A. A magnetically separable clinoptilolite supported CdS-PbS photocatalyst: Characterization and photocatalytic activity toward cefotaxime. Appl Surf Sci [Internet]. 2023;614:156252. Available from: https://doi.org/10.1016/j.apsusc.2022.156252

51. Rao R, Podila R, Tsuchikawa R, Katoch J, Tishler D, Rao AM, et al. Effects of Layer Stacking on the Combination Raman Modes in Graphene. ACS Nano. 2011;5:1594–9.

52. Pourtaheri A, Nezamzadeh-Ejhieh A. Enhancement in photocatalytic activity of NiO by supporting onto an Iranian clinoptilolite nano-particles of aqueous solution of cefuroxime pharmaceutical capsule. Spectrochim Acta - Part A Mol Biomol Spectrosc [Internet]. 2015;137:338–44. Available from: http://dx.doi.org/10.1016/j.saa.2014.08.058

53. Vahabirad S, Nezamzadeh-Ejhieh A, Mirmohammadi M. The coupled BiOI/(BiO)2CO3 catalyst: Brief characterization, and study of its photocatalytic kinetics. J Solid State Chem [Internet]. 2022;314:123405. Available from: https://doi.org/10.1016/j.jssc.2022.123405

54. Keyikoğlu R, Doğan IN, Khataee A, Orooji Y, Kobya M, Yoon Y. Synthesis of visible light responsive ZnCoFe layered double hydroxide towards enhanced photocatalytic activity in water treatment. Chemosphere. 2022;309.

55. Saadati A, Habibi-Yangjeh A, Feizpoor S, Keyikoglu R, Khataee A. Combining brown titanium dioxide with BiOBr and AgBr nanoparticles using a facile one-pot procedure to promote visible-light photocatalytic performance. J Photochem Photobiol A Chem [Internet]. 2022;431:114034. Available from: https://doi.org/10.1016/j.jphotochem.2022.114034

56. Hassandoost R, Kotb A, Movafagh Z, Esmat M, Guegan R, Endo S, et al. Nanoarchitecturing bimetallic manganese cobaltite spinels for sonocatalytic degradation of oxytetracycline. Chem Eng J. 2022;431:1–32.

57. Ghattavi S, Nezamzadeh-Ejhieh A. A visible light driven AgBr/g-C3N4 photocatalyst composite in methyl orange photodegradation: Focus on photoluminescence, mole ratio,

synthesis method of g-C3N4 and scavengers. Compos Part B Eng [Internet]. 2020;183:107712. Available from: https://doi.org/10.1016/j.compositesb.2019.107712

58. Mirsalari SA, Nezamzadeh-Ejhieh A. Focus on the photocatalytic pathway of the CdS-AgBr nano-catalyst by using the scavenging agents. Sep Purif Technol [Internet]. 2020;250:117235. Available from: https://doi.org/10.1016/j.seppur.2020.117235

59. Hsu FF, Lakshmi VM, Zenser T V. Characterization of new metabolites from in vivo biotransformation of 2-amino-3-methylimidazo[4,5-f]quinoline inmouse by mass spectrometry. J Mass Spectrom. 2009;44:1359–68.

60. Muszyńska B, Dąbrowska M, Starek M, Zmudzki P, Lazur J, Pytko-Polończyk J, et al. Lentinula edodes mycelium as effective agent for piroxicam mycoremediation. Front Microbiol. 2019;10:1–9.

61. Zhang Y, Zhang Y, Li X, Zhao X, Anning C, Crittenden J, et al. Photocatalytic water splitting of ternary graphene-like photocatalyst for the photocatalytic hydrogen production. Front Environ Sci Eng. 2020;14:1–13.

CHAPTER- 3

Enhanced Photocatalytic Hydrogen Production with GO-modified Cu-TiO_2 for Alcohol Dehydrogenation under UV and Sunlight

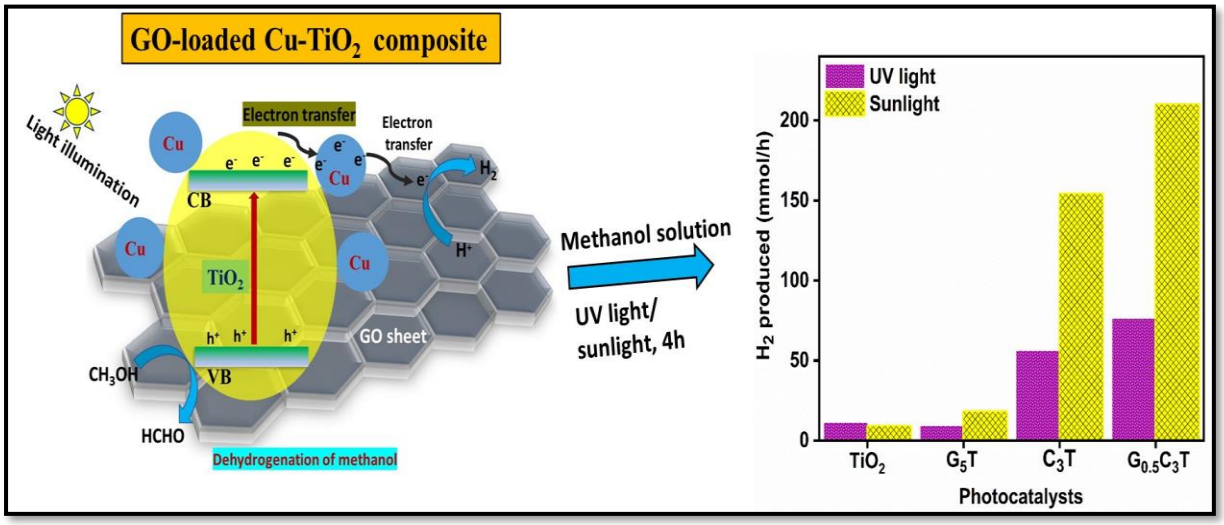

Schematic outline:

This study explored the alcohol dehydrogenation process using graphene oxide (GO)-modified Cu-TiO_2 photocatalyst under both UV light and sunlight. The photocatalyst was synthesized via a hydrothermal method. The research examined how different alcohols (methanol, ethanol, propanol) and their concentrations (both volume percentage and molarity) affect hydrogen (H_2) production. It also investigated the effects of various factors, including GO and Cu loading on TiO_2, their combined impact, reaction time, the type of alcohol, and the reaction conditions on photocatalytic hydrogen production.

3.1 Introduction

The current state of maximum energy growth relies on conventional resources such as fossil fuels[1]. With the continuous rise in energy consumption and the depletion of fossil fuels such as petroleum, coal, and natural gas, there is an urgent need to develop clean and environmentally friendly fuel options[2],[3]. Hydrogen energy, among the numerous alternative energy sources, is a crucial component of the renewable energy strategies of developed nations due to its immediate availability and high fuel efficiency[4]. It is a viable green energy source that has the potential to address environmental concerns associated with traditional fossil fuels. Hydrogen is presently produced through electrolysis, natural gas, naphtha, heavy oil, and coal, among other sources. Most (96%) of hydrogen production is generated directly from fossil fuels, while a small portion (4%) is produced indirectly using energy derived from fossil fuels as feedstock[5]. Nevertheless, for hydrogen to be employed in future energy supply systems, it must undergo various stages, including viable production, storage, and transportation, considering economic, technological, and environmental constraints.

The non-conventional methods for hydrogen production primarily include biomass, hydrocarbons, photocatalytic water splitting, dehydrogenation of waste alcoholic solvents, etc. In recent times, there has been a significant focus on photocatalytic approaches to hydrogen production due to the high cost, excessive energy use, and lack of environmental friendliness associated with traditional methods. One of the most eco-friendly ways to produce hydrogen in the future is to use energy-intensive and solar-powered semiconductors. Sun-light/Visible light-driven water splitting is proven to be less efficient and requires precious metal-based co-catalysts compared to UV-light-driven photocatalysts. One of the primary issues is photocatalysts' very low efficiency in converting sunlight into hydrogen. Current materials and technologies frequently fail to capture enough of the solar spectrum or efficiently convert it to chemical energy. Many effective photocatalysts rely on rare or expensive elements, such as Pt, Pd, Au, etc., making large-scale manufacture costly. Developing inexpensive and abundant materials remains a big challenge. The research is still ongoing to find and create novel photocatalytic materials that are effective, long-lasting, and affordable.

A wide range of semiconductor materials have been thoroughly investigated for the purpose of photocatalytic water splitting to generate hydrogen. In recent times, there has been considerable interest in alkanes, ethanol, benzyl alcohol, and glucose as potential precursors in hydrogen production using photocatalytic methods[6–9]. Significant quantities of organic acids

and alcohols are generated as byproducts in various industrial processes, such as hydrometallurgy and biomass processing. These byproducts unavoidably contaminate the environment[10]. Eliminating or degrading these chemicals into useful substances is a significant focus of modern environmental conservation efforts. Various approaches to the dehydrogenation of alcohols have been investigated, including heterogeneous photocatalytic systems using semiconductor-based nanoparticles[11,12], molecular donor-acceptor reactions[13], and photovoltaic cells containing electrocatalysts[14–16]. Sehrawat et al. fabricated a $Zn_{0.5}Cd_{0.5}S/MoS_2$ (ZCMS) composite and employed it for the degradation of ketorolac tromethamine drug and hydrogen evolution with benzyl alcohol(BA) oxidation. The 10 wt% ZCMS composite degraded 92.54% drug under solar light within 150 min and produced hydrogen with the rate of 2.3470 mmol $g^{-1}h^{-1}$ and converted 38.52% of BA into BAL (95.48%) selectivity[17]. Another study revealed that $ZnS/P–MoS_2$ composite, degraded 98.52% of brilliant green (BG) dye in 40 min under sunlight and converted 46.12% of BA into BAL (98.30%) selectivity with hydrogen evolution rate of 1.2306 mmol g^{-1} h^{-1} [18].

TiO_2 is the most extensively studied photocatalyst for this approach because of its favourable redox potential. Nevertheless, the recombination rate of the fast charge carrier and its limited utilisation of solar energy significantly restrict its practical uses. Therefore, extensive research is being conducted on developing heterostructure photocatalysts by combining them with other semiconductors with suitable band alignments[19–23]. One conventional method to enhance activity involves the deposition of noble metals as cocatalysts onto the TiO_2 surface[24–26]. Tkachenko et al.[27] fabricated the PtO_x/TiO_2 systems, demonstrating significant efficacy in photocatalytic hydrogen evolution from aqueous ethanol and glucose solutions under UV light. With varying Pt content (x = 0.2-0.4 wt%), the $PtO_x(0.29)/TiO_2$ photocatalyst produced the highest rate (0.7 mol $h^{-1}g_{(Pt)}^{-1}$) of hydrogen from glucose solution. Qui et al.[28] reported the $Cu@TiO_{2-x}$ hybrids exhibit enhanced photocatalytic hydrogen generation, with the $Cu@TiO_{2-x}$-1% sample achieving an H_2 evolution rate of 7218.8 mmol g^{-1} h^{-1}, which is 2.1 times greater than that of TiO_{2-x}.

Studies have reported that in recent decades, carbon-rich materials like graphene, carbon dots, reduced graphene oxide, and graphene oxide have been extensively researched to enhance the photocatalytic activity of semiconductors like TiO_2 due to their distinctive structure, high carrier mobility, and large specific surface area. Liu et al.[29] fabricated a TiO_2/rGO-Mo_2C photocatalyst and utilised it in the process of water splitting to produce hydrogen gas (H_2). The composite generated a rate of 880 μmol h^{-1} g^{-1} hydrogen, exhibiting an evident quantum

efficiency of 2.64%. This efficiency was approximately 5.5 times greater than that of the TiO_2/rGO composite and ~88 times more than that of bare TiO_2. Viable biomass-derived graphene aerogels correlate with green chemistry principles, resulting in cost-effective and ecologically friendly water remediation solutions[30–32]. Dhiman et al. synthesized a low-cost, green, efficient N-doped graphene aerogel for the degradation of telmisartan(TEL), a pharmaceutical drug which poses a threat to the environment. The photocatalyst degraded 99.8% of the drug within 70 minutes under visible light[33]. Aggarwal et al. prepared an onion-like carbon-based photocatalyst from diesel engine soot and utilised it for photocatalytic water splitting under visible light, and it produced a hydrogen rate of ~1075 $\mu M\ h^{-1}\ g^{-1}$[34].

Numerous studies utilising metal (Ag/Cu/Au/Pt)-TiO_2, GO-loaded TiO_2, and modified GO/metal-TiO_2 for the photocatalytic degradation of organic pollutants in the presence of UV/visible/sunlight have been conducted in the past[35–37]. However, reports of studies utilising these catalysts to produce hydrogen from alcohols are extremely scarce. Here in this study, we have prepared a ternary heterojunction GO-modified Cu-TiO_2 composite via the hydrothermal method and studied the photocatalytic application for the dehydrogenation of methanol under different light sources. To start with, the objective of this study is to regulate TiO_2's photocatalytic activity by altering its band energetics and surface structural properties using GO and Cu loading to create various ternary (GO/Cu-TiO_2) heterostructure composites. The incorporation of hybrid interfaces (Cu-TiO_2, GO-TiO_2) improved the photoexcited charge separation efficiency, leading to increased photocatalytic activity in the ternary composite. The effect of varying Cu and GO wt% over TiO_2 and prepared ternary composites was studied for photocatalytic methanol dehydrogenation under two light sources: UV lamp and sunlight. Other factors, such as the influence of chain length of alcohols, concentration, and time, were also evaluated. Focusing on the outstanding physical and chemical characteristics of GO and Cu, we present a straightforward and economical approach that integrates the merits of both materials to substantially enhance the photocatalytic activity of the GO-modified Cu-TiO_2 composite.

3.2 Experimental Section

3.2.1 Materials and Chemicals

The utilised materials were procured from commercial suppliers without undergoing any additional purification processes. A commercial type of TiO_2 (P25; 70% Anatase & 30% Rutile) was given as a gift by Degussa Corporation in Germany. Cupric acetate ($Cu(CH_3COO)_2 .H_2O$, 98–102%) supplied by Thermofisher science was used. Sigma Aldrich, India, supplied the graphite powder, potassium permanganate, IPA(isopropyl alcohol) and sodium nitrate utilised in this study. The deionised (DI) water was acquired from Organo Biotech Laboratories Pvt. Ltd. in India.

3.2.2 Synthesis of Cu-TiO_2

The photo-deposition method was employed for the Cu metal deposition over the bare TiO_2 surface[38]. In a standard method, 100mg of powdered TiO_2 was dispersed in a 10 mL test tube containing a 50% volume aqueous IPA solution. Different volumes of $Cu(CH_3COO)_2.H_2O$ (ranging from 1574 to 7870 μL, 0.01M) (for different wt%= 1,3,5) were then added. Subsequently, the test tube was sealed with a rubber septum after being purged with argon (Ar) gas for about 15 minutes to eliminate any other gases. After irradiating with a mercury arc lamp (125W) with continuous magnetic stirring for 4 hours, the suspension was centrifuged at 8000 rpm, rinsed multiple times with DI water and methanol, and dried overnight at 353 K.

3.2.3 Synthesis of GO-TiO_2 &GO modified Cu-TiO_2

The modified Hummers method was employed to synthesise graphene oxide (GO) from the graphite powder, as reported in our previous paper[28]. The hydrothermal method was followed to load different wt% GO over TiO_2 and Cu-TiO_2. Various quantities of graphene oxide (GO) were dispersed in a solution consisting of a 2:1 mixture of deionised water (20 ml): ethanol (10 ml). Ultrasonication was employed to exfoliate the mixture for a duration of 2 hours. To the resulting GO solution, a calculated amount of 200 mg of TiO_2 was added (for GO-TiO_2 composite) and Cu-TiO_2 (for GO@Cu-TiO_2 composite) and magnetically stirred for 2h to obtain a homogeneous suspension. Further, the suspension was transferred into the autoclave and heated at 180 ^oC for 5 h. The mixture was centrifuged, washed with distilled water, and dried at 60 ^oC.

3.2.4 Characterization

The X-ray diffractometer (SmartLab SE) was used to record the crystal structure of the powder samples. The diffraction angle (2θ) range ranged from 10° to 80°, and Cu-Kα (1.540598 Å) was used as the X-ray source. The surface morphology was examined using Field Emission Scanning Electron Microscopy (FE-SEM, JEOL JSM-7600F). The EDX spectra were obtained using the Bruker EDX equipment. Additionally, analysis was performed using High-Resolution Transmission Electron Microscopy (HRTEM, JEOL JEM-2100 model). The optical analysis was conducted using diffuse reflectance spectroscopy with a UV-VIS spectrophotometer (JASCO V-750) within the 200-800 nm wavelength range. The Raman spectroscopy was performed using the LabRam HR 124 Evolution Raman microscope, which utilised a 532 nm excitation wavelength. The oxidation state of various elements present in the composite was evaluated using XPS (X-ray photoelectron spectroscopy) Thermofisher Scientific ESCALAB. The surface area and pore diameter were measured with the help of BET and BJH methods using Quantachrome Nova-1000 surface analyzer.

3.2.5 Photocatalytic dehydrogenation of alcohols

The photocatalytic hydrogen production from the dehydrogenation of various alcohols was studied with the help of prepared composites. The amount of hydrogen generated during the dehydrogenation of alcohols was quantified utilising a NUCON Gas chromatograph (GC) employing argon gas as the carrier gas and a molecular sieve with 5X A column equipped with a thermal conductivity detector(TCD). The temperatures of the column, detector, and injector were adjusted to 40 °C, 110 °C, and 90 °C respectively. 50 mg of the catalyst was added in 10 ml 50vol% methanol solution in a test tube, and the test tube was sealed with the help of rubber septa after purging it with argon gas for 20 minutes in order to create an inert atmosphere. Afterwards, the test tube was magnetically stirred under a UV lamp (Hg arc lamp,125W, 300-390 nm, 10.4 mW cm^{-2}) for 4h, and it was taken out after regular intervals to study the hydrogen evolution. Utilising a gas-confined syringe, 1 ml of the gas produced in the test tube was drawn out and injected into the injector inlet of the GC. A standard of 505 ppm hydrogen was employed to evaluate the GC chromatograms recorded. The same procedure was followed to determine the amount of hydrogen produced by the catalysts under direct sunlight in May 2024, with an average temperature of 40°C and average solar intensity of ~680 W m^{-2}.

3.3 Results and Discussion

3.3.1 Characterization study

3.3.1.1 XRD analysis

The crystal planes and the diffraction angle values corresponding to the synthesised $G_{0.5}C_3T$, G_5T, and C_3T nanocomposites were analysed along with bare P25- TiO_2 from their recorded XRD spectra, as depicted in **Fig.3.1(a)**. For pure GO, the characteristic sharp peak was observed at an angle of 2θ = 10.5°, indicating the presence of the (002) lattice plane for graphene oxide (GO). Additionally, another peak was identified at 42.1° with the (101) lattice plane, validating the formation of GO. This information is illustrated in the supporting image, **Fig.3.1(b)**. The XRD profile of the bare TiO_2 sample exhibits distinct peaks at specific angles, namely 25.2º, 37.7º, 47.9º, 53.9º, 55.08º, 62.7º, 68.9º, 70.3º, and 75.16º. These peaks correspond to the (101), (004), (200), (105), (211), (204), (116), (220) and (215) diffraction planes of anatase TiO_2 (JCPDS card no. 21-1272). The peaks appearing at the 2θ = 27.3º, 36.1º, and 41.2º corresponds to the planes (110), (101), (111), respectively, of the rutile form of TiO_2. This information follows the reference to JCPDS Card No. 21-1276. After the photo-deposition of Cu metal over the TiO_2, no distinct peak was observed for the Cu metal co-catalyst. Prior reports have indicated that metal nanoparticles with a low weight percentage (<5wt%) are typically not observable in XRD spectra[20]. When GO is loaded onto TiO_2 (G_5T) and Cu-TiO_2 ($G_{0.5}C_3T$), the diffraction peak associated with GO becomes much weaker or non-existent. This is because both Cu and TiO_2 have a higher X-ray scattering coefficient than GO, attributed to their greater atomic numbers.

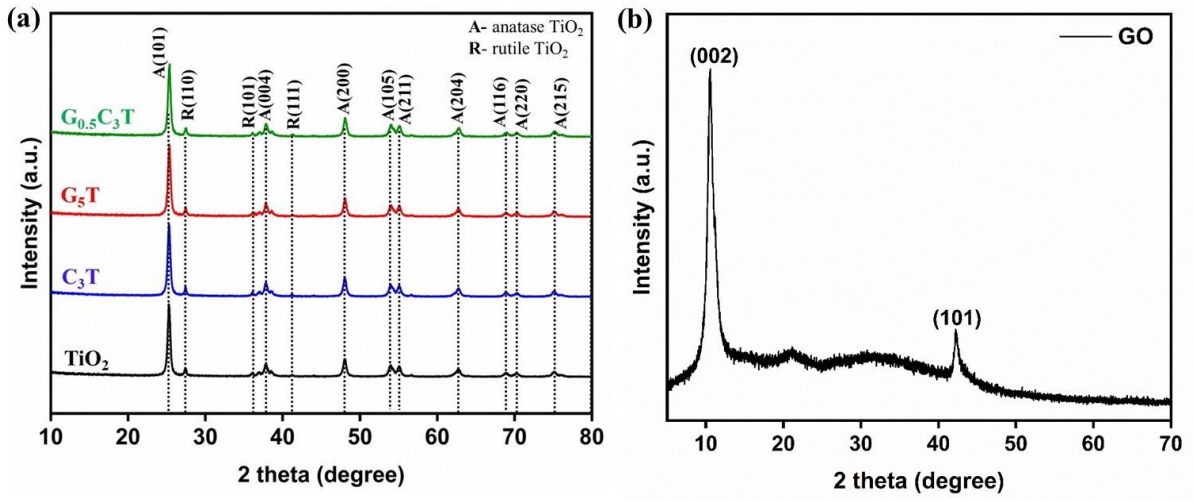

Fig.3.1: XRD pattern of the prepared composites.

3.3.1.2 Surface morphological studies

FE-SEM, EDX, and HR-TEM analyses were conducted on the newly synthesised C_3T and $G_{0.5}C_3T$ ternary nanocomposite in order to analyse its morphological and structural characteristics. As seen in **Fig.3.2(a)**, given that the C_3T composite had a low weight percentage deposition of Cu, the deposition of Cu on the TiO_2 surface was not observable. The presence of Cu in the C_3T composite was confirmed by EDX spectra in **Fig.3.2(c)**. The elemental composition of Cu was found to be 2.56 wt%, which nearly matched the 3wt% of Cu photo-deposited over TiO_2. The disparity between the desired and obtained elemental weight percentages may be attributed to the limited scanning of a specific area of the catalyst and the inevitable loss of some weight percentage of Cu during the washing process. **Fig.3.2(b)** depicts the non-uniform dispersion of Cu-TiO_2 nanoparticles over the GO sheets. The EDX spectra, **Fig.3.2(d)**, show the elemental composition of elements C, O, Ti, and Cu in the $G_{0.5}C_3T$ ternary composite.

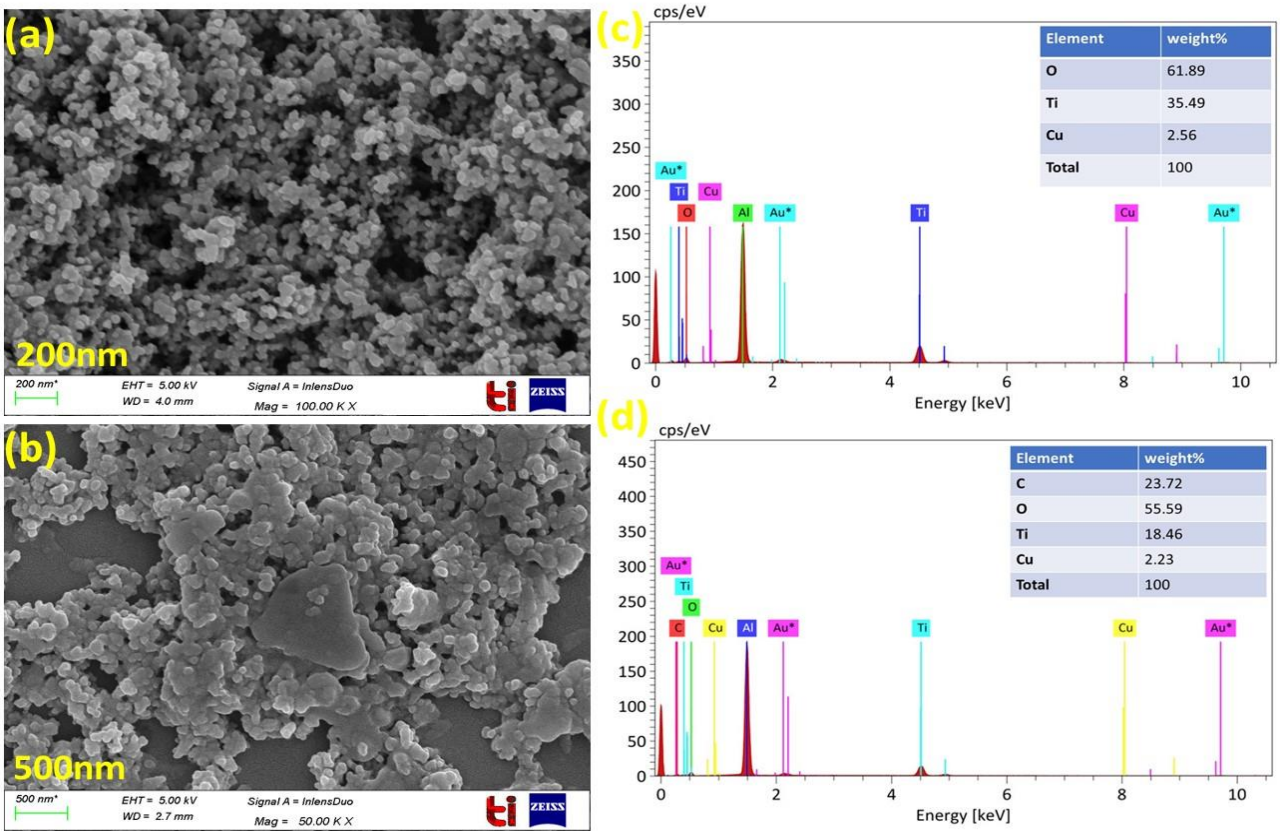

Fig.3.2: FE-SEM image & EDX spectra of (a,c) C_3T (b,d) $G_{0.5}C_3T$ composite.

The HRTEM analysis of the C_3T composite is represented in **Fig.3.3(a)**. The small spherical particles of Cu, which are dark grey in colour and highlighted by the red circle, can be clearly seen deposited on the light grey-coloured spherical-shaped TiO_2, circled in yellow. **Fig.3.3(b&c)** represents two different nm scales, i.e. 50 nm and 20nm, respectively, of the $G_{0.5}C_3T$ composite. The Cu-TiO_2 nanoparticles are clearly seen deposited over the GO sheets. The plane (111) was identified as a lattice fringe with a d-spacing of 0.208 nm for Cu nanoparticles, while a fringe with a lattice spacing of 0.363 nm was attributed to the (101) crystal plane of TiO_2 deposited on the GO sheet, **Fig.3.3(d)**inset.

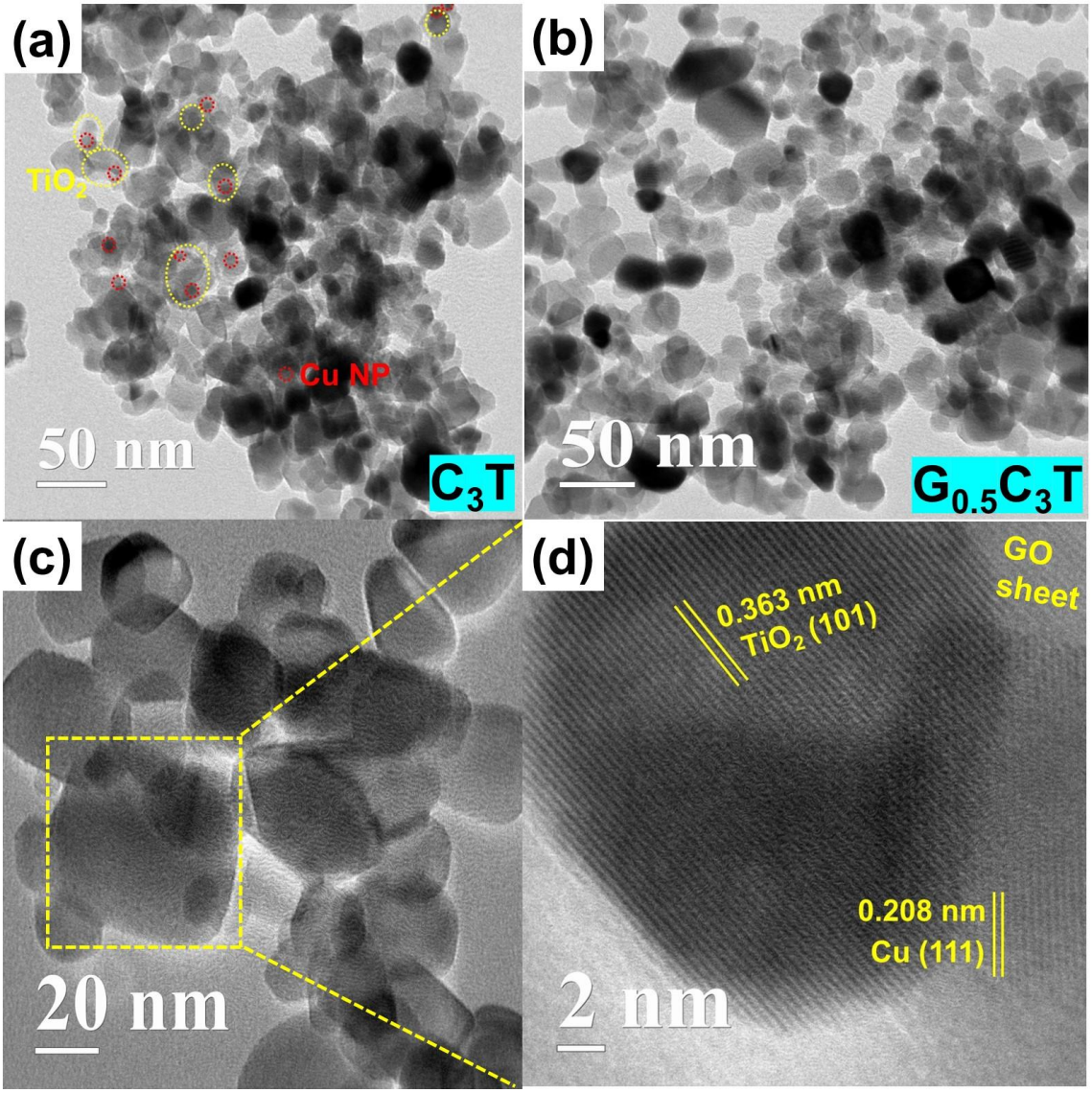

Fig.3.3: HRTEM images of (a) C_3T (b,c) $G_{0.5}C_3T$ composite (d) inset corresponding lattice fringes.

3.3.1.3 Raman analysis

Fig.3.4(a) analyses the Raman shifts of different synthesised samples ranging from 100 cm^{-1} to 2000 cm^{-1}. The prepared samples showed peaks at 146, 394, 515, and 635 cm^{-1} for E_g (O-Ti-O symmetric stretching), A_{1g} and E_g (O-Ti-O asymmetric stretching), and B_{1g} (O-Ti-O wag) modes, which were consistent with anatase TiO_2. After depositing the Cu, no shift or broadening of the peaks is observed in the C_3T composite, demonstrating the TiO_2 structure remained intact. The presence of GO in the $G_{0.5}C_3T$ composite was further confirmed by the Raman spectroscopy. In **Fig.3.4(b)**, the characteristic D and G bands of GO appeared at 1347 and 1595 cm^{-1} (as shown in the inset picture), confirming the formation of the $G_{0.5}C_3T$ composite.

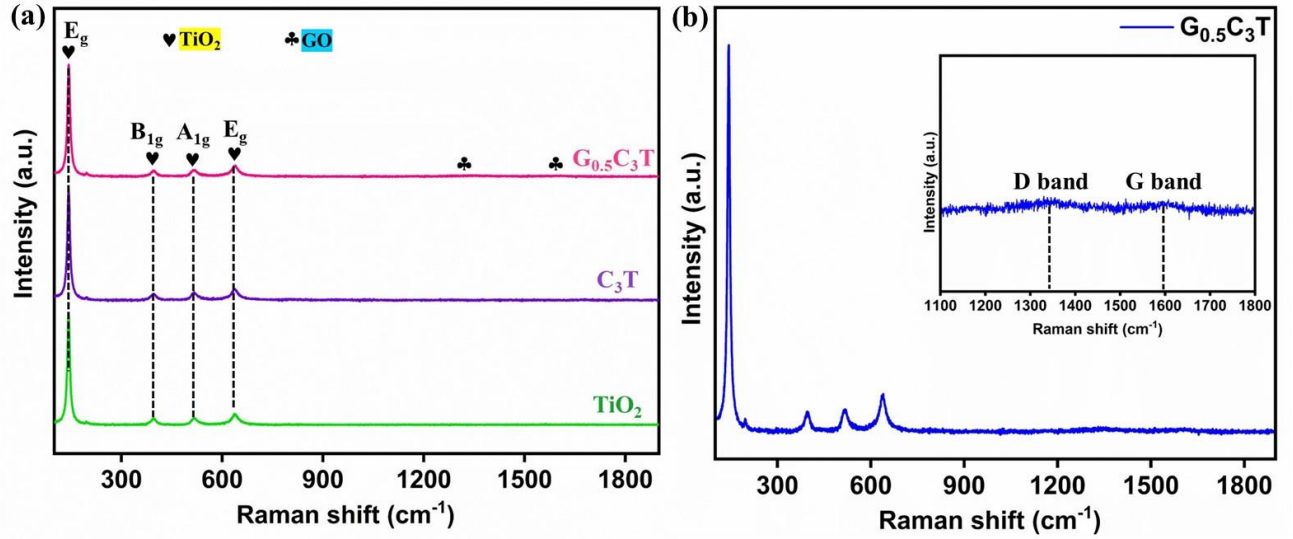

Fig.3.4: (a)Raman Spectra of TiO_2, C_3T, $G_{0.5}C_3T$ composite. (b) The inset image shows the GO-loaded sample's characteristic D and G bands.

3.3.1.4 Optical studies

Using diffuse reflectance spectroscopy, the light absorption, or optical characteristics, of the as-fabricated samples were visualised. The results are shown in **Fig.3.5**. The comparative photo absorption capacities of bare TiO_2 and photo-deposited Cu-TiO_2 and GO-modified Cu-TiO_2 composites were studied. The bare TiO_2 exhibits a significant absorption in the UV spectrum, with a maximum absorption at approximately 329 nm. The broad absorption band in the visible range, spanning 500-800 nm, was observed following the deposition of plasmonic metal (Cu).

This observation confirmed the deposition of Cu nanoparticles over the TiO_2, which explains the wide peak observed in the C_3T and $G_{0.5}C_3T$ composites.

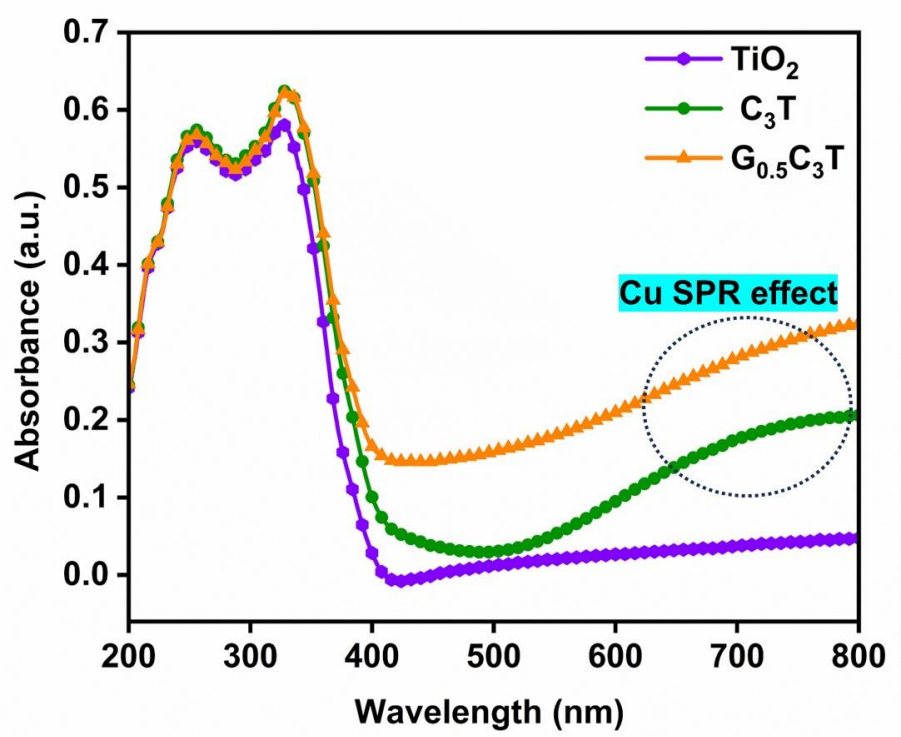

Fig.3.5: Diffuse reflectance spectra of the synthesised composites.

The Kubelka-Munk equation was utilised to analyse the DRS spectra using the following equation no.3.1. The bandgap energy of the composites was obtained by extending the linear portion of the curve in Tauc's plot (αhν vs. hν) to calculate the value of (αhν) when it intersects with the x-axis.

$$\alpha h\nu = A(h\nu - E_g)^n \qquad \text{(equation no. 3.1)}$$

where α denotes the absorption coefficient, h is the Planck's constant, υ is light's frequency, A = constant, n= ½ or 2 (for allowed direct and indirect electronic transitions respectively), E_g denotes the bandgap energy.

The E_g values were determined for n= ½ (allowed direct transition) for bare TiO_2, C_3T, and $G_{0.5}C_3T$ composite. The calculated values were 3.25 eV, 2.92 eV, and 2.67 eV, respectively, as shown in **Fig.3.6**. Significantly, the band gap value decreases from 3.2 eV (for TiO_2) to 2.67 eV (for $G_{0.5}C_3T$), signifying the role of Cu and GO in reducing the band gap and enhancing the optical properties of the TiO_2 composites in the visible range.

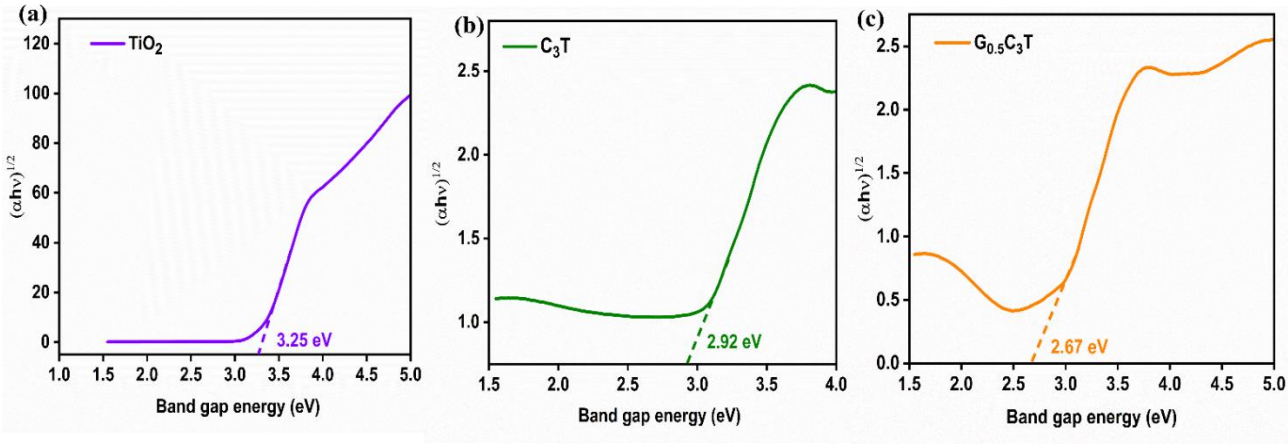

Fig.3.6: Tauc plots for allowed direct transition of prepared samples (a) TiO_2, (b) C_3T and (c) $G_{0.5}C_3T$ composites.

3.3.1.5 BET analysis

To describe the surface characteristics and pore size distributions of the as-synthesised materials, the N_2 adsorption-desorption isotherms (as shown in **Fig.3.7**) were examined. The bare TiO_2 and synthesized $G_{0.5}C_3T$ composite both followed type IV isotherm with type H3 hysteresis loop representing the mesoporous nature and slit-shape-like pores. The surface area determined using the BET technique of bare TiO_2 was 48.5 m^2/g, which slightly increased to 51.4 m^2/g in the case of $G_{0.5}C_3T$ composite, which might be due to the deposition of GO and Cu over TiO_2. The pore size was also determined from the BJH curve; the average pore size was found to be 5.34 nm in the case of TiO_2 and 12.85 nm in the case of the $G_{0.5}C_3T$ composite.

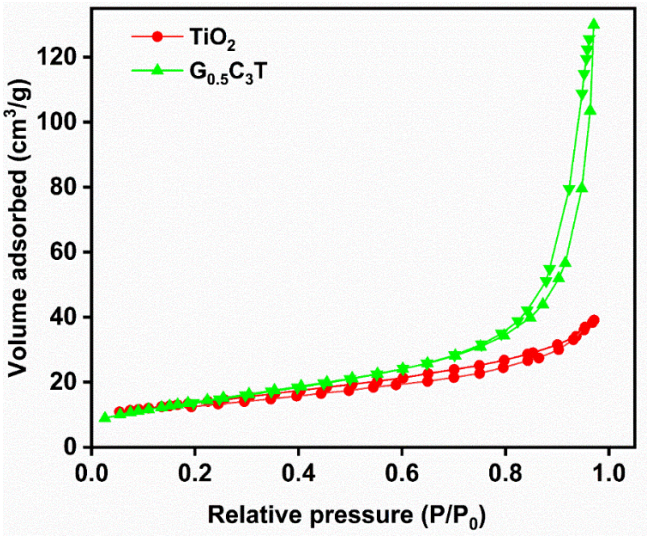

Fig.3.7: N_2 adsorption-desorption isotherm of the composites.

3.3.1.6 XPS analysis

X-ray photoelectron spectroscopy (XPS) was used to determine the elemental composition and elemental states of the synthesised $G_{0.5}C_3T$ composite. The XPS spectra of Ti 2p, as shown in **Fig.3.8(a)**, contained peaks at 458.6 eV ($2p_{3/2}$) and 464.3 eV ($2p_{1/2}$). The existence of Ti in (+4) oxidation state is indicated by its high agreement with the characteristic binding energy of Ti in pure TiO_2. The 529.8 eV and 531.6 eV peaks in the O 1s spectra of **Fig.3.8(b**) correspond to O^{2-} and C–O in the TiO_2 lattice, respectively [39,40]. The binding energy peaks at 284.2 eV,285.07 eV, 286.9 eV, and 289 eV correspond to the C=C, C–C, C-O and C= O groups, respectively. For O 1s (GO), the peaks at 530 eV,532 eV, and 533 eV fit for the O-C=O, C=O, and C-O, respectively, thus confirming the formation of the GO composite[41]. The XPS spectra of C 1s in **Fig.3.8(c)** displayed peaks at 284.87 eV and 288.9 eV, which fitted precisely to C–Cand C= O, respectively. The XPS spectra in **Fig.3.8(d)** displayed two binding energy peaks at 932.6 eV ($2p_{3/2}$) and 952.2 eV($2p_{1/2}$) for the Cu 2p orbitals. The difference between these peaks, which is 6 eV, indicates Cu in the (0) oxidation state. The observed satellite peak of Cu 2p is expected to be present in the presence of Cu_2O and CuO[42,43].

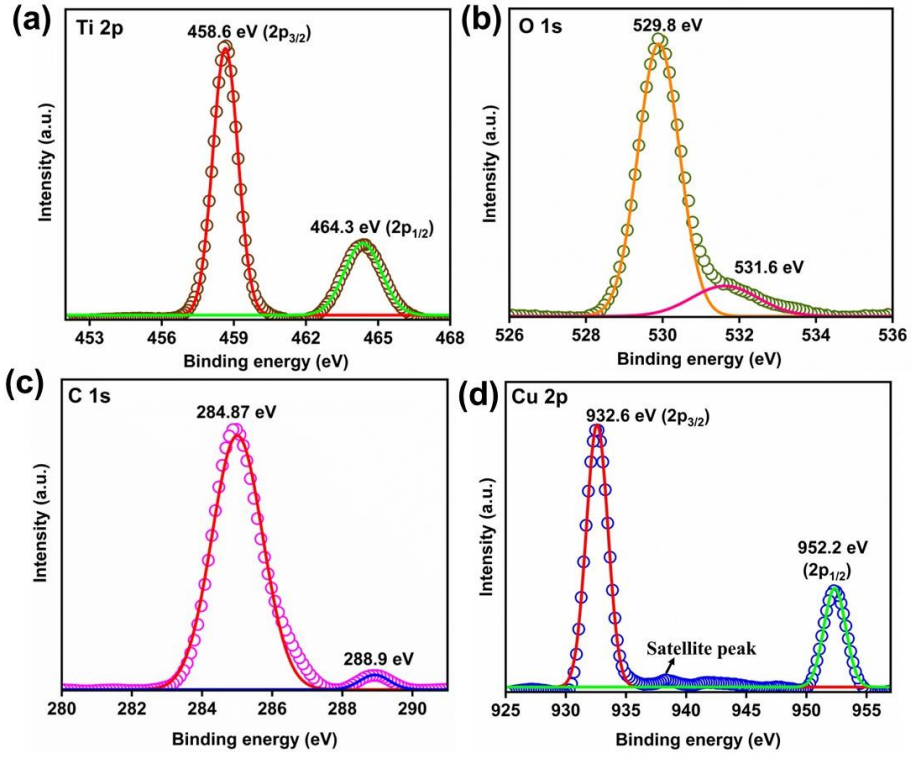

Fig.3.8: XPS spectra of prepared $G_{0.5}C_3T$ composite: (a) Ti 2p, (b) O 1s, (c) C 1s and (d) Cu 2p.

3.3.2 Photocatalytic Hydrogen production under UV and sunlight

3.3.2.1 Influence of loading of metal(Cu) and GO over TiO_2

The influence of photo-deposition of diff. wt% (1,3,5) Cu metal over TiO_2 was examined for the hydrogen evolution from photocatalytic dehydrogenation of methanol solution (50vol%), shown in **Fig.3.9(a)**. The photocatalytic activity of TiO_2 was very low, producing 38 mmol of hydrogen after 4h in UV light as compared to C_1T(115 mmol), C_3T(217 mmol), and C_5T(163 mmol). The findings suggested that a 3wt% Cu-TiO_2 (C_3T) composite yielded the greatest quantity of hydrogen, thereby optimising the Cu content. Similarly, the effect of different weight% (0.5,1, 3, 5) of GO loading on TiO_2 was examined in terms of the hydrogen evolution that occurred during the photocatalytic methanol dehydrogenation of a 50% solution exposed to UV light for 4h. **Fig.3.9(b)** illustrates the amount of hydrogen generated by different GT composites, indicating that the 5 wt% GO-TiO_2 (G_5T) composite produced the highest amount of hydrogen compared to the other weight% synthesised composites. The bare TiO_2 showed the least amount of hydrogen evolved, which was 38 mmol, as compared to $G_{0.5}T$(11mmol)<G_1T(18mmol)<G_3T(26mmol)<G_5T(42mmol). The performance of TiO_2, C_3T, and ternary different wt% (0.5,1, 3, 5) GO/C_3T photocatalysts in hydrogen evolution under UV light with a methanol solution(50vol%) for 4h is illustrated in **Fig.3.9(c)**. Among all of the composites, the $G_{0.5}C_3T$ produced the highest amount of hydrogen (294 mmol), which is approx. 7.7 times as compared to bare TiO_2 (38 mmol).

The prepared catalysts were evaluated under direct sunlight under identical experimental conditions, as shown in **Fig.3.10(a-c)**. The results followed the same trend with different wt% Cu and GO loading as shown under UV light, but the amount of hydrogen produced was much higher than that produced by UV light. The C_3T composite produced 636 mmol of hydrogen in sunlight, as compared to 217 mmol produced under UV light. The G_5T composite produced ~ 2 times higher hydrogen in sunlight than that under UV light.

The results compared the efficiency of the GO-modified C_3T composites under two different light sources (as shown in **Table 3.1**). The GO-modified C_3T ternary composites possessed higher photocatalytic dehydrogenation ability (both in UV and sunlight) than bare TiO_2, binary Cu-TiO_2 and GO-TiO_2 composites. The 0.5 wt% GO loaded over C_3T ($G_{0.5}C_3T$) composite displayed the highest efficiency amongst all composites, highlighting the synergistic effect of GO, Cu, and TiO_2. The different wt% loadings of GO over C_3T followed the order: $G_{0.5}C_3T$ >

G_1C_3T > G_3C_3T > G_5C_3T. The $G_{0.5}C_3T$ composite produced ~3folds higher hydrogen in sunlight than the UV light source.

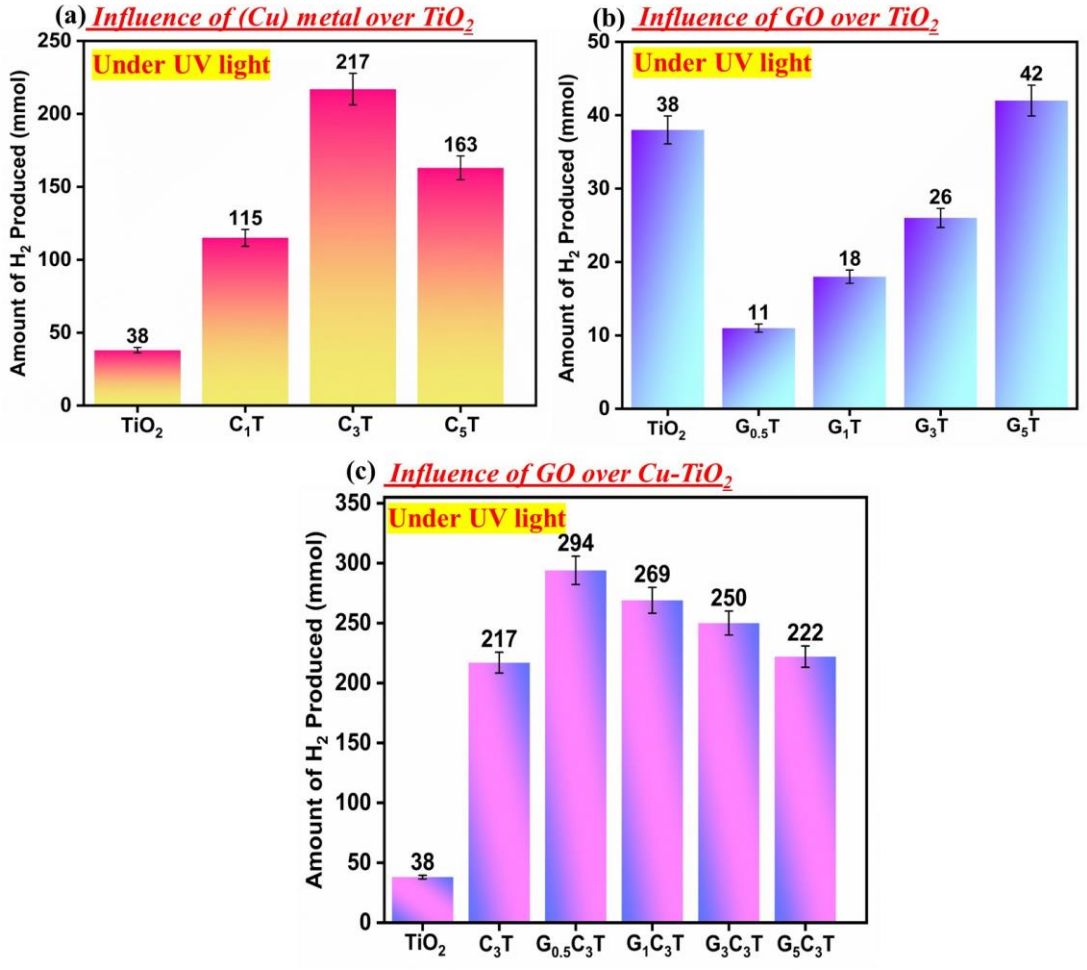

Fig.3.9: Histogram representing the influence of (a) Cu metal and (b) GO over TiO_2 (c) GO modified Cu- TiO_2 on the amount of hydrogen gas produced (mmol) by different catalysts in 10ml methanol solution(50 vol%) under UV light for 4 h.

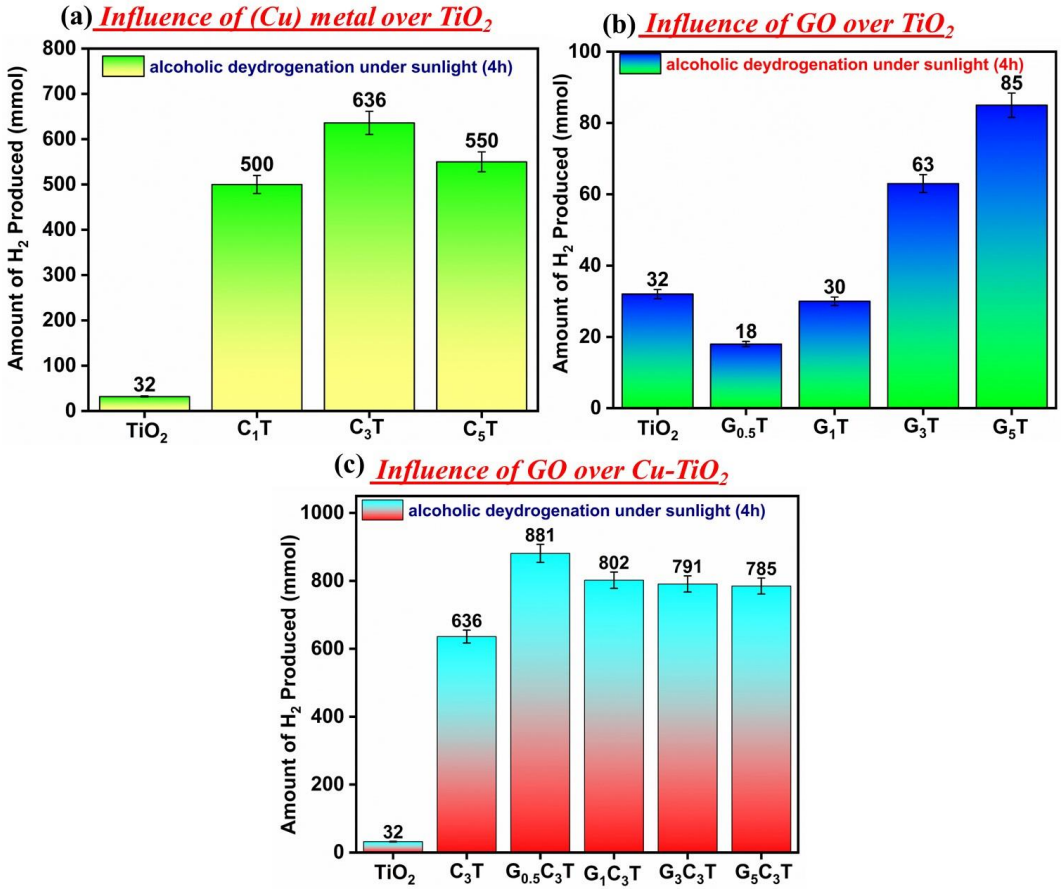

Fig.3.10: Histogram representing the influence of (a) Cu metal and (b) GO over TiO_2 (c) GO modified Cu- TiO_2 on the amount of hydrogen gas produced (mmol) by various catalysts in 10ml methanol solution (50 vol%) under sunlight for 4 h.

The GC chromatograms related to hydrogen production after 4h by different catalysts under UV are shown in **Fig.3.11**. The findings suggested that increasing the weight percent (1,3,5 wt.%) of GO into the photocatalyst resulted in a decline in the amount of hydrogen production. This can be attributed to the fact that excess GO would increase photon absorption and scattering that occurred during the photocatalytic process[44].

Sr. no.	Catalyst	Methanol dehydrogenation (in mmol) (under UV light)	Methanol dehydrogenation (in mmol) (under sunlight)
1.	TiO_2	38	32
2.	G_5T	42	85
3.	C_3T	217	636
4.	$G_{0.5}C_3T$	294	881

Table 3.1: Comparison of the synthesized photocatalysts for methanol dehydrogenation.

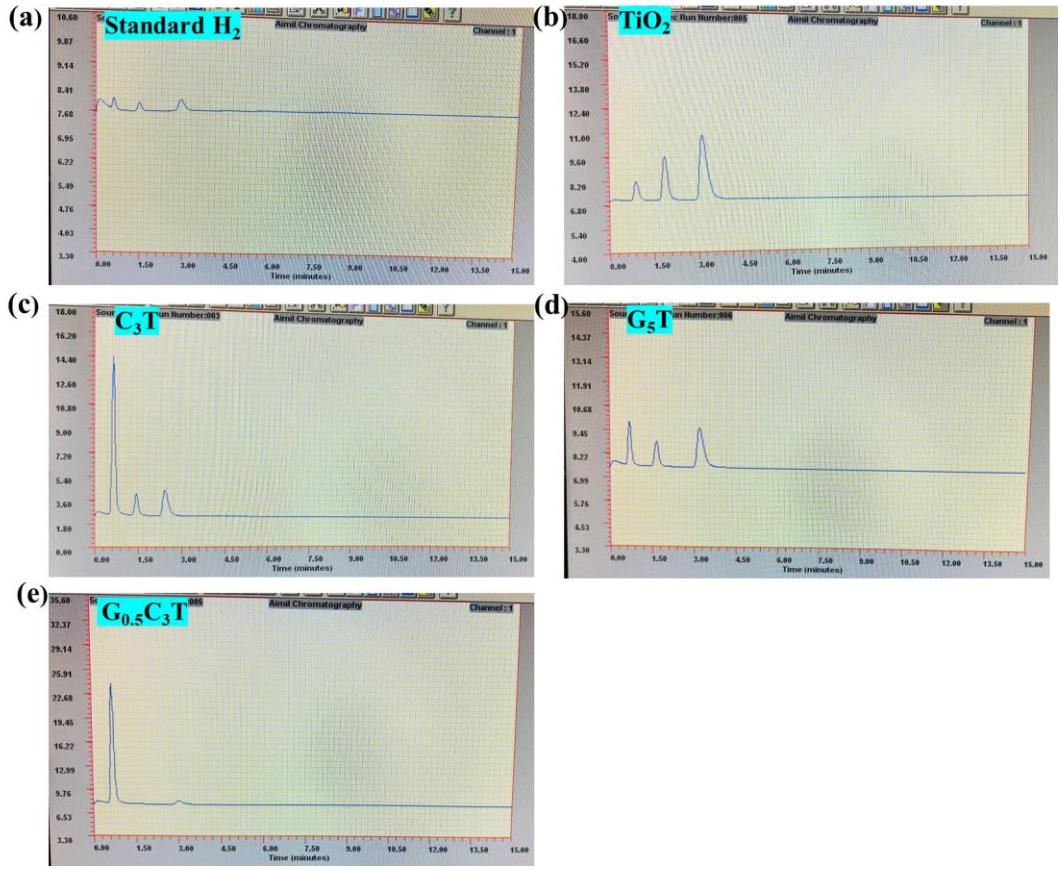

Fig.3.11: GC spectra of methanol dehydrogenation by different prepared catalysts in UV light after 4h.

The results indicate that the addition of an optimal amount of GO improved the activity of photocatalytic hydrogen generation. **Fig.3.12(a and b)** demonstrates the time course study of the reaction that took over 4h under UV light and sunlight, respectively. The samples were taken out after every one-hour time interval and analysed with the help of GC. The graph shows that the $G_{0.5}C_3T$ composite produced the maximum amount of hydrogen among different catalysts over a time period of 4h. The hydrogen evolution rate was compared for TiO_2, C_3T, G_5T, and $G_{0.5}C_3T$ photocatalysts under UV light and sunlight irradiation. **Fig.3.12(c)** illustrates the hydrogen evolution rate was much higher for the $G_{0.5}C_3T$ catalyst for methanol dehydrogenation under sunlight(210 mmol/h) than under UV light(76 mmol/h). Similarly, for other catalysts, the hydrogen evolution rate was also higher in sunlight than in UV light, indicating the importance of the source of light used. The catalysts exhibited the following order when exposed to UV light: TiO_2 (10mmol/h) <G_5T (11 mmol/h)< C_3T (55 mmol/h)< $G_{0.5}C_3T$ (74 mmol/h). Under sunlight, the catalysts followed the order: TiO_2 (8mmol/h) <G_5T (21mmol/h)< C_3T (159 mmol/h)< $G_{0.5}C_3T$ (220 mmol/h).

A comparison table was drawn to better understand the photocatalytic hydrogen produced by the prepared composites compared to that of other recently reported literature in **Table 3.2**.

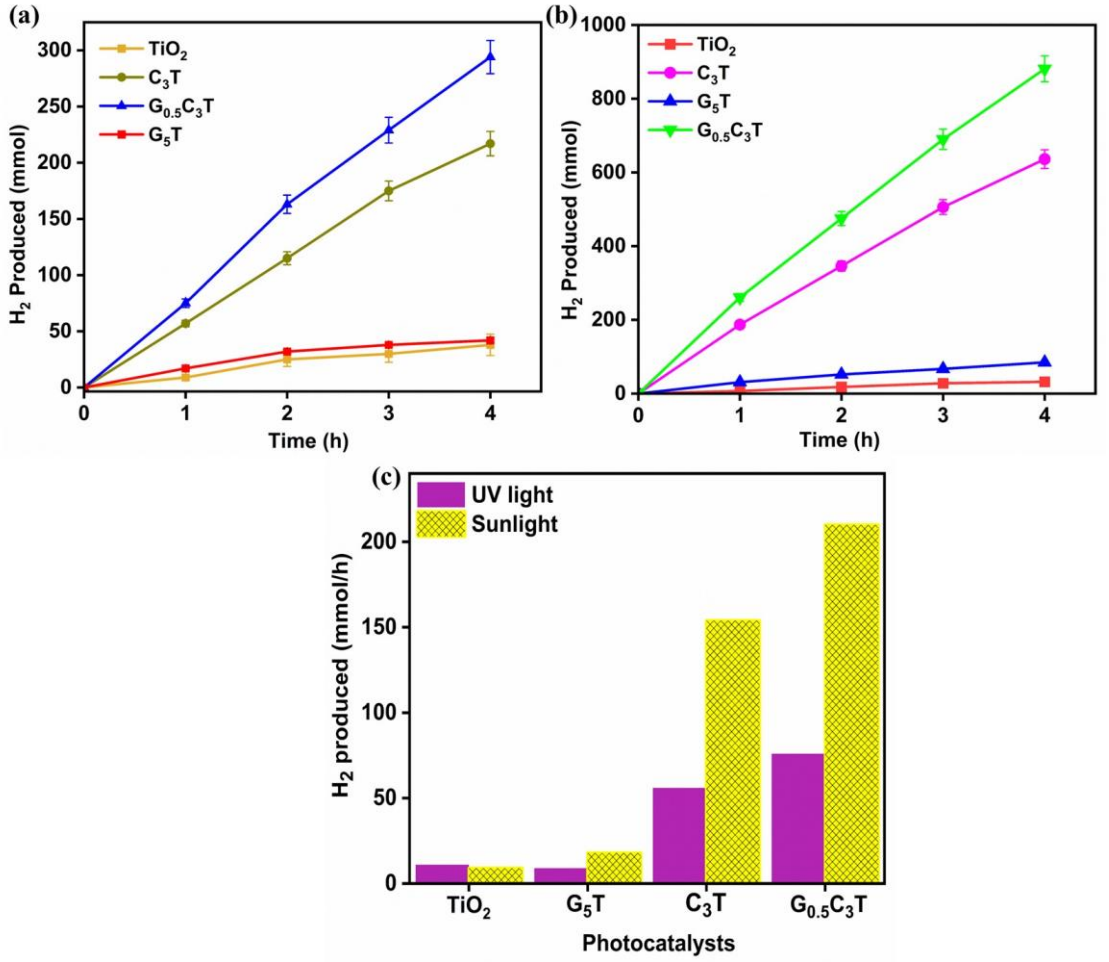

Fig.3.12: Time course graph of H_2 production from dehydrogenation of methanol solution by different catalysts under (a) UV irradiation, (b) sunlight, and (c) Comparative hydrogen evolution rates for methanol dehydrogenation under UV and sunlight.

Sr.no.	Photo-catalyst	Light source	Reaction time	Alcohol used	H_2 production	References
1.	Pt/P25	UV	2h	Methanol	71.53 mmol g^{-1} h^{-1}	[45]
2.	1wt% Cu-TiO_2	UV	3h	Methanol	23.2 mmol g^{-1} h^{-1}	[46]
3.	Pd/ TiO_2	Visible lamp	2h	Methanol	22835 $\mu mol \cdot g^{-1} \cdot h^{-1}$	[47]

4.	Rh-Cu/TiO_2	UV	6h	Methanol	9272 $\mu mol \cdot g^{-1} \cdot h^{-1}$	[48]
5.	$G_{0.5}C_3T$	UV	4h	Methanol	1470 mmol h^{-1} g^{-1}	This work
6.	$G_{0.5}C_3T$	sunlight	4h	Methanol	4405 mmol h^{-1} g^{-1}	This work

Table 3.2: Comparison table of different photocatalysts for methanol dehydrogenation under light irradiation.

3.3.2.2 Influence of chain length and concentration of solution

To check the behaviour of different alcohols (methanol, ethanol, propanol), the dehydrogenation of these alcohols with the best-proved catalyst, $G_{0.5}C_3T$, under the optimised conditions mentioned above was conducted. **Fig.3.13(a)** illustrates the results that in the same vol% of alcohols, methanol produced the highest amount of hydrogen (294 mmol) as compared to ethanol(185 mmol) and propanol(90 mmol). In terms of hydrogen production, the most effective organic compounds were methanol>ethanol> propanol. The breakdown of these organic molecules contributes to increased hydrogen production, as hydrogen is one of their constituents. In this manner, adding sacrificial reagents can improve the process of photocatalytic hydrogen production. Organic compounds, including alcohols, and aldehydes, organic acids have been tested and found to be effective as electron donors for hydrogen production in photocatalytic reactions [48]. Among these compounds, methanol has been identified as the most efficient sacrificial reagent compared to other alcohols. According to reports, the amount of hydrogen produced reduces as the carbon number increases in the alcohol(methanol>ethanol> propanol)[48,49]. The primary cause of this effect is the decrease in the production of formaldehyde for higher alcohols. This occurs because the process of forming formaldehyde requires breaking C-C bonds. As the chain length and complexity of the alcohol molecule increase, the steric hindrance is enhanced, leading to a decrease in hydrogen production.

The results were different when the same concentration of different alcohol was taken in **Fig.3.13(b&d)**. It was found that ethanol showed the highest amount of hydrogen production. The probable reason could be that the stability of the intermediate species generated during this process can impact the effectiveness of hydrogen generation. Ethanol, methanol, and propanol undergo dehydrogenation to produce distinct intermediate species, and the stability of these

intermediates can differ. The intermediate of ethanol, acetaldehyde, may have characteristics that promote more efficient dehydrogenation and hydrogen release compared to the intermediates produced from methanol and propanol.

The above-mentioned experiments were performed under sunlight in order to examine the influence of light sources on hydrogen production. Although the results followed the same pattern as discussed under UV light, the amount of hydrogen produced during the dehydrogenation of alcohols was much higher, emphasising the importance of the source (i.e. sunlight). In comparison to ethanol (625 mmol) and propanol solutions (472 mmol), **Fig.3.13(c)** shows that hydrogen production was highest (in 50vol%) with methanol solution (881 mmol). Of the three different alcohols, the ethanol solution produced the highest amount of hydrogen in the case of 0.5M solutions (**Fig.3.13(d)**).

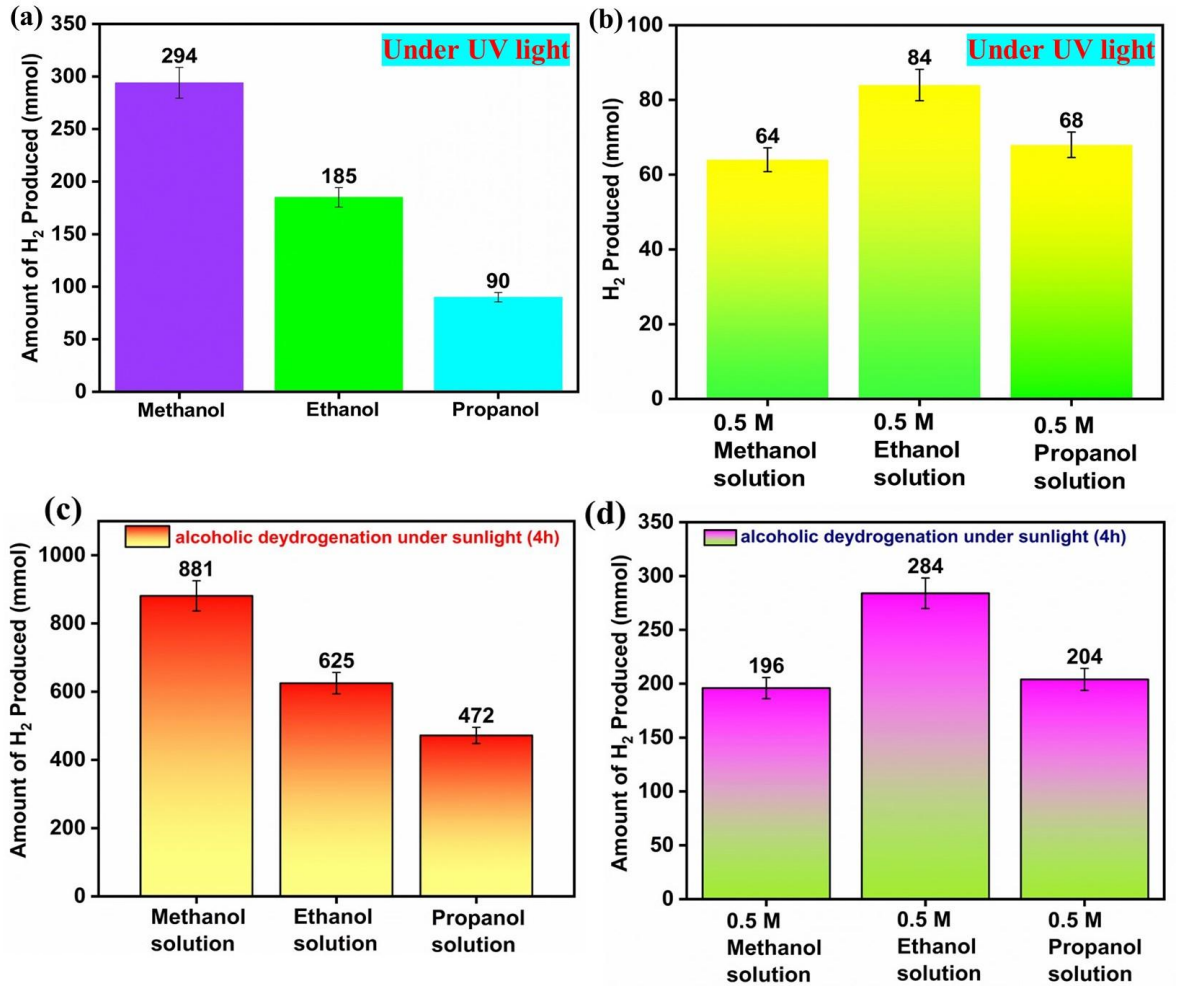

Fig.3.13: The influence of (a&c) different alcohol (50 vol%) solutions (b&d) same concentration of alcoholic solutions (0.5 M) on hydrogen production studied with the help of $G_{0.5}C_3T$ composite under UV and sunlight.

Fig.3.14(a) illustrates the amount of hydrogen produced using various molar concentrations of methanol solution under the same reaction conditions. As the concentration of the solution increased, the amount of hydrogen evolution correspondingly increased. The highest amount of hydrogen evolution was achieved using a 12.35 M methanol solution (estimated to be 50vol%), justifying the use of the 50vol% methanol solution taken during the dehydrogenation process.

3.3.2.3 Reusability test

The reusability of the $G_{0.5}C_3T$ catalyst was assessed through four cycles for the photocatalytic methanol dehydrogenation using the same experimental conditions indicated above. The catalyst was retrieved from the solution using centrifugation, rinsed with distilled water, dried, and subsequently reused for further runs. **Fig.3.14(b)** demonstrates that the catalyst produced a significant amount of hydrogen up to four cycles under the same experimental conditions in comparison to the original run.

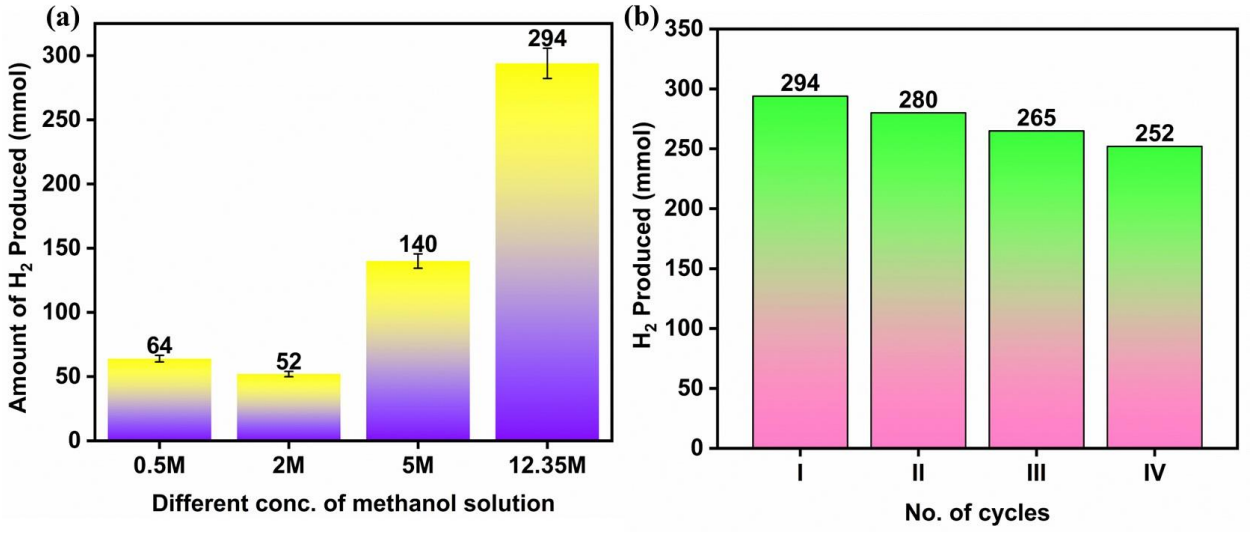

Fig.3.14: (a)The influence of different molar concentrations of methanol solutions over hydrogen production with the $G_{0.5}C_3T$ composite under UV light, (b)H_2 production by the $G_{0.5}C_3T$ photocatalyst for four cycles.

3.3.2.4 Proposed photocatalytic dehydrogenation of methanol mechanism

Scheme 3.1 depicts the most plausible mechanism that could be occurring given the current experimental conditions. The band edge positions for TiO_2 were calculated from the Valence band XPS spectra (**Fig.3.15**). The valence band (VB) position was determined to be +2.85 eV, and the conduction band (CB) position was calculated to be -0.4 eV using the band gap value for the semiconductor TiO_2, which is 3.25 eV. The current mechanism is suggested based on

the findings derived from the activity results for the superior activity of the $G_{0.5}C_3T$ catalyst and the characterisation studies stated above. When exposed to ultraviolet (UV) radiation /sunlight, the photocatalyst TiO_2 undergoes a process where electrons in the valence band (VB) of TiO_2 get excited and go to the conduction band (CB). However, the catalyst's photocatalytic hydrogen production is not high due to the rapid recombination rate of the electron-hole pairs. To delay this quick recombination rate, Cu metal was photo-deposited over TiO_2 composite, and due to the SPR and electron trapping effect of Cu, the electrons get captured by the metal, thus decreasing the recombination rate, which enhances the photocatalytic property of the TiO_2 catalyst for hydrogen production. These e^-s are subsequently transferred to the GO surface, which has exceptional conduction and electron storage properties. Due to the lower reduction potential of GO (-0.08 eV) than TiO_2 (-0.24 eV), the e^-s get transferred on the GO sheet, thus further enhancing the electron-hole recombination rate and resulting in the reduction of H^+ to hydrogen[50,51]. Methanol molecules present in the reaction are oxidised by the holes in the VB of TiO_2 to formaldehyde. The above-suggested mechanism explains the higher photocatalytic efficiency of the $G_{0.5}C_3T$ catalyst, indicating the importance of loading GO and Cu metal over TiO_2 and their combined cooperative effect on the catalyst.

The photooxidation reaction of dehydrogenation of methanol is assumingly supposed to take place by the following chemical equations:

$$CH_3OH \xrightarrow{h\nu,photocatlyst} HCH0 + H_2\ (\Delta G° = 64\ kJpermol),$$

$$HCHO + H_2O \xrightarrow{h\nu,photocatlyst} HCOOH + H_2\ \ (\Delta G° = 47\ kJpermol),$$

$$HCOOH \xrightarrow{h\nu,photocatlyst} CO_2 + H_2\ \ (\Delta G° = -95.8\ kJpermol).$$

This mechanism is supported by earlier findings[52–54]. Nalajala et al. performed the HPLC analysis to explain the mechanism with the help of the obtained products. The results emphasised that the test solution exhibited a new peak that corresponded to formaldehyde, in addition to methanol and water, along with a trace amount of formic acid formation; however, no CO_2 was observed[52].

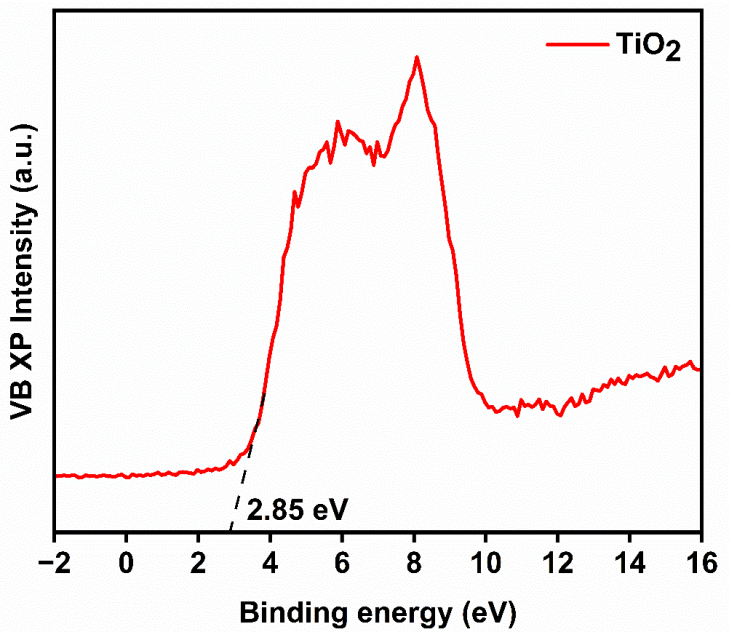

Fig.3.15: XPS valence band spectra of the semiconductor TiO_2.

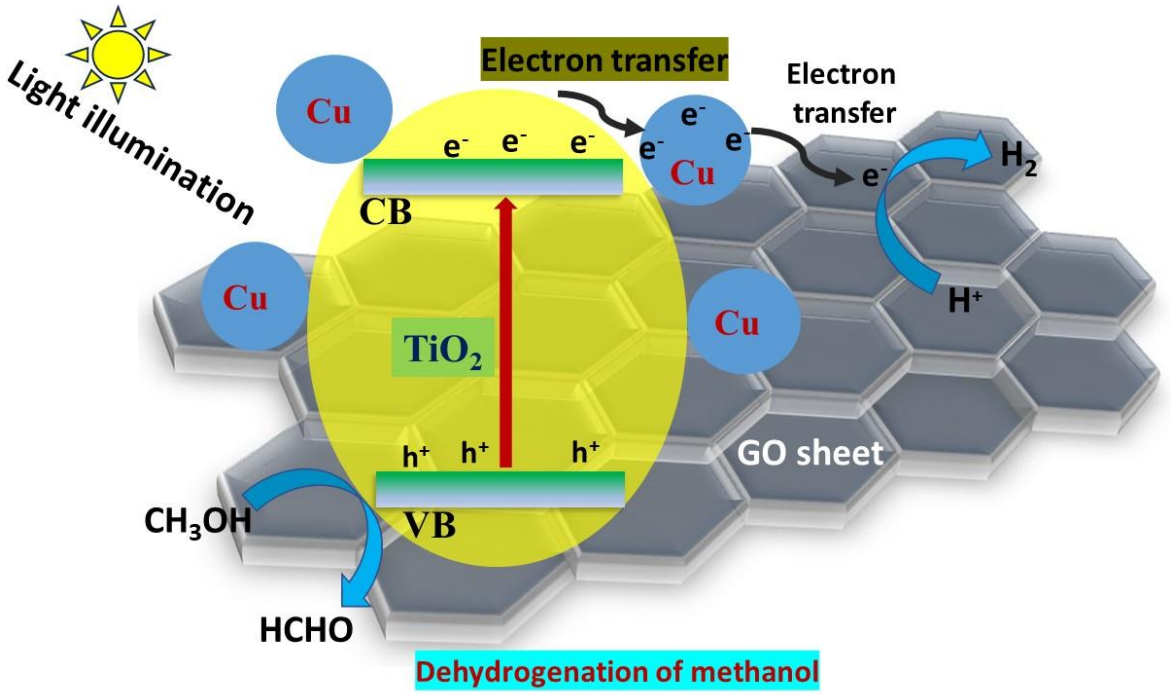

Scheme 3.1: The plausible reaction mechanism of photocatalytic dehydrogenation of methanol over $G_{0.5}C_3T$ composite under light irradiation.

3.4 Conclusion

To summarise, this work involved the synthesis of a ternary GO-modified Cu-TiO_2 photocatalyst using hydrothermal and photo-deposition methods. The attributes of the optimal $G_{0.5}C_3T$ have been extensively examined using various techniques, including analysis of its structural, morphological, chemical composition, optical properties, etc. These investigations have confirmed the successful formation of the nanomaterial. The photoactivity of TiO_2 has been extensively improved by photo-depositing Cu metal and GO loading over its surface, which resulted in higher photocatalytic methanol dehydrogenation under UV and sunlight irradiation. Various parameters, such as the influence of different wt% of Cu metal and GO loading, source of light, the influence of chain length of alcohols, concentration, and time kinetics, were studied thoroughly. For practical purposes, the recyclability of the catalyst was studied, and the results demonstrated that the catalyst produced a significant amount of hydrogen up to four cycles. For photocatalytic methanol dehydrogenation, the $G_{0.5}C_3T$ composite produced ~3fold higher hydrogen in sunlight than the UV light source. The results validate that GO loading and Cu metal are highly encouraging substitute co-catalysts for costly noble metal-based co-catalysts (such as Pd, Pt, and Au) in activating TiO_2 for solar hydrogen generation in alcohol-water mixtures. In the future, GO-modified metal-TiO_2 or other semiconductors could enable the examination of hydrogen production from various waste industrial alcohols or laboratory organic solvents. This process is considered a green fuel solution, and it utilises low-cost synthesised photocatalysts to convert these materials into usable energy sources.

References

1. Nahar G, Mote D, Dupont V. Hydrogen production from reforming of biogas: Review of technological advances and an Indian perspective. Renew Sustain Energy Rev. 2017;76:1032–52.

2. Wolff CM, Frischmann PD, Schulze M, Bohn BJ, Wein R, Livadas P, et al. All-in-one visible-light-driven water splitting by combining nanoparticulate and molecular co-catalysts on CdS nanorods. Nat Energy [Internet]. 2018;3:862–9. Available from: https://doi.org/10.1038/s41560-018-0229-6

3. Landman A, Dotan H, Shter GE, Wullenkord M, Houaijia A, Maljusch A, et al. Photoelectrochemical water splitting in separate oxygen and hydrogen cells. Nat Mater [Internet]. 2017;16:646–51. Available from: https://doi.org/10.1038/nmat4876

4. Nowotny J, Sorrell CC, Sheppard LR, Bak T. Solar-hydrogen: Environmentally safe fuel for the future. Int J Hydrogen Energy [Internet]. 2005;30:521–44. Available from: https://www.sciencedirect.com/science/article/pii/S0360319904002447

5. Kumar R, Kumar A, Pal A. An overview of conventional and non-conventional hydrogen production methods. Mater Today Proc [Internet]. 2021;46:5353–9. Available from: https://www.sciencedirect.com/science/article/pii/S2214785320366839

6. Xing C, Liu Y, Zhang Y, Wang X, Guardia P, Yao L, et al. A Direct Z-Scheme for the Photocatalytic Hydrogen Production from a Water Ethanol Mixture on CoTiO3/TiO2 Heterostructures. ACS Appl Mater Interfaces [Internet]. 2021;13:449–57. Available from: https://doi.org/10.1021/acsami.0c17004

7. Al-Qurahi MAA, Demir MC, Tümer B, Gökçal B, Tuncel A. Formic acid dehydrogenation catalyzed by bimetallic nanoalloys supported by monodisperse-porous microspheres: Catalytic and visible light driven photocatalytic hydrogen generation. Int J Hydrogen Energy [Internet]. 2024;51:111–32. Available from: https://www.sciencedirect.com/science/article/pii/S0360319923049868

8. Zhang L, Liu L, Pan Z, Zhang R, Gao Z, Wang G, et al. Visible-light-driven non-oxidative dehydrogenation of alkanes at ambient conditions. Nat Energy [Internet]. 2022;7:1042–51. Available from: https://doi.org/10.1038/s41560-022-01127-1

9. Zhang L, Jiang D, Irfan RM, Tang S, Chen X, Du P. Highly efficient and selective photocatalytic dehydrogenation of benzyl alcohol for simultaneous hydrogen and benzaldehyde production over Ni-decorated Zn0.5Cd0.5S solid solution. J Energy Chem [Internet]. 2019;30:71–7. Available from: https://www.sciencedirect.com/science/article/pii/S2095495618301591

10. Mogyorósi K, Kmetykó Á, Czirbus N, Veréb G, Sipos P, Dombi A. Comparison of the substrate dependent performance of Pt-, Au-and Ag-doped TiO 2 photocatalysts in H 2-production and in decomposition of various organics. React Kinet Catal Lett. 2009;98:215–25.

11. Yüksel YE. Elementary science teacher candidates' views on hydrogen as future energy carrier. Int J Hydrogen Energy. 2019;44:9817–22.

12. Lan L, Daly H, Sung R, Tuna F, Skillen N, Robertson PKJ, et al. Mechanistic Study of Glucose Photoreforming over TiO2-Based Catalysts for H2 Production. ACS Catal [Internet]. 2023;13:8574–87. Available from: https://doi.org/10.1021/acscatal.3c00858

13. Dawood F, Anda M, Shafiullah GM. Hydrogen production for energy: An overview. Int J Hydrogen Energy [Internet]. 2020;45:3847–69. Available from: https://www.sciencedirect.com/science/article/pii/S0360319919345926

14. Peng Z, Su Y, Siaj M. Encapsulation of tin oxide layers on gold nanoparticles decorated one-dimensional CdS nanoarrays for pure Z-scheme photoanodes towards solar hydrogen evolution. Appl Catal B Environ [Internet]. 2023;330:122614. Available from: https://www.sciencedirect.com/science/article/pii/S0926337323002576

15. López-Tenllado FJ, Hidalgo-Carrillo J, Montes-Jiménez V, Sánchez-López E, Urbano FJ, Marinas A. Photocatalytic production of hydrogen from binary mixtures of C-3 alcohols on Pt/TiO2: Influence of alcohol structure. Catal Today [Internet]. 2019;328:2–7. Available from: https://www.sciencedirect.com/science/article/pii/S0920586118311015

16. Liu J, Wan J, Liu L, Yang W, Low J, Gao X, et al. Synergistic effect of oxygen defect and doping engineering on S-scheme O-ZnIn2S4/TiO2-x heterojunction for effective photocatalytic hydrogen production by water reduction coupled with oxidative dehydrogenation. Chem Eng J [Internet]. 2022;430:133125. Available from: https://www.sciencedirect.com/science/article/pii/S138589472104701X

17. Sehrawat P, Raj A, Singh S, Mehta SK, Bhinder SS, Kansal SK. Solar-driven S-scheme Zn0.5Cd0.5S/MoS2 composite for photocatalytic ketorolac tromethamine degradation and hydrogen generation coupled with benzyl alcohol oxidation. Int J Hydrogen Energy [Internet]. 2024;62:17–30. Available from: https://doi.org/10.1016/j.ijhydene.2024.03.036

18. Sehrawat P, Mehta SK, Kansal SK. Synergistic enhancement of photocatalytic activity in ZnS/P-doped-MoS2 composite for hydrogen generation simultaneously oxidation of benzyl alcohol through water splitting and dye degradation. Int J Hydrogen Energy [Internet]. 2024;80:573–85. Available from: https://doi.org/10.1016/j.ijhydene.2024.07.147

19. Zhao H, Yu X, Li C-F, Yu W, Wang A, Hu Z-Y, et al. Carbon quantum dots modified TiO2 composites for hydrogen production and selective glucose photoreforming. J Energy Chem [Internet]. 2022;64:201–8. Available from: https://www.sciencedirect.com/science/article/pii/S209549562100245X

20. Deng M, Yang H, Peng L, Zhang L, Tan L, He G, et al. Insight into the boosted activity of TiO2–CoP composites for hydrogen evolution reaction: Accelerated mass transfer, optimized interfacial water, and promoted intrinsic activity. J Energy Chem [Internet]. 2022;74:111–20. Available from: https://www.sciencedirect.com/science/article/pii/S2095495622003540

21. Chen J-L, Liu M-M, Xie S-Y, Yue L-J, Gong F-L, Chai K-M, et al. Cu2O-loaded TiO2 heterojunction composites for enhanced photocatalytic H2 production. J Mol Struct [Internet]. 2022;1247:131294. Available from: https://www.sciencedirect.com/science/article/pii/S002228602101423X

22. Mohd Shah NRA, Mohamad Yunus R, Rosman NN, Wong WY, Arifin K, Jeffery Minggu L. Current progress on 3D graphene-based photocatalysts: From synthesis to photocatalytic hydrogen production. Int J Hydrogen Energy [Internet]. 2021;46:9324–40. Available from: https://www.sciencedirect.com/science/article/pii/S0360319920346541

23. Chen WT, Dong Y, Yadav P, Aughterson RD, Sun-Waterhouse D, Waterhouse GIN. Effect of alcohol sacrificial agent on the performance of Cu/TiO2 photocatalysts for UV-driven hydrogen production. Appl Catal A Gen [Internet]. 2020;602:117703. Available from: https://doi.org/10.1016/j.apcata.2020.117703

24. Eder M, Courtois C, Petzoldt P, Mackewicz S, Tschurl M, Heiz U. Size and Coverage Effects of Ni and Pt Co-Catalysts in the Photocatalytic Hydrogen Evolution from Methanol on TiO2(110). ACS Catal [Internet]. 2022;12:9579–88. Available from: https://doi.org/10.1021/acscatal.2c02230

25. Patra KK, Ghosalya MK, Bajpai H, Raj S, Gopinath CS. Oxidative Disproportionation of MoS2/GO to MoS2/MoO3–x/RGO : Integrated and Plasmonic 2D-Multifunctional Nanocomposites for Solar Hydrogen Generation from Near-Infrared and Visible Regions. J Phys Chem C [Internet]. 2019;123:21685–93. Available from: https://doi.org/10.1021/acs.jpcc.9b05983

26. Conte F, Rossetti I, Ramis G, Vaulot C, Hajjar-Garreau S, Bennici S. Low Metal Loading (Au, Ag, Pt, Pd) Photo-Catalysts Supported on TiO2 for Renewable Processes. Materials (Basel). 2022.

27. Tkachenko P, Volchek V, Kurenkova A, Gerasimov E, Popovetskiy P, Asanov I, et al. Photocatalytic H2 generation from ethanol and glucose aqueous solutions by PtOx/TiO2 composites. Int J Hydrogen Energy [Internet]. 2023;48:22366–78. Available from: https://www.sciencedirect.com/science/article/pii/S0360319922055835

28. Qiu P, Lu M, Cheng G, Li W, Liu L, Xiong J. Co-implantation of oxygen vacancy and well-dispersed Cu cocatalyst into TiO2 nanoparticles for promoting solar-to-hydrogen evolution. Int J Hydrogen Energy [Internet]. 2023;48:933–42. Available from: https://www.sciencedirect.com/science/article/pii/S0360319922044834

29. Liu J, Wang P, Fan J, Yu H, Yu J. In Situ Synthesis of Mo2C Nanoparticles on Graphene Nanosheets for Enhanced Photocatalytic H2-Production Activity of TiO2. ACS Sustain Chem Eng [Internet]. 2021;9:3828–37. Available from: https://doi.org/10.1021/acssuschemeng.0c08903

30. Tripathi VK, Shrivastava M, Dwivedi J, Gupta RK, Jangir LK, Tripathi KM. Biomass-based graphene aerogel for the removal of emerging pollutants from wastewater. React Chem Eng. 2024;753–76.

31. Kaushik J, Himanshi, Kumar V, Tripathi KM, Sonkar SK. Sunlight-promoted photodegradation of Congo red by cadmium-sulfide decorated graphene aerogel. Chemosphere [Internet]. 2022;287:132225. Available from: https://doi.org/10.1016/j.chemosphere.2021.132225

32. Kaushik J, Sharma C, Lamba NK, Sharma P, Das GS, Tripathi KM, et al. 3D Porous MoS2-Decorated Reduced Graphene Oxide Aerogel as a Heterogeneous Catalyst for Reductive Transformation Reactions. Langmuir. 2023;39:12865–77.

33. Dhiman N, Tripathi VK, Dwivedi J, Gupta RK, Tripathi KM. Photoactive Graphene Aerogel from Biomass for the Visible-Light-Induced Degradation of Pharmaceutical Residues. ACS Sustain Resour Manag. 2024;1:1068–75.

34. Aggarwal R, Sonkar SK, Tripathi KM. Visible-light promoted hydrogen production by diesel soot derived onion like carbon nanoparticles. Carbon N Y [Internet]. 2023;208:436–42. Available from: https://doi.org/10.1016/j.carbon.2023.03.064

35. Kaur D, Singh K, Reynolds WT, Pal B. Graphene oxide-coated Ag-TiO2 hybrid nanocomposites for superior photocatalytic activity. Environ Sci Pollut Res [Internet]. 2023;30:97660–72. Available from: https://doi.org/10.1007/s11356-023-29301-2

36. Kaur D, Pal B. Improved photocatalytic activity of graphene oxide modified Ag-TiO2 for degradation of piroxicam-20 and dehydrogenation of methanol under light irradiation. J Taiwan Inst Chem Eng [Internet]. 2024;155:105282. Available from: https://www.sciencedirect.com/science/article/pii/S1876107023006090

37. Kaur M, Pal B, Kaur D. Modified Ag-ZnO coated graphene oxide ternary composite for superior photocatalytic degradation of crystal violet dye under visible light irradiation. Diam Relat Mater [Internet]. 2024;143:110935. Available from: https://www.sciencedirect.com/science/article/pii/S0925963524001481

38. Bhardwaj S, Dogra D, Pal B, Singh S. Photodeposition time dependant growth, size and photoactivity of Ag and Cu deposited TiO2 nanocatalyst under solar irradiation. Sol Energy. 2019;194:618–27.

39. Palmisano G, Loddo V, El Nazer HH, Yurdakal S, Augugliaro V, Ciriminna R, et al. Graphite-supported TiO2 for 4-nitrophenol degradation in a photoelectrocatalytic reactor. Chem Eng J. 2009;155:339–46.

40. Rao R, Podila R, Tsuchikawa R, Katoch J, Tishler D, Rao AM, et al. Effects of Layer Stacking on the Combination Raman Modes in Graphene. ACS Nano. 2011;5:1594–9.

41. Alkhouzaam A, Qiblawey H, Khraisheh M, Atieh M, Al-Ghouti M. Synthesis of graphene oxides particle of high oxidation degree using a modified Hummers method. Ceram Int [Internet]. 2020;46:23997–4007. Available from: https://doi.org/10.1016/j.ceramint.2020.06.177

42. Luo D, Yan R, Fu C, Zhen Z, Yue H, Wu P, et al. Cu(0)/TiO2 composite byproduct from photo-reduction of acidic Cu-containing wastewater and its reuse as a catalyst. J Water Process Eng [Internet]. 2019;32:100958. Available from: https://www.sciencedirect.com/science/article/pii/S2214714419306828

43. Ghodselahi T, Vesaghi MA, Shafiekhani A, Baghizadeh A, Lameii M. XPS study of the Cu@Cu2O core-shell nanoparticles. Appl Surf Sci [Internet]. 2008;255:2730–4. Available from: https://www.sciencedirect.com/science/article/pii/S0169433208018254

44. Zhang Y, Zhang Y, Li X, Zhao X, Anning C, Crittenden J, et al. Photocatalytic water splitting of ternary graphene-like photocatalyst for the photocatalytic hydrogen production. Front Environ Sci Eng. 2020;14:1–13.

45. Chen W, Liu X, Zheng H, Fu X, Yuan Y. One-Pot Synthesis of Hexamethylenetetramine Coupled with H2 Evolution from Methanol and Ammonia by a Pt/TiO2 Nanophotocatalyst. ACS Omega [Internet]. 2022;7:19614–21. Available from: https://doi.org/10.1021/acsomega.2c01323

46. Wang K, Bielan Z, Endo-Kimura M, Janczarek M, Zhang D, Kowalski D, et al. On the mechanism of photocatalytic reactions on Cu x O@ TiO 2 core–shell photocatalysts. J Mater Chem A. 2021;9:10135–45.

47. Wang B, Zhong S, Tang S, Yue H, Ma K, Liu C, et al. Photocatalytic Production of Methyl Formate by Methanol Self-Coupling: From Oxidative Dehydrogenation to Direct Dehydrogenation. Ind Eng Chem Res. 2021;60:9684–95.

48. Camposeco R, Hinojosa-Reyes M, Zanella R. Highly efficient photocatalytic hydrogen evolution by using Rh as co-catalyst in the Cu/TiO2 system. Int J Hydrogen Energy [Internet]. 2021;46:26074–86. Available from: https://www.sciencedirect.com/science/article/pii/S0360319921004134

49. Lin W-C, Yang W-D, Huang I-L, Wu T-S, Chung Z-J. Hydrogen Production from Methanol/Water Photocatalytic Decomposition Using Pt/TiO2− x N x Catalyst. Energy & Fuels. 2009;23:2192–6.

50. Rather RA, Singh S, Pal B. Core–shell morphology of Au-TiO2@ graphene oxide nanocomposite exhibiting enhanced hydrogen production from water. J Ind Eng Chem. 2016;37:288–94.

51. Kaur D, Pal B. Improved photocatalytic activity of graphene oxide modified Ag-TiO2 for degradation of piroxicam-20 and dehydrogenation of methanol under light irradiation. J Taiwan Inst Chem Eng [Internet]. 2024;155:105282. Available from: https://doi.org/10.1016/j.jtice.2023.105282

52. Nalajala N, Salgaonkar KN, Chauhan I, Mekala SP, Gopinath CS. Aqueous Methanol to Formaldehyde and Hydrogen on Pd/TiO2 by Photocatalysis in Direct Sunlight: Structure Dependent Activity of Nano-Pd and Atomic Pt-Coated Counterparts. ACS Appl Energy Mater [Internet]. 2021;4:13347–60. Available from: https://doi.org/10.1021/acsaem.1c03080

53. Rather RA, Singh S, Pal B. A Cu+1/Cu0-TiO2 mesoporous nanocomposite exhibits

improved H2 production from H2O under direct solar irradiation. J Catal [Internet]. 2017;346:1–9. Available from: https://www.sciencedirect.com/science/article/pii/S0021951716302755

54. Choi H-J, Kang M. Hydrogen production from methanol/water decomposition in a liquid photosystem using the anatase structure of Cu loaded TiO2. Int J Hydrogen Energy [Internet]. 2007;32:3841–8. Available from: https://www.sciencedirect.com/science/article/pii/S0360319907002923

CHAPTER- 4

Graphene Oxide modified Ag-TiO_2 Hybrid Nanocomposites for Improved Photocatalytic Activity

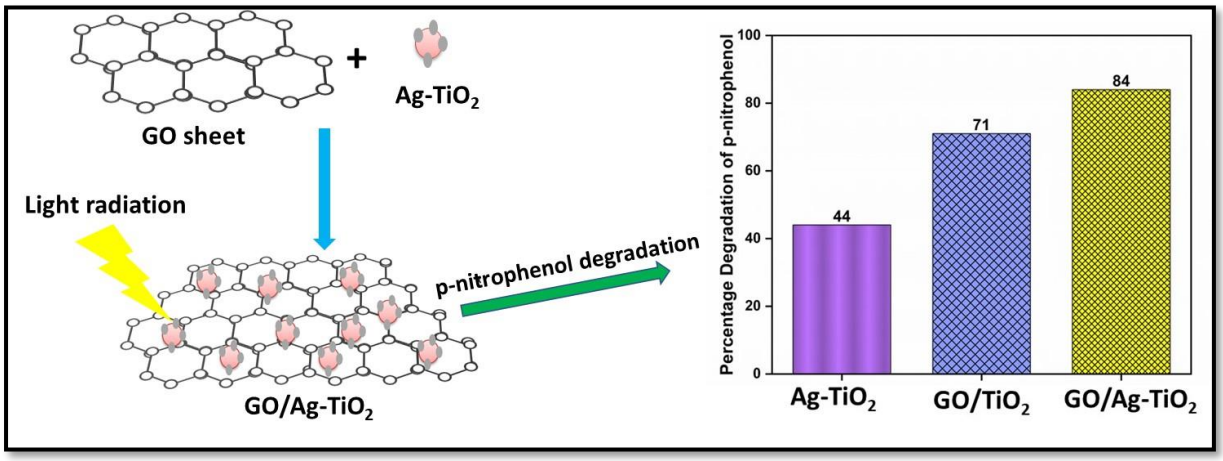

Schematic outline:

This report explores the creation of graphene oxide (GO) and Ag-TiO_2 nanocomposites to enhance photocatalytic activity. GO, obtained from anthracite coal, features a high sp^2 carbon content, improving conductivity and light absorption. The goal is to develop GO-TiO_2 composites that enable efficient electron transfer, reducing recombination. By adding silver nanoparticles (Ag) to TiO_2, photocatalytic performance is further enhanced. Characterization using XRD, HR-TEM, SEM, and Raman spectroscopy confirms the successful integration of the components. Testing with phenol and 4-nitrophenol shows that the GO/Ag-TiO_2 composite achieves 62% phenol degradation under UV light and 34% under visible light, along with 85% degradation of p-nitrophenol under UV. These results demonstrate the synergistic effects of Ag, TiO_2, and GO, highlighting the potential of these nanocomposites for effective pollutant removal.

4.1 Introduction

In recent years, graphene oxide (GO) has attracted a significant amount of interest due to its fascinating structural and electronic properties [1–3]. It has become a promising candidate in a wider variety of applications, such as energy storage [4,5], optoelectronic devices [6,7], sensors [8,9], biomedical applications [10,11], photocatalysis [12,13] etc. But till now, expensive carbon-based precursors such as graphite have been extensively used to prepare the graphene oxides [14–17]. As a result, the commercial utilization of these materials is rather narrow. Therefore, the synthesis of graphene oxide materials from cheaper resources, including natural and industrial wastes, attracted a substantial extent of attention [18–23].

In present times, due to its high abundance and lower cost, coal has emerged as a new generation precursor for preparing graphene oxides [24–28]. It consists of an infinite three-dimensional network structure comprising of sp^2 and sp^3 carbon atoms linked through aliphatic and ether groups[29–31]. The fractions of sp^2 carbon are around 70%, 75%, 85%, and 94% for lignite, sub-bituminous, bituminous, and anthracite coal, respectively[29,30]. Such features enable coal to be a potentially valuable precursor for preparing graphene oxide.

TiO_2-derived photocatalysts have been extensively used for the removal of toxic pollutants from wastewater due to their low cost, non-toxic nature and enhanced stability[32–34]. But because of its wider band gap (~3.2 eV), it can only act as an efficient photocatalyst under UV radiation only [35]. It has been reported that depositing metal (e.g. Ag, Cu, Au) (Rather et al., 2017; Yurdakal et al., 2017; Aulakh and Pal, 2019; Aulakh et al., 2020) or graphene oxide [40–42] on TiO_2 surface, its photocatalytic efficiency under visible light can be enhanced significantly.

In this report, we have prepared graphene oxide (GO) using the methodology developed by Mahajan et al.[25] from anthracite coal as it contains extremely high concentrations of sp^2 carbon, resulting in excellent absorbance in the visible region and high conductivity, resulting in facile electron transfer. The obtained GO was then deposited on the TiO_2 surface and examined the photocatalytic activity. Phenol and p-nitrophenol have been chosen as the model pollutants. These compounds have been extensively used in pharmaceutical, textiles and agrochemical industries [43]. Despite their widespread range of utility, these compounds are extremely harmful towards humans, animals and plants (Michałowicz J. and Duda W., 2007; Asadollahi-Baboli, 2012; Majewska et al., 2021). Furthermore, superior stability and low

biodegradable nature conceal their efficient removal from wastewater. Hence, their efficient removal becomes particularly essential.

4.2 Experimental section

4.2.1 Materials

Commercial TiO_2 (P25) was received as a gift from Degussa Corporation, Germany. Anthracite coal was procured from the Kashmir region. Silver nitrate ($AgNO_3$) and Graphite powder were purchased from Sigma Aldrich, India. Distilled water was obtained from the distillation plant (Milli-Q, Millipore). All chemicals were utilized without any additional purification.

4.2.2 Preparation of Graphene oxides

The graphene oxide from anthracite coal was obtained using one pot process[25]. Firstly, raw coal was mechanically powdered and then purified by dissolving in dilute acid (50ml of HCl (37%) and 50ml HF (45-50%) with approx. 500 ml of DI water), stirred in PP bottle for 1-2 days. Afterwards, the resulting mixture was washed with DI water until it showed pH 7 and filtered the resultant purified slurry, was dried at room temperature. 5g of purified coal was refluxed with 80 ml of HNO_3 in a round bottom flask at 120°C for 5h. The resultant mixture was cooled at room temperature, washed several times with DI water and ultrasonicated for 2 h to further exfoliate the oxidized coal. Subsequently, it was centrifuged at @4000rpm, washed a number of times with DI water and dried at 60° C. The graphene oxide from graphite powder was synthesized using modified Hummer's method [47]. Firstly, a (1:1) mixture of graphite powder and $NaNO_3$ was added to a conical flask, and then 23 ml of H_2SO_4 was added into it, followed by 3h stirring (~20°C). Afterwards, 3g $KMnO_4$ was added slowly, and the reaction mixture was vigorously stirred for 2h at 20°C. 46 ml of distilled water was added to the above mixture slowly and stirred for 2 h at 98° C. To the above solution, 100 ml DI water was added and 10 ml H_2O_2 after 5 min. The obtained product was washed with DI water and ethyl alcohol 3-4 times, and the final product dried at 55°C for 12 h.

4.2.3 Preparation of Ag-TiO_2

The photo-deposition method was followed for the deposition of Ag metal onto TiO_2 [48]. In a typical method, 100 mg of TiO_2 was dispersed in 50vol% of (5 ml IPA and 5 ml DI water) followed by the addition of $AgNO_3$ (0.01M; 93 0µL) in a test tube. The above test tube was purged with Ar gas and sealed and photo-irradiated under UV light using a mercury arc lamp

with continuous magnetic stirring for 2h. The obtained solution was centrifuged @ 6000rpm, washed with ethyl alcohol and water and dried at 80°C overnight. This compound will sometimes be referred to as **ATO** throughout the chapter.

4.2.4 Preparation of GO/TiO_2 and GO/Ag-TiO_2

The GO/TiO_2 and GO/Ag-TiO_2 composite was synthesized using the hydrothermal method [49]. 10 mg of GO was dissolved in a 2:1 solution of (80 ml DI water and 40 ml ethanol) and exfoliated by ultrasonication for 2h. To the resulting GO solution, 200 mg of TiO_2 was added (for GO/TiO_2 composite) or Ag-TiO_2 (for GO/Ag-TiO_2 composite) and further agitated for 2h to afford a homogeneous suspension. The obtained suspension was added into a 200 ml Teflon-sealed autoclave and placed in a muffle furnace at 120°C for 3h. Finally, the obtained composite was recovered by filtration, washed 3-4 times with DI water, and dried at 70°C for 12 h. These composites will be occasionally denoted as **GTO** and **AGTO**, respectively, throughout the chapter.

4.2.5 Characterization

XRD (X-ray diffraction) diffractograms were recorded using the X-ray diffractometer, PANALYTICAL X'Pert PRO with Cu Kα (λ=1.540Å), using a scanning rate of 10 min^{-1}. The surface morphology was studied by scanning electron microscopy (SEM) using a JEOL JSM-7600 F microscope operated at 30 kV. The microstructural and crystallographic details were furthermore scrutinized by recording the high-resolution transmission electron microscopy (HRTEM) images in JEOLJEM-2100 plus microscope operating at 200 kV. The concentration of phenol and p-nitrophenol in the solutions was measured by determining the absorbance values at 269 and 401 nm, respectively, using a Shimadzu UV-2600 spectrophotometer. The Raman spectra were recorded using LabRam HR Evolution Raman microscope with an excitation wavelength of 532 nm. The HRMS (High resolution mass spectroscopy) on Waters, QTOF mass spectrometer with UPLC (XEVO G2 XS) was used to investigate the intermediate by products formed during photocatalytic degradation of phenol. The diffused reflectance spectra (DRS) of each individual composite were measured in the range 350-800 nm using DRS and Avantes spectrometer to record the solid state absorption spectra. To determine the solution phase, UV-visible and photoluminescence spectra, 1mg of the different nanostructures were dispersed in 5 ml distilled water to afford homogeneous dispersions. The absorption and emission spectra were recorded using Shimadzu UV 2600 and spectrometer and Perkin-Elmer LS55 spectro-fluorimeter, respectively.

4.2.6 Photocatalytic Activity

The photocatalytic activity of the prepared composites was evaluated by monitoring the change in absorbance of phenol/p-nitrophenol solution in the presence of UV and visible light using a 125 W Hg arc and 50W LED lamp, respectively. Then, 5 mg of (TiO_2, Ag-TiO_2, GO/TiO_2, GO/Ag-TiO_2) catalyst was added in 10 ml of phenol (1 μM) /p-nitrophenol solution (0.1 mM) in test tubes placed under UV lamp for various time intervals, the absorbance change were analyzed by a UV-Visible spectrophotometer. The same procedure was used to examine the photocatalytic degradation of phenol using synthesized catalysts under visible lamp. Before every photocatalytic reaction, different mixtures were stirred in the dark for 30 minutes in order to complete the adsorption process. The photocatalytic degradation efficiency (%D) was calculated using equation 4.1.

$$\%\boldsymbol{D} = \frac{\boldsymbol{A_0 - A}}{\boldsymbol{A_0}} \times \mathbf{100} \qquad \text{(equation no. 4.1)}$$

Where A_0 and A are the initial and final absorbance of phenol/p-nitrophenol at 269/401 nm, respectively.

4.3 Results and Discussions

4.3.1 Structural Analysis

The formation and crystallinity of the as-prepared composites were confirmed by examining their XRD patterns (**Fig.4.1**). In the XRD pattern of graphene oxide (GO), the characteristic signals of the anthracite coal have almost completely disappeared along with the concurrent appearance of the distinctive peak for GO (**Fig.4.1(a)**)[50]. The overall diffraction pattern includes the (200), (111) lattice planes of Ag-nanoparticles (Fig. 1b). It also contains (101), (004), (200), (105), (211), (204), (116), (220), (215) crystallographic planes of anatase TiO_2 (JCPDS card no. 21-1272) as well as (110), (101), and (111) lattice plane of rutile TiO_2 (JCPDS Card No. 21-1276) (**Fig.4.1(b)**). The peaks show no appreciable changes from their pristine analogues. Upon loading of Ag-TiO_2, the diffraction peak corresponding to GO becomes relatively much weaker. This is because both Ag and TiO_2 have higher x-ray scattering coefficients compared to GO due to higher atomic numbers.

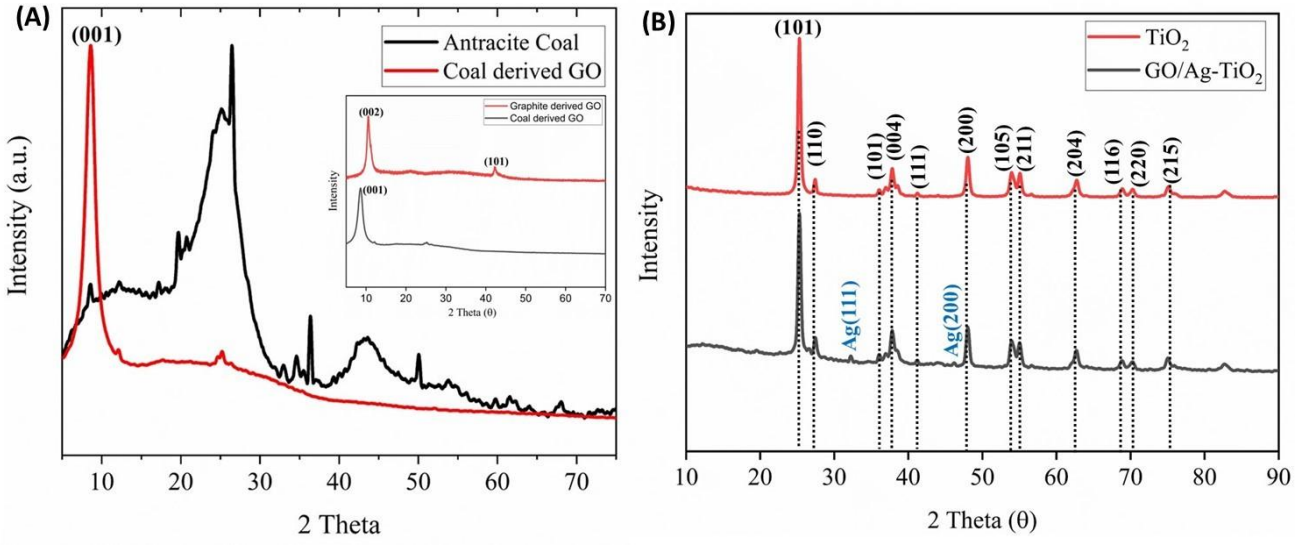

Fig.4.1: XRD patterns of (a) GO, (b) TiO_2, GO/Ag-TiO_2 composites.

The SEM images (**Fig.4.2(a-b)**) of the hybrid structures show that graphene oxide layers undergo stacking to result in a flower-shaped morphology. In the case of GO/Ag-TiO_2 hybrid, the Ag-TiO_2 nanoparticles undergo the deposition of the external surface of graphene oxide microstructures. In order to check the homogeneity of the deposition process, SEM micrographs were collected in different areas (**Fig.4.2(c-d)**). It has been observed that the Ag-TiO_2 nanoparticles are deposited at different extents in the different locations of the sample, thereby suggesting non-uniformity of the deposition process.

In order to scrutinize the crystallinity and morphology more, transmission electron microscopic studies were performed (**Fig.4.3**). The TEM image of GO/Ag-TiO_2 hybrids consists of light grey coloured layers, medium grey coloured cubes and dark grey coloured spherical particles corresponding to GO, TiO_2 and Ag nanoparticles respectively (**Fig.4.3(a)**). It can be clearly observed that the flower-shaped morphology is no longer present, thereby suggesting that the incorporation of Ag-TiO_2 can cause the graphene layers to move away from each other. The HR-TEM pattern of the composites revealed the presence of (200) and (101) lattice fringes corresponding to Ag nanoparticles (face-centred cubic lattice) and anatase TiO_2, respectively (**Fig.4.3(b)**). Such observations confirm the formation of GO/Ag-TiO_2 binary composites.

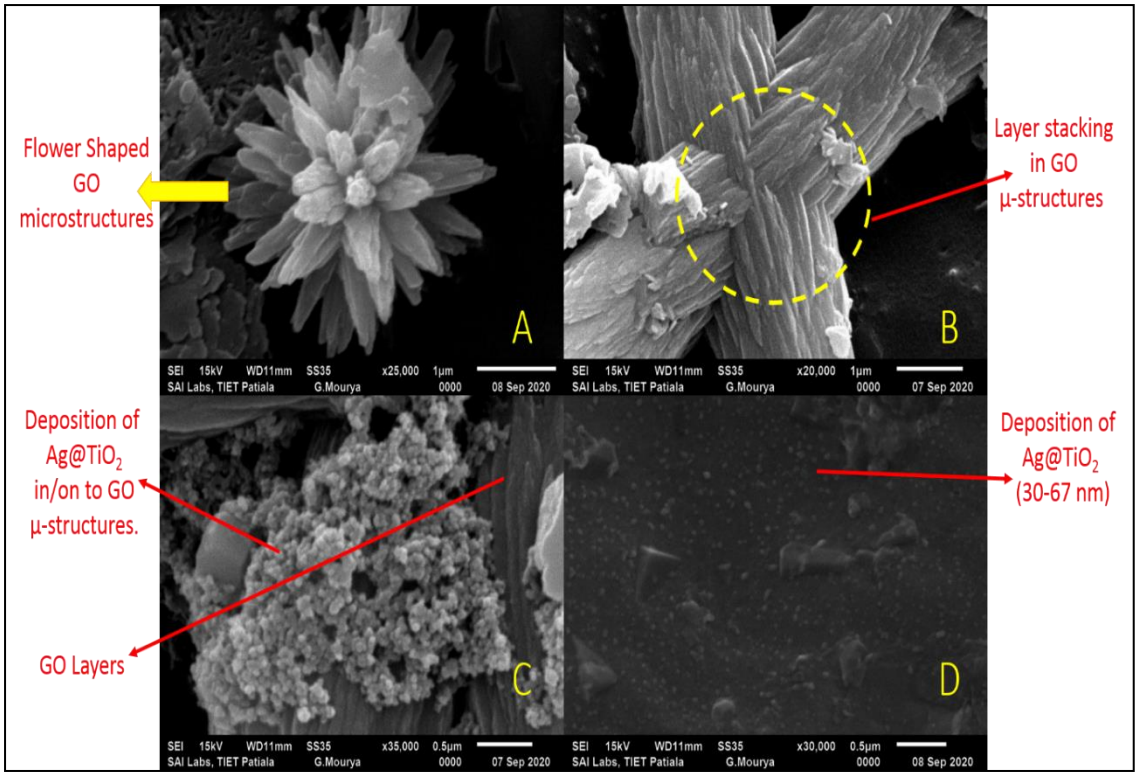

Fig.4.2: SEM micrographs showing (a) Flower shaped Coal derived Graphene Oxide, (b) Stacking between different layers of GOs, (c-d) Surface deposition of Ag-TiO_2 nanoparticles onto the GO micro(μ)-structures.

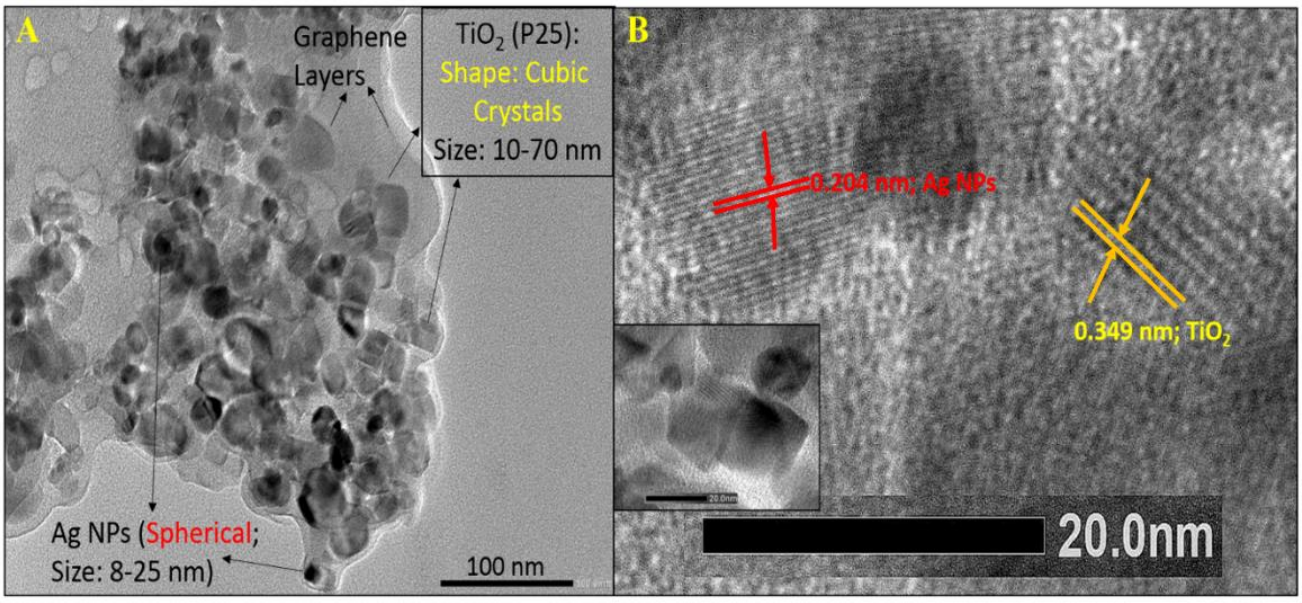

Fig.4.3: (a) HR-TEM image (b) Lattice Fringes of GO/Ag-TiO_2 composites.

In order to analyze the structure further, Raman spectra of GO, GO/TiO_2 and GO/Ag-TiO_2 were recorded (**Fig. 4**). In the Raman spectra of GO **Fig.4.4(a)**, there are two broad signals at 1346 and 1593 cm^{-1} due to D and G band of GO indicating a significant amount of disorder [51].

Apart from these two, there is a peak at 1924 cm^{-1} because of iTALO mode resulting from the stacking of graphene layers, and the calculated I_D/I_G ratio resulted in 0.84 [52]. Interestingly, upon loading of TiO_2 and Ag-TiO_2, the signal corresponding to the iTALO mode has disappeared, whereas the peaks related to the D and G bands remain practically identical (**Fig.4.4(b)**). Such observation is consistent with the delamination of graphene layers upon loading of TiO_2 and Ag-TiO_2. Furthermore, the signals at 397, 513 and 639 cm^{-1} are characteristic peaks of TiO_2 [53].

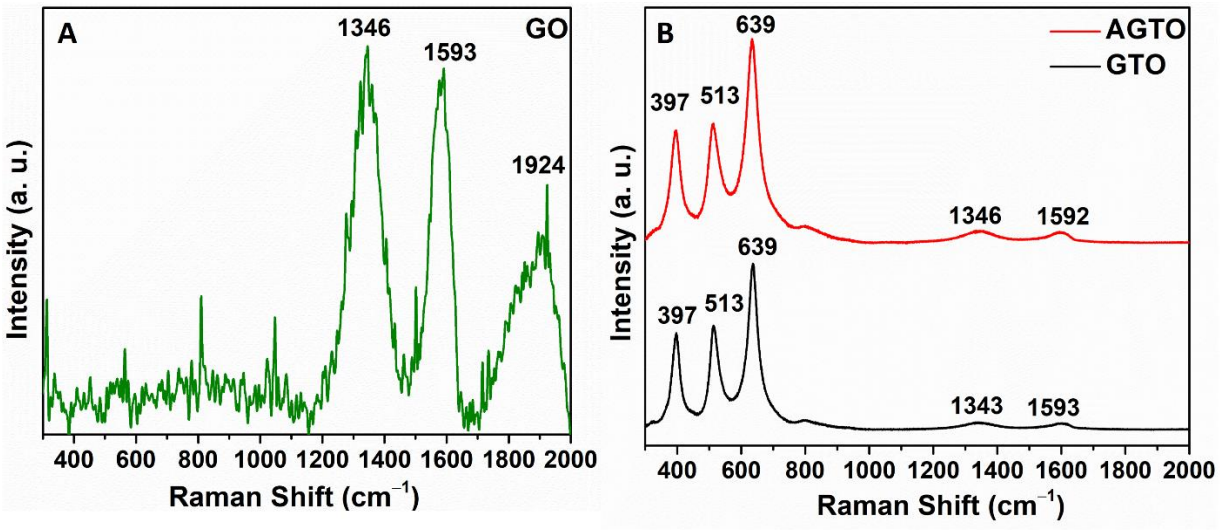

Fig.4.4: Raman Spectra of (a) GO and (b) GO/TiO_2 (GTO) and GO/Ag-TiO_2 (AGTO) composites.

4.3.2 Optical Properties

In order to monitor the optical properties, solution phase UV-visible spectra of the suspensions as well the solid-state DRS patterns were recorded for the composites as well as their individual constituents (**Fig.4.5(a,b)** and **Fig.4.6**). The UV-visible absorbance spectra of GO showed a characteristic peak at 227 nm, which results from $\pi \rightarrow \pi^*$ transitions because of the aromatic C=C bonds [54] and TiO_2 show characteristic signals at 327 nm, respectively (**Fig.4.5a**), whereas Ag nanoparticles show representative peaks at 214 and 417 nm (**Fig.4.5b**). The GO/TiO_2 and GO/Ag-TiO_2 hybrids possess all the distinct signals of each discrete component (**Fig.4.5b**). The DRS spectra also displayed exactly similar patterns (**Fig.4.6**). In order to examine the electron-hole pair recombination process, the photoluminescence (PL) spectra of Ag-TiO_2 and GO/Ag-TiO_2 were recorded (**Fig.4.5c**). It has been observed that upon loading with GO on Ag-TiO_2, the PL intensity decreases, thereby indicating quenching of the emission process due to a lower degree of electron-hole pair recombination.

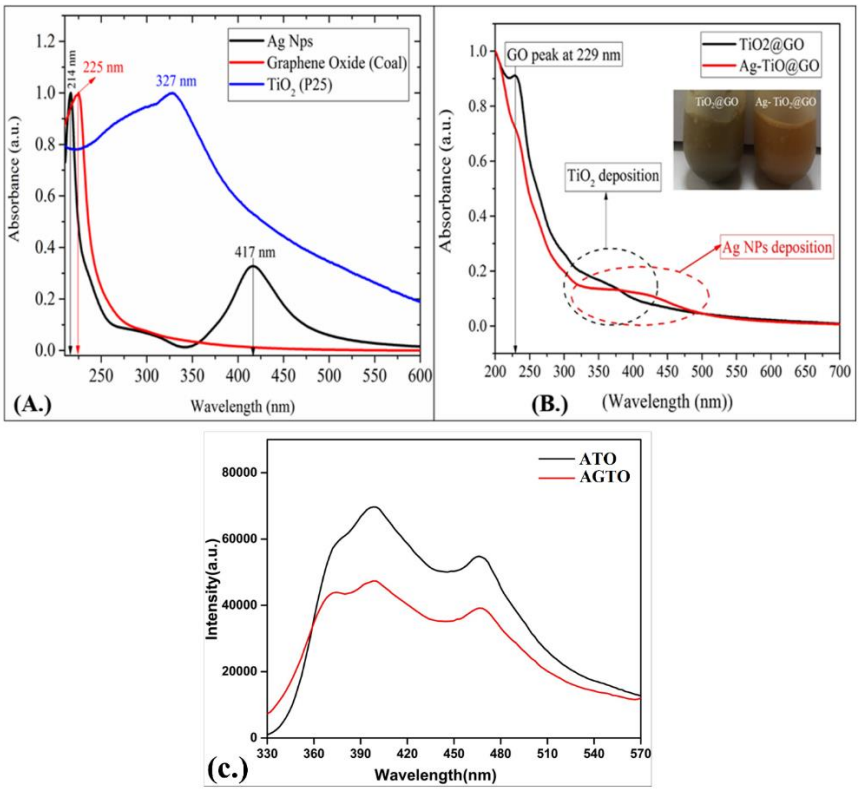

Fig.4.5: (a) UV-Visible spectra of Ag NPs, GO, and TiO_2 (b) Changes in the UV-Visible spectra of GO after deposition of TiO_2 and Ag-TiO_2 and (c) Photoluminescence spectra of ATO and AGTO composites.

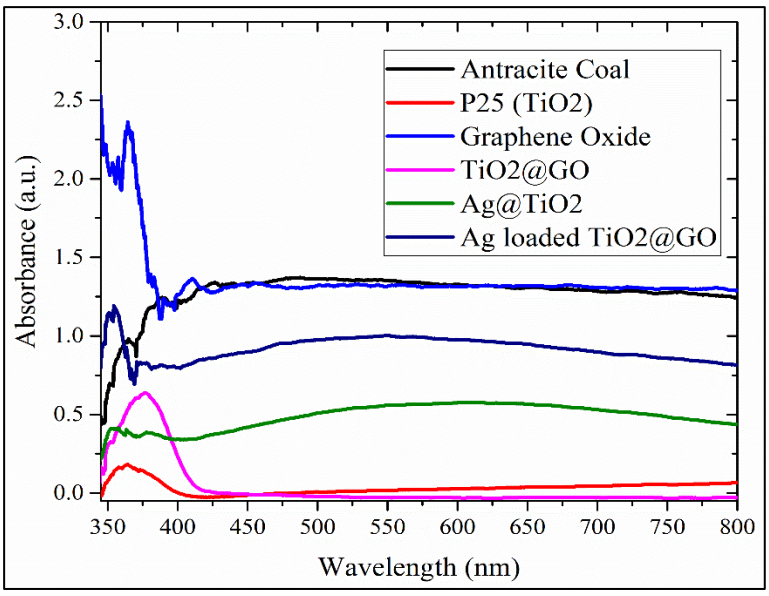

Fig.4.6: The DRS spectra of Anthracite coal, P25, GO sheets, TiO_2@GO, Ag@ TiO_2, and Ag-TiO_2@GO**.**

4.3.3 Photocatalytic Activities

The photocatalytic activity of GO, TiO_2, GO/TiO_2, Ag-TiO_2 and GO/Ag-TiO_2 were scrutinized towards the degradation of phenol (neutral pH) under both visible and UV light irradiation by monitoring the absorbance at 269 nm (**Fig.4.7**). Under visible light radiation, the GO, TiO_2, GO/TiO_2 and Ag-TiO_2 have 15%, 4%, 6% and 16% photocatalytic removal efficiency towards phenol, respectively. The poor photocatalytic activity can be attributed to their poor absorbance in the visible region and higher electron-hole pair recombination. Moreover, the GO/TiO_2 hybrid has inferior photocatalytic activity compared to GO. This can be due to the blockage of active sites present in the external surface of GO upon TiO_2 loading. Interestingly, the GO/Ag-TiO_2 heterostructure had significantly higher photodegradation efficiency (34%). Such observation revealed that the synergistic effect of GO, Ag, and TiO_2 are extremely crucial to afford optimum photocatalytic activity. Interestingly, under UV light irradiation, the photocatalytic activities of Ag-TiO_2 (38%) and GO/Ag-TiO_2 (62%) composites were significantly higher. Because exposure to UV light can lead to higher energy electronic transitions originating from inner core-filled bands to afford high energy holes to afford higher photocatalytic activity.

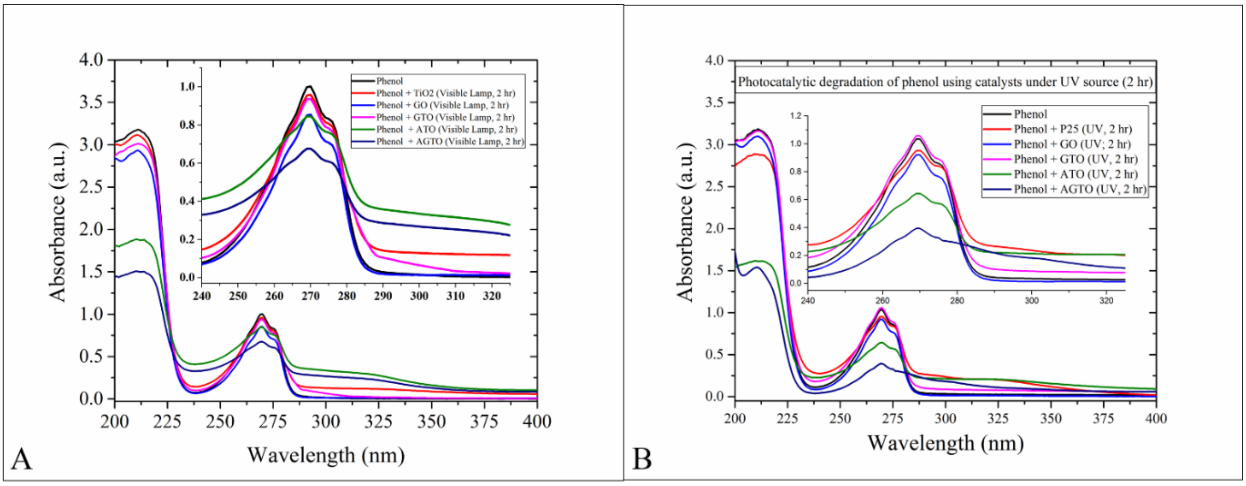

Fig.4.7: Photocatalytic degradation of Phenol using different catalysts under (a) Visible and (b) UV light irradiation for 2 h.

All these photodegradation reactions obey pseudo-first-order kinetics (**Fig.4.8**) (equation 4.2). The corresponding rate constant values are 3.94×10^{-3} and 8.05×10^{-3} min^{-1} for the Ag-TiO_2 and GO/Ag-TiO_2 hybrids, respectively. In order to confirm the reproducibility, photodegradation reactions in the presence of GO/Ag-TiO_2 composite have been repeated three times. The

photodegradation efficiencies after 2 h were practically constant (60, 62 and 63%), thereby confirming the consistency of the result.

$$\ln \frac{C_0}{C_t} = kt \qquad \text{(equation no. 4.2)}$$

Where C_0 = the Initial Concentration of the substrate, Ct = Concentration of the substrate at time t, and k= rate constant.

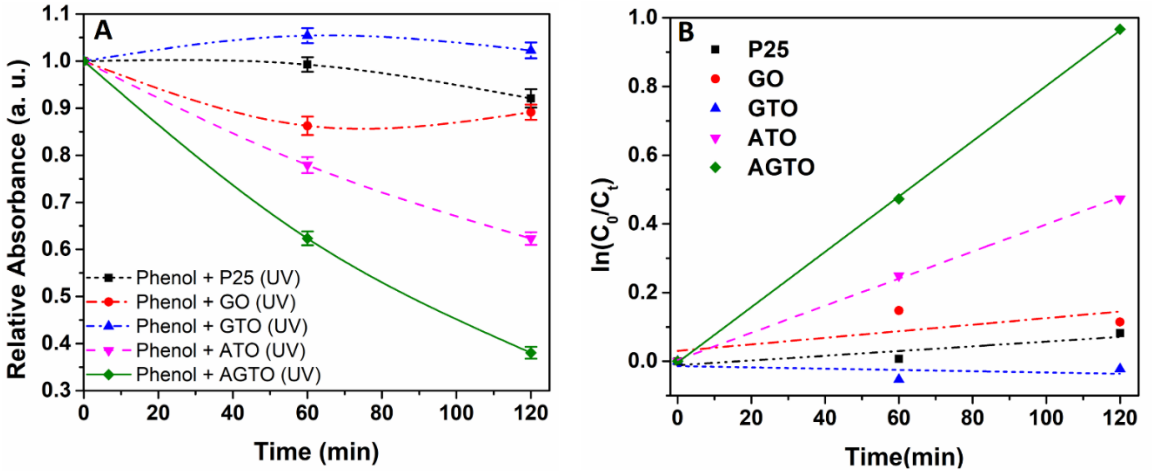

Fig.4.8: (a) variation in absorbance (at 269 nm) with time for different photocatalysts under UV irradiation (b) pseudo first order kinetic fitting for different photocatalysts in the presence of UV irradiation.

The photocatalytic activity under UV radiation of the coal-derived GO/Ag-TiO_2 hybrid was compared with its graphite-derived analogue to validate the choice of precursor (**Fig.4.9**). It has been observed that the coal-derived nanocomposite shows 89% photocatalytic phenol degradation within 4 hours and 35 minutes whereas the graphite derives analogue shows 85% activity in 5 hours and 25 minutes. Coal-derived GO is composed of carbon atoms that are planar, graphenic, sp^2 and sp^3 linked. Nonetheless, in coal the wide range of functional chemistry and molecular compounds leads to tunable electronic and optical properties as compared to conventional sources like graphite-derived GO. Such observation confirms that the coal-derived heterostructure acts as a superior photocatalyst compared to its corresponding graphite derivative.

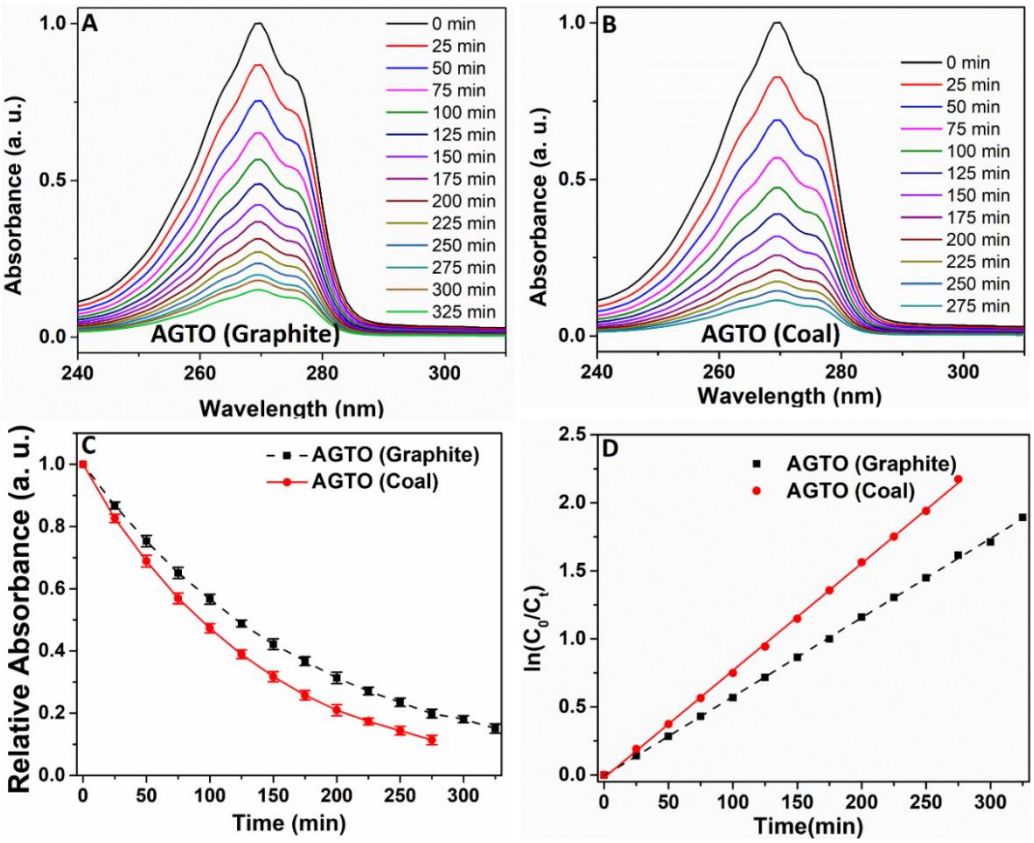

Fig.4.9: Comparison of photocatalytic efficiency of different Ag-TiO_2/GO composites under UV light (a) Changes in the UV spectra with time for graphite-derived AGTO composite (b) Changes in the UV spectra with time for coal-derived AGTO composite (c) variation in absorbance (at 269 nm) with time for AGTO composites (d) pseudo first order kinetic fitting for AGTO composites.

Inspired by the above observations, the photocatalytic activity of GO, Ag-TiO_2 and GO/Ag-TiO_2 towards p-nitrophenol degradation was examined (**Fig.4.10**) under UV light irradiation. Among all these catalysts, the GO/Ag-TiO_2 hybrid had the best photocatalytic activity. This composite possesses 85% degradation efficiency towards photocatalytic p-nitrophenol removal in 60 minutes, whereas GTO (71%) and ATO (44%) show relatively inferior photocatalytic activity within the same time interval (as shown in **Table 4.1**). This observation also reveals that the cooperative effect of Ag NPs, GO, and TiO_2 is extremely important to maximize the photocatalytic activity.

Sr. no.	Catalyst	% Degradation (p-nitrophenol)
1.	ATO	44
2.	GTO	71
3.	AGTO	85

Table 4.1: Comparison of the synthesized photocatalysts for p-nitrophenol degradation.

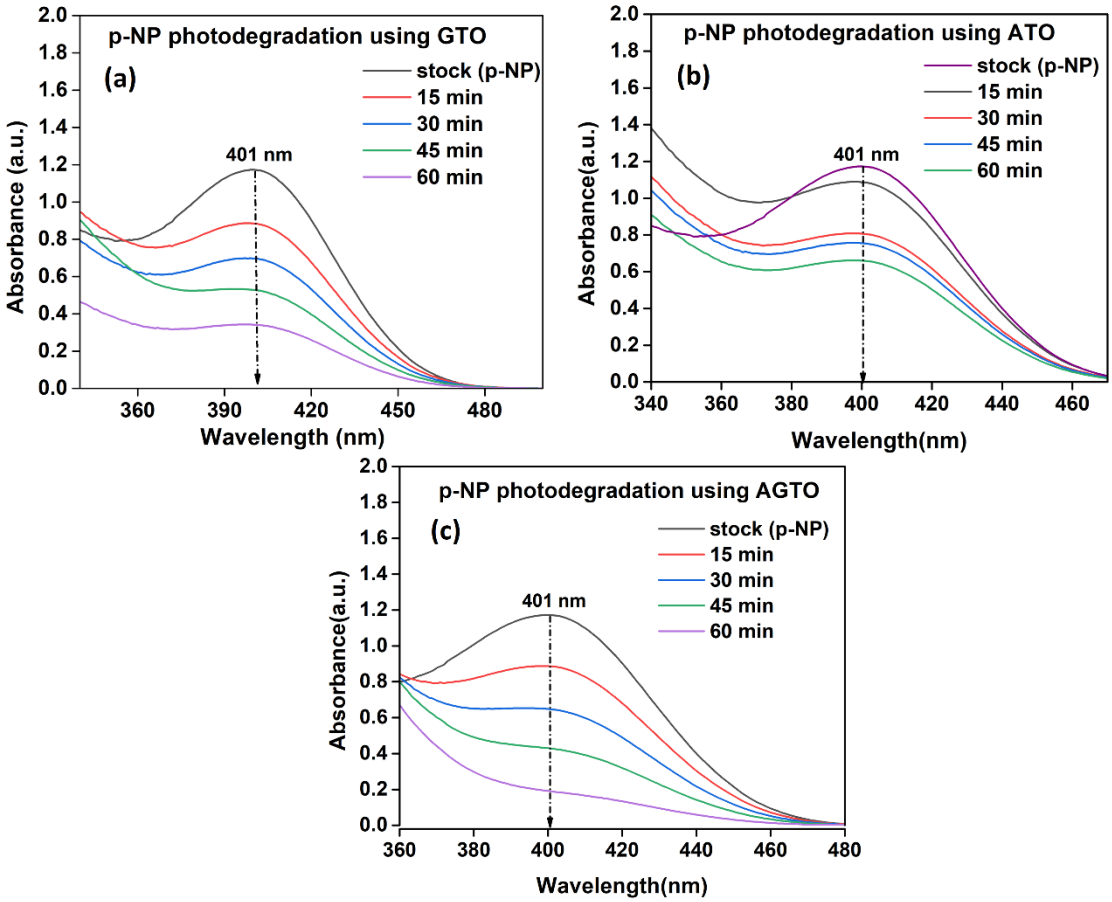

Fig.4.10: Photodegradation of p-nitrophenol in the presence of different catalysts.

Similar to phenol degradation, photocatalytic p-nitrophenol degradation also obeys pseudo-first-order kinetics (**Fig.4.11**). The GTO, ATO and AGTO possess the rate constant values of 0.020, 0.010 and 0.029 min^{-1} respectively.

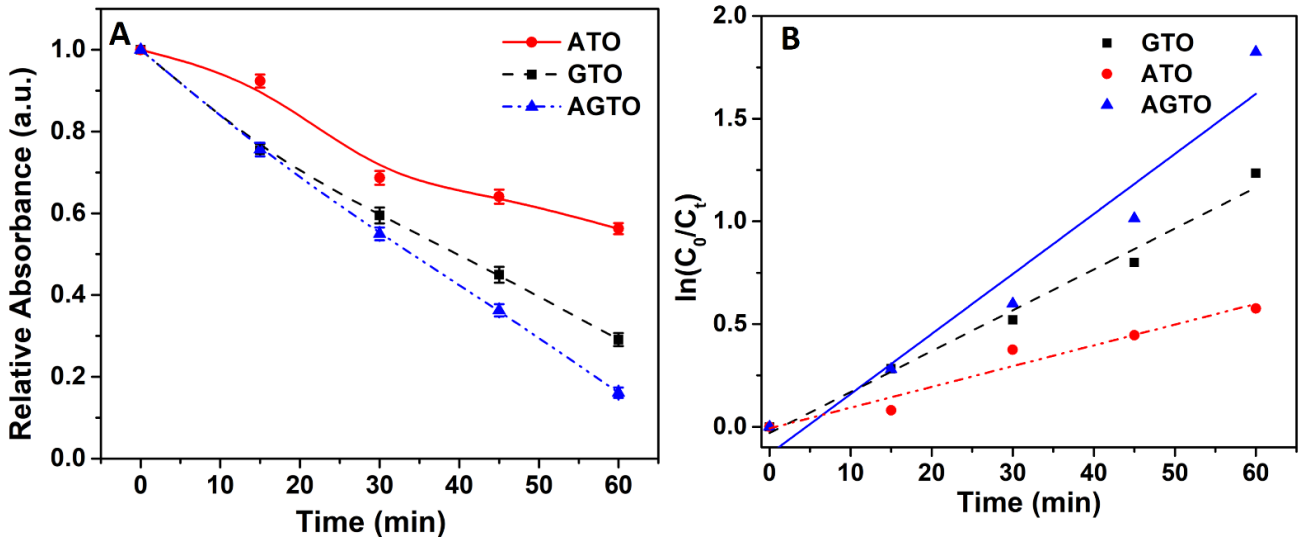

Fig.4.11: (a) variation in absorbance (at 401 nm) with time for different photocatalysts under UV irradiation (b) pseudo first order kinetic fitting for different photocatalysts in the presence of UV irradiation.

Importantly, the p-nitrophenol undergoes much more facile degradation than phenol. The presence of electron-withdrawing nitro groups enhances the positive charge density on the hydroxyl group, thereby enhancing its hydrogen bond acceptance ability. Moreover, the nitro groups can also participate in additional non-covalent interactions with the photocatalysts. Due to these factors, p-nitrophenol can undergo stronger binding with photocatalysts to result in more efficient degradation.

Remarkably, the GO/Ag-TiO_2 heterostructure (**AGTO)** shows shorter reaction time and comparable degradation efficiency towards photocatalytic p-nitrophenol removal under UV light irradiation with much smaller catalyst dosage as shown in **Table 4.2** [55–57].

Photocatalyst	**Catalyst dosage (g L^{-1}) ***	**Concentration of the Pollutant (M)**	**pH**	**Light Source**	**Photocatalytic Efficiency (%)**	**Time (minutes)**	**References**
B-doped TiO_2	1.0	7.2×10^{-6}	-	125 W Hg lamp	90	180	[57]
FeTPP/NaY, H_2O_2	1.0	2×10^{-4}	6.5	12 W UV lamps	86	180	[55]

$K_{0.33}MnO_2 \cdot 1.14 H_2O$	1.0	1.8×10^{-4}	-	TQ150–Z0 lamp (power 150 W)	100	150	[56]
AGTO	0.5	1×10^{-4}	-	125 W Hg arc	85	60	This Work

Table 4.2: Comparative photodegradation efficiency of **AGTO** towards p-nitrophenol degradation under UV light irradiation with the reported literature.

In order to identify the active species, different control experiments have been performed (**Fig.4.12**). The UV-light promoted photocatalytic p-nitrophenol degradation activity of the **AGTO** composite under different reaction conditions after 1-hour of reaction time were compared. It has been observed that the photocatalytic activity remains practically identical even after extensive argon purging. Such observation rules out any role of the electrons as well as the superoxide radicals in the photocatalytic reactions. Whereas the addition of 0.5 ml *iso*-propanol in the 10 ml reaction mixture reduces the degradation efficiency quite significantly. Such observations suggest that the holes (h^+) and hydroxyl radicals (·OH) act as active species in the photocatalytic degradation process.

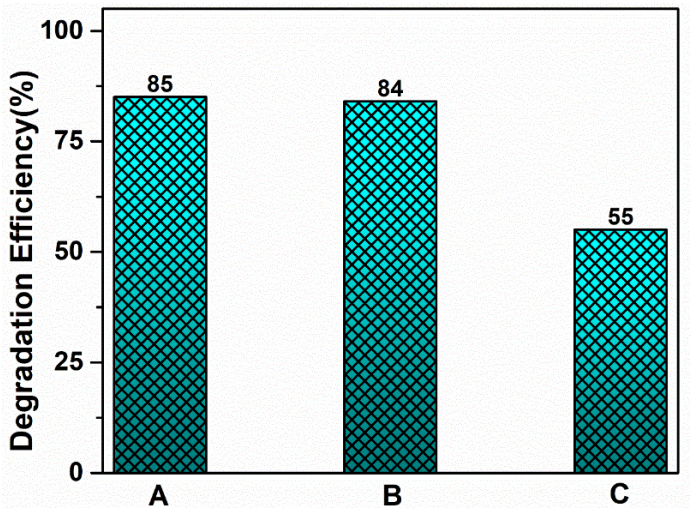

Fig.4.12: Variation photocatalytic p-nitrophenol degradation efficiency of **AGTO** catalyst after 60 minutes reaction time under different conditions (A) Reaction mixture under ambient atmosphere (B) Reaction mixture under argon atmosphere (C) Reaction mixture containing 0.5ml *isopropanol*.

Based on the above observation, the following mechanism has been proposed (**Scheme 4.1**). It involves the excitation of TiO_2 by the incident light to generate an electron-hole pair. Furthermore, the Ag nanoparticles can also undergo excitation through the surface plasmon resonance phenomenon to afford additional electron-hole pairs. The excited electron (e^-) from the TiO_2 conduction band or Ag nanoparticles undergo facile transfer to the GO surface to reduce the probability of electron-hole pair recombination. The holes (h^+) oxidize the water molecules to generate hydroxyl (·OH) radicals. The hydroxyl (·OH) radicals and holes (h^+) finally react with the organic pollutants (phenol/p-nitrophenol) to afford the degradation products.

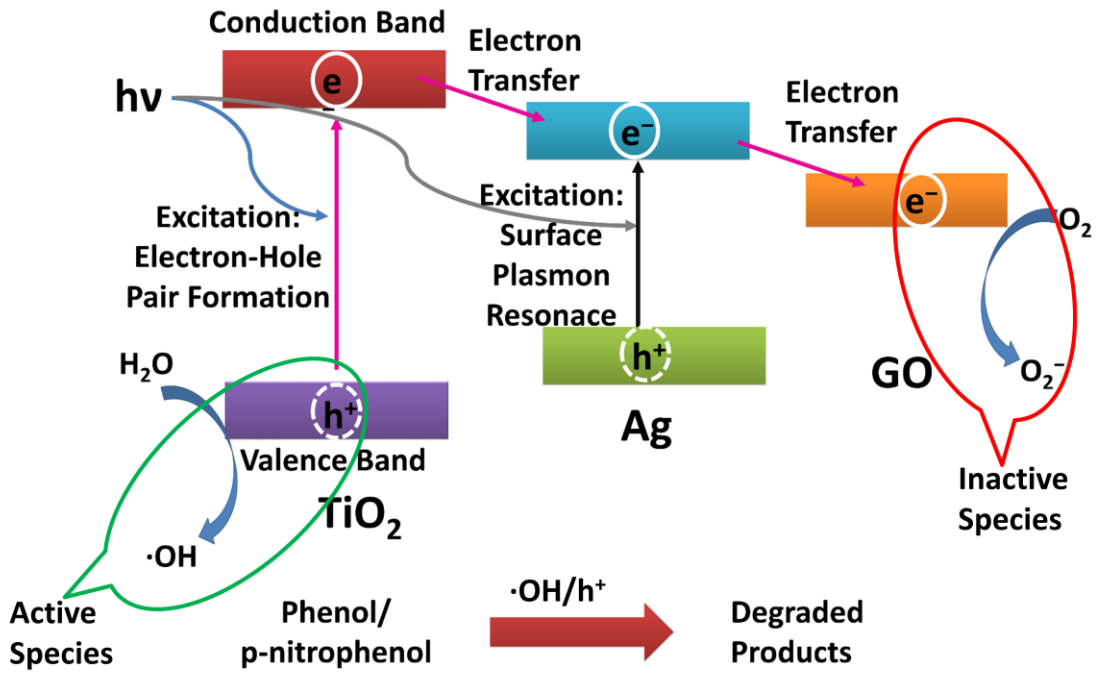

Scheme 4.1: Schematic representation showing the proposed reaction mechanism for the photocatalytic degradation.

4.3.3.1 Phenol degradation mechanism study using HRMS analysis

Phenol degradation was carried out by taking 5mg of AGTO catalyst in 10ml of phenol (1 µM) solution in a test tube and kept under the dark for 30 min afterwards, placed under UV light for 2h. The degraded solution was collected and centrifuged, and the UV-visible absorbance spectra were recorded. The photocatalytic degradation efficiency of AGTO was found to be 65%. The degraded solution sample was used for HRMS analysis to identify the phenol degradation intermediates and to better understand the photodegradation mechanism. The analysis was carried out using the positive mode of electrospray ionization. The fragmented

mass pattern **(Fig.4.12)** depicted fragments of m/z = 110 (catechol, hydroquinone),108 (o & p-benzoquinone), 90 (oxalic acid), and 60 (acetic acid), respectively. **Fig.4.13** depicts a plausible phenol degradation pathway based on the intermediate compounds found in the mass pattern. Phenol degradation was initiated with the ·OH radical attack (confirmed by scavenger test) on the phenol ring (m/z = 94), which resulted in the formation of catechol, hydroquinone, o & p-benzoquinone as intermediates. After gradual photooxidation by the ·OH radical, small fragments were formed (oxalic acid, propionic acid, acetic acid), which mineralized into small compounds like CO_2 and H_2O[58]. The phenol fragment of (m/z = 94) was not observed in the spectra, which suggests that the phenol ring degraded down into smaller fragments, which eventually degraded into smaller compounds.

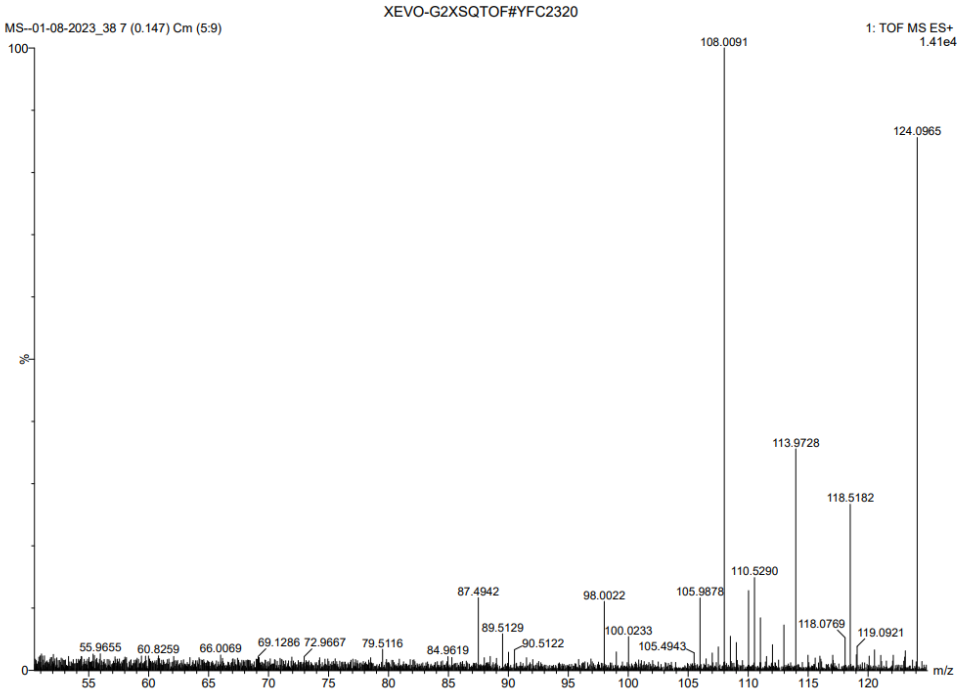

Fig.4.12: HRMS spectra of degraded phenol after photocatalytic reaction with AGTO composite.

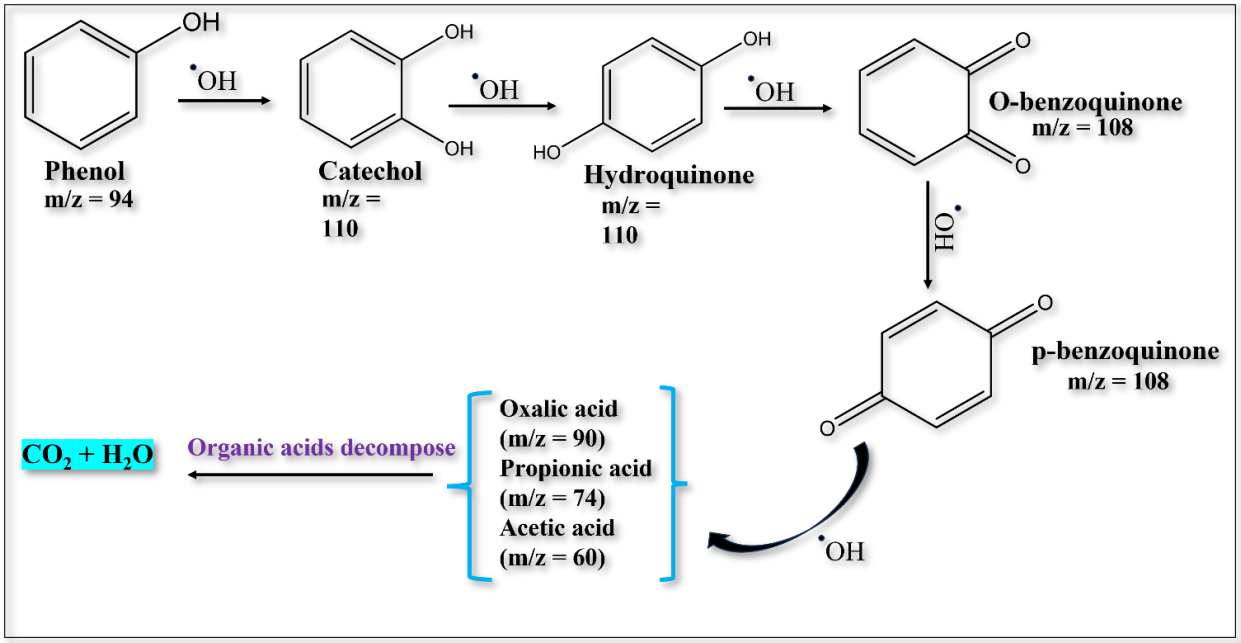

Fig.4.13: The proposed pathway of phenol degradation after photocatalytic degradation with AGTO composite under UV light irradiation.

4.4 Conclusion

In summary, different graphene oxide-derived composites have been prepared, and their activity towards degradation of phenol and p-nitrophenol was evaluated under UV as well as visible light irradiation. The formation of Ag-TiO_2/GO ternary nanocomposites was confirmed by different spectroscopic and microscopic techniques such as XRD, HR-TEM, Raman, etc. It has been observed that the Ag-TiO_2/GO hybrids show the highest catalytic activities among all different composites. Such observation suggests that the synchronized effect of Ag, TiO_2 and GO plays a crucial role in maximizing the photocatalytic activity. Also, the coal-derived GO based heterostructure has been shown to possess superior photocatalytic efficiency compared to its graphene-derived analogue. Furthermore, photocatalytic degradation of p-nitrophenol is much more facile compared to the phenol. The control experiments suggest that the holes and hydroxyl radicals are the predominant active species in the photodegradation process, while the electrons and superoxide radicals do not have any significant roles. Such observation will endorse an emerging direction to prepare different nanostructures from cheaper, naturally abundant resources to afford fascinating physicochemical properties such as enhanced photocatalytic activity.

References

1. Pacilé D, Meyer JC, Fraile Rodríguez A, Papagno M, Gómez-Navarro C, Sundaram RS, et al. Electronic properties and atomic structure of graphene oxide membranes. Carbon N Y. 2011;49:966–72.

2. Saxena S, Tyson TA, Shukla S, Negusse E, Chen H, Bai J. Investigation of structural and electronic properties of graphene oxide. Appl Phys Lett. 2011;99:13104.

3. Sharma N, Tomar S, Shkir M, Kant Choubey R, Singh A. Study of Optical and Electrical Properties of Graphene Oxide. Mater Today Proc. 2021;36:730–5.

4. Ambrosi A, Pumera M. Electrochemically Exfoliated Graphene and Graphene Oxide for Energy Storage and Electrochemistry Applications. Chem – A Eur J. 2016;22:153–9.

5. Tian Y, Yu Z, Cao L, Zhang XL, Sun C, Wang D-W. Graphene oxide: An emerging electromaterial for energy storage and conversion. J Energy Chem. 2021;55:323–44.

6. Ke S, He Y, Zhu L, Jiang Z, Mao H, Zhu Y, et al. Indium-Gallium-Zinc-Oxide Based Photoelectric Neuromorphic Transistors for Modulable Photoexcited Corneal Nociceptor Emulation. Adv Electron Mater. 2021;n/a:2100487.

7. Wan X, Huang Y, Chen Y. Focusing on Energy and Optoelectronic Applications: A Journey for Graphene and Graphene Oxide at Large Scale. Acc Chem Res. 2012;45:598–607.

8. Xue J, Gao Z, Xiao L. The Application of Stimuli-Sensitive Actuators Based on Graphene Materials . Front. Chem. . 2019. p. 803.

9. Rowley-Neale SJ, Randviir EP, Abo Dena AS, Banks CE. An overview of recent applications of reduced graphene oxide as a basis of electroanalytical sensing platforms. Appl Mater Today. 2018;10:218–26.

10. Chung C, Kim Y-K, Shin D, Ryoo S-R, Hong BH, Min D-H. Biomedical Applications of Graphene and Graphene Oxide. Acc Chem Res. 2013;46:2211–24.

11. Yim Y, Shin H, Ahn SM, Min D-H. Graphene oxide-based fluorescent biosensors and their biomedical applications in diagnosis and drug discovery. Chem Commun. 2021;57:9820–33.

12. Jamjoum HAA, Umar K, Adnan R, Razali MR, Mohamad Ibrahim MN. Synthesis, Characterization, and Photocatalytic Activities of Graphene Oxide/metal Oxides Nanocomposites: A Review . Front. Chem. . 2021. p. 789.

13. Putri LK, Tan L-L, Ong W-J, Chang WS, Chai S-P. Graphene oxide: Exploiting its unique properties toward visible-light-driven photocatalysis. Appl Mater Today. 2016;4:9–16.

14. Feicht P, Biskupek J, Gorelik TE, Renner J, Halbig CE, Maranska M, et al. Brodie's or Hummers' Method: Oxidation Conditions Determine the Structure of Graphene Oxide. Chem – A Eur J. 2019;25:8955–9.

15. Marcano DC, Kosynkin D V, Berlin JM, Sinitskii A, Sun Z, Slesarev A, et al. Improved

Synthesis of Graphene Oxide. ACS Nano. 2010;4:4806–14.

16. Yu H, Zhang B, Bulin C, Li R, Xing R. High-efficient Synthesis of Graphene Oxide Based on Improved Hummers Method. Sci Rep. 2016;6:36143.

17. Zito CA, Perfecto TM, Mazon T, Dippel A-C, Koziej D, Volanti DP. Reoxidation of graphene oxide: Impact on the structure, chemical composition, morphology and dye adsorption properties. Appl Surf Sci. 2021;567:150774.

18. Amir Faiz MS, Che Azurahanim CA, Yazid Y, Suriani AB, Siti Nurul Ain MJ. Preparation and characterization of graphene oxide from tea waste and it's photocatalytic application of TiO2/graphene nanocomposite. Mater Res Express. 2020;7:15613.

19. Jiang C, An D, Wang Z, Zhang S, An X, Bo J, et al. A sustainable reduction route of graphene oxide by industrial waste lignin for versatile applications in energy and environment. J Clean Prod. 2020;268:122019.

20. Liu S, Xue J, Liu X, Chen H, Li X. Pitch derived graphene oxides: Characterization and effect on pyrolysis and carbonization of coal tar pitch. J Anal Appl Pyrolysis. 2020;145:104746.

21. Powell C, Beall GW. Graphene oxide and graphene from low grade coal: Synthesis, characterization and applications. Curr Opin Colloid Interface Sci. 2015;20:362–6.

22. Sierra U, Álvarez P, Blanco C, Granda M, Santamaría R, Menéndez R. Cokes of different origin as precursors of graphene oxide. Fuel. 2016;166:400–3.

23. Yadav KK, Singh H, Rana S, Sunaina, Sammi H, Nishanthi ST, et al. Utilization of waste coir fibre architecture to synthesize porous graphene oxide and their derivatives: An efficient energy storage material. J Clean Prod. 2020;276:124240.

24. Hoang VC, Hassan M, Gomes VG. Coal derived carbon nanomaterials – Recent advances in synthesis and applications. Appl Mater Today. 2018;12:342–58.

25. Lee S-Y, Mahajan RL. A facile method for coal to graphene oxide and its application to a biosensor. Carbon N Y. 2021;181:408–20.

26. Pakhira B, Ghosh S, Maity S, Sangeetha DN, Laha A, Allam A, et al. Extraction of preformed graphene oxide from coal: its clenched fist form entrapping large molecules. RSC Adv. 2015;5:89076–82.

27. Xu B, Maimaiti H, Wang S, Awati A, Wang Y, Zhang J, et al. Preparation of coal-based graphene oxide/SiO2 nanosheet and loading ZnO nanorod for photocatalytic Fenton-like reaction. Appl Surf Sci. 2019;498:143835.

28. Zhang C, Xie Y, Zhang C, Lin J. Upgrading coal to multifunctional graphene-based materials by direct laser scribing. Carbon N Y. 2019;153:585–91.

29. Haenel MW. Recent progress in coal structure research. Fuel. 1992;71:1211–23.

30. Mathews JP, Chaffee AL. The molecular representations of coal – A review. Fuel. 2012;96:1–14.

31. Vasireddy S, Morreale B, Cugini A, Song C, Spivey JJ. Clean liquid fuels from direct

coal liquefaction: chemistry, catalysis, technological status and challenges. Energy Environ Sci. 2011;4:311–45.

32. Guo Q, Zhou C, Ma Z, Yang X. Fundamentals of TiO2 Photocatalysis: Concepts, Mechanisms, and Challenges. Adv Mater. 2019;31:1901997.

33. Schneider J, Matsuoka M, Takeuchi M, Zhang J, Horiuchi Y, Anpo M, et al. Understanding TiO2 Photocatalysis: Mechanisms and Materials. Chem Rev. 2014;114:9919–86.

34. Meng A, Zhang L, Cheng B, Yu J. Dual Cocatalysts in TiO2 Photocatalysis. Adv Mater. 2019;31:1807660.

35. Zhao Y, Li C, Liu X, Gu F, Jiang H, Shao W, et al. Synthesis and optical properties of TiO2 nanoparticles. Mater Lett. 2007;61:79–83.

36. Kaur Aulakh M, Sharma R, Pal B, Prakash R. Photo-induced oxidation and reduction by plasmonic Ag-TiO2 nanocomposites under UV/sunlight. Sol Energy. 2020;196:427–36.

37. Yurdakal S, Tek BS, Değirmenci Ç, Palmisano G. Selective photocatalytic oxidation of aromatic alcohols in solar-irradiated aqueous suspensions of Pt, Au, Pd and Ag loaded TiO2 catalysts. Catal Today. 2017;281:53–9.

38. Aulakh MK, Pal B. A co-relation study of efficient photocatalytic reduction of aromatic nitriles and band energies of Cu loaded elongated TiO2 nanocatalysts. J Taiwan Inst Chem Eng. 2019;96:559–65.

39. Rather RA, Singh S, Pal B. A C3N4 surface passivated highly photoactive Au-TiO2 tubular nanostructure for the efficient H2 production from water under sunlight irradiation. Appl Catal B Environ. 2017;213:9–17.

40. Kurniawan TA, Mengting Z, Fu D, Yeap SK, Othman MHD, Avtar R, et al. Functionalizing TiO2 with graphene oxide for enhancing photocatalytic degradation of methylene blue (MB) in contaminated wastewater. J Environ Manage. 2020;270:110871.

41. Tismanar I, Obreja AC, Buiu O, Duta A. VIS-active TiO2 – graphene oxide composite thin films for photocatalytic applications. Appl Surf Sci. 2021;538:147833.

42. Yadav HM, Kim J-S. Solvothermal synthesis of anatase TiO2-graphene oxide nanocomposites and their photocatalytic performance. J Alloys Compd. 2016;688:123–9.

43. Mäki-Arvela P, Murzin DY. Hydrodeoxygenation of Lignin-Derived Phenols: From Fundamental Studies towards Industrial Applications. Catal. . 2017.

44. Michałowicz J. DW. Phenols – Sources and Toxicity. Polish J Environ Stud. 2007;16:347–62.

45. Majewska M, Khan F, Pieta IS, Wróblewska A, Szmigielski R, Pieta P. Toxicity of selected airborne nitrophenols on eukaryotic cell membrane models. Chemosphere. 2021;266:128996.

46. Asadollahi-Baboli M. Exploring QSTR analysis of the toxicity of phenols and thiophenols using machine learning methods. Environ Toxicol Pharmacol. 2012;34:826–

31.

47. Hunge YM, Yadav AA, Dhodamani AG, Suzuki N, Terashima C, Fujishima A, et al. Enhanced photocatalytic performance of ultrasound treated GO/TiO2 composite for photocatalytic degradation of salicylic acid under sunlight illumination. Ultrason Sonochem. 2020;61:104849.

48. Bhardwaj S, Dogra D, Pal B, Singh S. Photodeposition time dependant growth, size and photoactivity of Ag and Cu deposited TiO2 nanocatalyst under solar irradiation. Sol Energy. 2019;194:618–27.

49. Noreen Z, Khalid NR, Abbasi R, Javed S, Ahmad I, Bokhari H. Visible light sensitive Ag/TiO2/graphene composite as a potential coating material for control of Campylobacter jejuni. Mater Sci Eng C. 2019;98:125–33.

50. Trikkaliotis DG, Mitropoulos AC, Kyzas GZ. Low-cost route for top-down synthesis of over- and low-oxidized graphene oxide. Colloids Surfaces A Physicochem Eng Asp [Internet]. 2020;600:124928. Available from: https://doi.org/10.1016/j.colsurfa.2020.124928

51. Jabbar A, Yasin G, Khan WQ, Anwar MY, Korai RM, Nizam MN, et al. Electrochemical deposition of nickel graphene composite coatings: effect of deposition temperature on its surface morphology and corrosion resistance. RSC Adv. 2017;7:31100–9.

52. Rao R, Podila R, Tsuchikawa R, Katoch J, Tishler D, Rao AM, et al. Effects of Layer Stacking on the Combination Raman Modes in Graphene. ACS Nano. 2011;5:1594–9.

53. Vasilaki E, Georgaki I, Vernardou D, Vamvakaki M, Katsarakis N. Ag-loaded TiO2/reduced graphene oxide nanocomposites for enhanced visible-light photocatalytic activity. Appl Surf Sci. 2015;353:865–72.

54. Trikkaliotis DG, Christoforidis AK, Mitropoulos AC, Kyzas GZ. Graphene oxide synthesis, properties and characterization techniques: A comprehensive review. ChemEngineering. 2021;5.

55. Moosavifar M, Heidari SM, Fathyunes L, Ranjbar M, Wang Y, Arandiyan H. Photocatalytic Degradation of Dye Pollutant Over FeTPP/NaY Zeolite Nanocomposite. J Inorg Organomet Polym Mater. 2020;30:1621–8.

56. González-Morán S, González B, Vicente MA, Trujillano R, Rives V, Gil A, et al. Application of birnessite-type solids prepared by sol–gel and oxidation methods in photocatalytic degradation of 4-nitrophenol. Environ Technol. 2022;43:402–10.

57. Yadav V, Verma P, Sharma H, Tripathy S, Saini VK. Photodegradation of 4-nitrophenol over B-doped TiO2 nanostructure: effect of dopant concentration, kinetics, and mechanism. Environ Sci Pollut Res. 2020;27:10966–80.

58. Honarmandrad Z, Javid N, Malakootian M. Removal efficiency of phenol by ozonation process with calcium peroxide from aqueous solutions. Appl Water Sci [Internet]. 2021;11:1–9. Available from: https://doi.org/10.1007/s13201-020-01344-7

Summary and Future Outlook

Among various photocatalysts, Titanium dioxide (TiO_2) is an established photocatalyst known for its robust photocatalytic oxidation, high room temperature activity, and excellent photostability. Although TiO_2 have significant potential for photocatalytic applications, its effectiveness is hindered by its rather small specific surface area, rapid recombination of photogenerated charge carriers, and limited efficiency in utilising solar or visible light due to the wide band gap. The core focus of this thesis is to synthesize GO-modified metal-TiO_2 composites with efficient e^--h^+ pair separation for photocatalysis using the synergic influence of metal (plasmonic/transition) and graphene oxide (carbonaceous material) on them. The developed nanocomposites, such as different wt% GO/Ag-TiO_2 and GO/Cu-TiO_2, have been found to exhibit improved photocatalytic performance than their individual counterparts (bare TiO_2 and their binary composites) for the photodegradation of several toxic pharmaceutical and industrial pollutants. In addition, the GO-modified metal- TiO_2 catalysts performed well in tests evaluating its potential for use in the generation of green and renewable energy (H_2). The enhancement in the photocatalytic properties is credited to the construction of a ternary heterojunction composite that features (i) increased specific surface area due to the incorporation of GO, resulting in an abundance of photocatalytic active sites (ii) accelerated separation and transport of photoexcited charge carriers across the interface contacts of metal (M), TiO_2, and GO, and (iii) an expanded light absorption range due to surface-deposited metals. Based on the research work, it is anticipated that these GO-modified metal TiO_2 composites with promising photocatalytic activity can be further investigated in other scientific fields such as sensing, fuel cells, batteries, bacterial disinfection, carbon dioxide (CO_2) reduction, nitrogen oxide (NOx) conversion, hydrogen (H_2) generation from biomass or water splitting, and many more. In extension to this, it is proposed that the strategy of promoting the photocatalysis activity via the combined effect of M and GO can be expanded for the modification of other semiconductor metal oxides.

List of Publications

1. **D. Kaur** and B. Pal, "Improved photocatalytic activity of graphene oxide modified Ag-TiO_2 for degradation of piroxicam-20 and dehydrogenation of methanol under light irradiation," ***J. Taiwan Inst. Chem. Eng.*, vol. 155, no. October 2023, p. 105282, 2024, doi: 10.1016/j.jtice.2023.105282. (I.F.= 5.5)**
2. **D. Kaur** and B. Pal, "Highly enhanced photocatalytic hydrogen production via GO-modified Cu-TiO_2 system for dehydrogenation of alcohols under UV & sunlight irradiation," ***Solar Energy.*, vol. 282, no. November 2024, p. 112905, 2024, doi: 10.1016/j.solener.2024.112905. (I.F.= 6.0)**
3. **D. Kaur**, K. Singh, W. T. Reynolds, and B. Pal, "Graphene oxide-coated Ag-TiO_2 hybrid nanocomposites for superior photocatalytic activity," ***Environ. Sci. Pollut. Res.*, vol. 30, no. 43, pp. 97660–97672, 2023, doi: 10.1007/s11356-023-29301-2. (I.F.= 5.8)**

Other publications

1. M. Kaur, B. Pal, and **D. Kaur***, "Modified Ag-ZnO coated graphene oxide ternary composite for superior photocatalytic degradation of crystal violet dye under visible light irradiation," ***Diam. Relat. Mater.*, vol. 143, no. February, p. 110935, 2024, doi: 10.1016/j.diamond.2024.110935. (I.F.=4.3)**
2. A. Bathla, **D. Kaur**, and B. Pal, " Impact of metal ions (Cr +6 /Mn +7) loaded CaCO 3 extracted from tap water for adsorption/ degradation of toxic pollutants under sunlight," ***Mater. Express*, vol. 12, no. 1, pp. 106–113, 2022, doi: 10.1166/mex.2022.2132. (I.F.=1.65)**

Conferences and Workshops

1. Volunteered in **SCI-FEST 2022**, held at Thapar Institute of Engineering and Technology, Patiala, on 7th June, 2022.

2. Attended "International conference on emerging trends in science and technology" **(ICETST-2022),** organized by the Department of Applied Sciences, Punjab Engineering College, Chandigarh. 10th -11th June, 2022

3. Volunteered and participated in 7 days, Hands on training program on insights into the applications of high-end instruments in chemical sciences, under the **DST-STUTI** scheme held at Thapar Institute of Engineering and Technology, Patiala. 21st -27th February, 2023

4. ***Poster presentation on the topic***, "Improved photocatalytic activity of GO@Ag-TiO_2 towards piroxicam-20 under visible light irradiation" Ist International conference on recent advances in chemistry-2023, **(CRAC-2023),** held at Punjabi University, Patiala. 23rd-24th February, 2023.

5. ***Poster presentation on the topic,*** " Improved photocatalytic activity of Graphene oxide modified Ag-TiO_2 for degradation of piroxicam-20 and dehydrogenation of methanol under light irradiation" International conference on advances in chemical and applied sciences for sustainable development, **(ACASSD-2024)**, held at JECRC University, Jaipur, Rajasthan. 29th- 30th March, 2024.

6. ***Poster presentation on the topic***, "Efficient hydrogen production using GO-modified Cu-TiO_2 system for photocatalytic dehydrogenation of alcohol" 24th National Symposium on Catalysis (CATSYMP-24) "Catalysis for Sustainable Chemicals, Materials & Energy" (CSCME-2025) held at Thapar Institute of Engineering and Technology, Patiala, 24-26th February, 2025.

7. Received **Young Scientist Award for Best Oral Presentation** on the topic, "Efficient hydrogen production using GO-modified Cu-TiO_2 system for photocatalytic alcohol dehydrogenation" International Conference on Energy, Functional Materials/ Molecules and Nanotechnology (ICEFN & NWSSWM) 2025, held at Kumaun University, Nainital. 20th-22nd March 2025.

plag check.docx

ORIGINALITY REPORT

13%	6%	11%	2%
SIMILARITY INDEX	INTERNET SOURCES	PUBLICATIONS	STUDENT PAPERS

PRIMARY SOURCES

1	Mizanur Rahaman, Md Hasive Ahmed, Sarker Md Sadman, Muhammad Rakibul Islam. "Defect mediated visible light induced photocatalytic activity of Co3O4 nanoparticle decorated MoS2 nanoflower: A combined experimental and theoretical study", Heliyon, 2023 Publication	1%
2	Muhammad Rafique, Syeda Hajra, Muneeb Irshad, Muhammad Usman, Muhammad Imran, Mohammad A. Assiri, Waqar Muhammad Ashraf. " Hydrogen Production Using TiO -Based Photocatalysts: A Comprehensive Review ", ACS Omega, 2023 Publication	1%
3	Quanjun Xiang, Jiaguo Yu. "Graphene-Based Photocatalysts for Hydrogen Generation", The Journal of Physical Chemistry Letters, 2013 Publication	1%
4	ksascholar.dri.sa Internet Source	1%

Journal of the Taiwan Institute of Chemical Engineers 155 (2024) 105282

Contents lists available at ScienceDirect

Journal of the Taiwan Institute of Chemical Engineers

journal homepage: www.journals.elsevier.com/journal-of-the-taiwan-institute-of-chemical-engineers

Improved photocatalytic activity of graphene oxide modified Ag-TiO_2 for degradation of piroxicam-20 and dehydrogenation of methanol under light irradiation

Davinder Kaur, Bonamali Pal *

School of Chemistry and Biochemistry, TIET-Virginia Tech Center of Excellence in Emerging Materials, Thapar Institute of Engineering and Technology, Patiala 147004, India

ARTICLE INFO

Keywords:
Graphene oxide
Piroxicam-20
Photodegradation
Photocatalytic dehydrogenation
Reaction intermediates
Visible light

ABSTRACT

Background: Graphene oxide (GO), an atomic sheet structure made of sp^2-bonded carbon atoms with superior optoelectronic, and catalytic properties, has attracted much interest. Incorporating a carbon-rich material, onto metal-loaded TiO_2 is reported to increase the photocatalytic properties of resultant composites.

Methods: This research aimed at the deposition of different amounts (1–5 wt.%) of GO using the ultrasonication method on bare TiO_2 and Ag (3 wt.%)-TiO_2 (AT3) and studied their influence on piroxicam-20 degradation under visible light and methanol dehydrogenation under UV light. The prepared composites' structural, optical, and morphological properties were characterized using XRD, DRS, HR-TEM, FE-SEM, and XPS.

Significant findings: HRTEM analysis confirmed the existence of GO layers and spherical-shaped Ag nanoparticles deposited over the TiO_2 surface. GO(5 wt.%)@Ag(3 wt.%)-TiO_2 (G5@AT3) displayed better photodegradation efficiency (78 %) ($k = 0.0082\ min^{-1}$) under 120 min, and GO(1 wt.%)@Ag(3 wt.%)-TiO_2 (G1@AT3) composite produced higher amount (427 mmol) of H_2 from photocatalytic dehydrogenation of CH_3OH under 5 h relative to TiO_2 (2 mmol) AT3 (166 mmol) and GO(5 wt.%)@TiO_2 composite (GT5) (11 mmol). HRMS analysis was performed to identify the piroxicam-20 degradation intermediates. Thus, this research provides a proactive strategy highlighting the cooperative effect of Ag and GO loading to improve the photocatalytic efficiency of TiO_2 photocatalyst using both UV–visible light irradiation.

1. Introduction

Graphene oxide (GO), a widely used graphitic substance, has received significant attention during the past few years. It is a graphene aromatic lattice containing alcohols, epoxides, carboxylic groups, and ketone carbonyls. Functional groups containing oxygen on their surface make them hydrophilic and a good option for supporting metal oxide-based semiconductors [1,2]. For a variety of applications, GO displayed superior optical, electronic, and catalytic properties [3,4]; hence, GO-based materials have been widely reported for the photodegradation of various organic pollutants present in waste effluent [5–9]. Different antibiotic residue levels with associated harmful effects on aquatic and terrestrial organisms have been found in pharmaceutical and agricultural effluents [10]. Medications including piroxicam, diclofenac, naproxen, and ibuprofen fall under Nonsteroidal anti-inflammatory medicines (NSAIDs) [11–13]. NSAIDs are of particular importance among the different pharmacological families due to their enormous consumption as they are given for numerous diseases. Numerous NSAIDs have been found in surface and subsurface water, wastewater effluents, and biological sludge [14,15]. The wastewater containing drug residues must be treated to prevent pharmaceuticals from entering the environment. Derikvandi et al. photocatalytically degraded Metronidazole, one such water pollutant drug with the help of clinoptilolite nanoparticles supported ZnO and NiO photocatalysts [16].

Another major growing issue is the massive amounts of alcoholic solvents that are often drained away after usage since they are a combination of several solvents. Various alcoholic solvents such as glycol, methanol, butanol, cyclohexanol, higher chain alcohols, and cyclic alcohols are used in chemical labs and various food, cosmetic, and fertilizer industries. The photocatalytic dehydrogenation of alcohols is a promising method for the conversion of alcoholic solvents into hydrogen along with some useful organic products [17]. In this occurrence, there

* Corresponding author.
E-mail address: bpal@thapar.edu (B. Pal).

https://doi.org/10.1016/j.jtice.2023.105282
Received 12 October 2023; Received in revised form 1 December 2023; Accepted 4 December 2023

Solar Energy 282 (2024) 112905

Contents lists available at ScienceDirect

Solar Energy

journal homepage: www.elsevier.com/locate/solener

Highly enhanced photocatalytic hydrogen production via GO-modified Cu-TiO_2 system for dehydrogenation of alcohols under UV & sunlight irradiation

Davinder Kaur, Bonamali Pal *

[1] Department of Chemistry and Biochemistry, TIET-Virginia Tech Center of Excellence in Emerging Materials, Thapar Institute of Engineering and Technology, Patiala 147004, India

ARTICLE INFO

Keywords:
Hydrogen production
Methanol dehydrogenation
Sunlight
Graphene oxide
Copper photodeposition

ABSTRACT

The high efficiency of the production of hydrogen from alcohols is vital to the advancement of energy technology. This study thoroughly investigates the process of alcohol dehydrogenation utilising GO-modified Cu-TiO_2 photocatalyst under UV light and sunlight exposure. GO-modified Cu-TiO_2 photocatalyst was synthesised using the hydrothermal method. Various experimental techniques, including FESEM, HRTEM, XPS, and DRS, confirmed the formation of the ternary composite. The influence of different alcohols (methanol, ethanol, propanol) and their concentrations (same vol% and molarity) on the amount of hydrogen (H_2) production was examined in this study. The study thoroughly investigated the impact of various parameters, such as the influence of GO and Cu loading on TiO_2 and their combined effect, time course, nature of alcohol and the reaction conditions on the photocatalytic hydrogen production. The GO(0.5 wt%)/Cu(3 wt%)-TiO_2 ($G_{0.5}C_3T$) composite demonstrated the highest quantity of hydrogen production during methanol dehydrogenation when subjected to both UV and sunlight irradiation. The composite exhibited remarkably about three-fold higher hydrogen evolution in sunlight(881 mmol) than in UV light(294 mmol). The exceptional performance of this composite can be attributed to the efficient transfer of charge carriers and the delayed recombination of electron-holes, which is a result of the cooperative effect of GO and Cu deposited over the TiO_2 system. This approach offers a proactive strategy, signifying the synergetic effect of loading GO and Cu over TiO_2 to enhance the photocatalytic hydrogen production, which is regarded as a green fuel solution, and turns these materials into useful energy sources by using inexpensively synthesised photocatalysts.

1. Introduction

The current state of maximum energy growth relies on conventional resources such as fossil fuels [1]. With the continuous rise in energy consumption and the depletion of fossil fuels such as petroleum, coal, and natural gas, there is an urgent need to develop clean and environmentally friendly fuel options [2,3]. Hydrogen energy, among the numerous alternative energy sources, is a crucial component of the renewable energy strategies of developed nations due to its immediate availability and high fuel efficiency [4]. It is a viable green energy source that has the potential to address environmental concerns associated with traditional fossil fuels. Hydrogen is presently produced through electrolysis, natural gas, naphtha, heavy oil, and coal, among other sources. Most (96 %) of hydrogen production is generated directly from fossil fuels, while a small portion (4 %) is produced indirectly using energy derived from fossil fuels as feedstock [5]. Nevertheless, for hydrogen to be employed in future energy supply systems, it must undergo various stages, including viable production, storage, and transportation, considering economic, technological, and environmental constraints.

The non-conventional methods for hydrogen production primarily include biomass, hydrocarbons, photocatalytic water splitting, dehydrogenation of waste alcoholic solvents, etc. In recent times, there has been a significant focus on photocatalytic approaches to hydrogen production due to the high cost, excessive energy use, and lack of environmental friendliness associated with traditional methods. One of the most eco-friendly ways to produce hydrogen in the future is to use energy-intensive and solar-powered semiconductors. Sun-light/Visible

* Corresponding author.
E-mail address: bpal@thapar.edu (B. Pal).

https://doi.org/10.1016/j.solener.2024.112905
Received 19 June 2024; Received in revised form 17 August 2024; Accepted 28 August 2024
Available online 31 August 2024

Environmental Science and Pollution Research (2023) 30:97660–97672
https://doi.org/10.1007/s11356-023-29301-2

RESEARCH ARTICLE

Graphene oxide-coated Ag-TiO_2 hybrid nanocomposites for superior photocatalytic activity

Davinder Kaur[1] · Karanveer Singh[1] · William T. Reynolds Jr[2] · Bonamali Pal[1]

Received: 23 May 2023 / Accepted: 8 August 2023 / Published online: 19 August 2023

Abstract
Graphene oxide (GO) has now emerged as one of the most promising materials in different areas such as photocatalysis, adsorption, and energy storage due to its high surface area, unique layered structure, etc. Among various types of precursors, anthracite coal has attracted a lot of attention nowadays as it affords GO a high concentration of sp^2 carbons resulting in high conductivity and superior absorbance in the visible region. In this report, we have prepared GO-TiO_2 nanocomposites as it is supposed to possess high photocatalytic activity owing to facile electron transmission from the conduction band of TiO_2 to the GO surface resulting in a much lower degree of electron–hole pair recombination. To boost the photocatalytic activity further, TiO_2 was coated with Ag nanoparticles as well. These hybrid structures were characterized by different analytical techniques, for example, XRD, HR-TEM, SEM, and Raman spectroscopy. The XRD pattern of these composites consists of characteristic peaks corresponding to GO, TiO_2, and Ag. The HR-TEM studies confirm the presence of GO layers, cube-shaped TiO_2, and spherical Ag nanoparticles. Phenol and 4-nitrophenol have been used as model pollutants to evaluate the photooxidation efficiencies under both UV and visible light irradiation. Under UV irradiation, the GO/Ag-TiO_2 ternary nanocomposite shows better photooxidation efficiency (62%) compared to Ag-TiO_2 (38%), GO-TiO_2 (9%), GO (17%), and TiO_2 (8%) toward phenol degradation. The GO/Ag-TiO_2 is also having the highest photocatalytic activity toward the removal of phenol under visible light irradiation (34%). The ternary heterostructure (85%) also possesses superior photooxidation activity compared to Ag-TiO_2 (44%) and GO-TiO_2 (71%) toward the degradation of p-nitrophenol under UV light radiation for 60 min. The above observation reveals that the cooperative effect of Ag, TiO_2, and GO is playing a crucial role to result in the high photooxidation activity of the GO/Ag-TiO_2 hetero-nanocomposites.

Keywords Coal-derived graphene oxide · Ag-TiO_2 · Hybrid composites · Photocatalysis · Degradation of phenolic compounds

Introduction

In recent years, graphene oxide (GO) has attracted a significant amount of interest due to its fascinating structural and electronic properties (Pacilé et al. 2011; Saxena et al. 2011; Sharma et al. 2021). It has become a promising candidate in a wider variety of applications such as energy storage (Ambrosi and Pumera 2016; Tian et al. 2021), optoelectronic devices (Wan et al. 2012; Ke et al. 2021), sensors (Rowley-Neale et al. 2018; Xue et al. 2019), biomedical applications (Chung et al. 2013; Yim et al. 2021), and photocatalysis (Putri et al. 2016; Jamjoum et al. 2021). But till now, expensive carbon-based precursors such as graphite have been extensively used to prepare the graphene oxides (Marcano et al. 2010; Yu et al. 2016; Feicht et al. 2019; Zito et al. 2021). As a result, the commercial utilization of these materials is rather narrow. Therefore, the synthesis of graphene oxide materials from cheaper resources including natural and industrial wastes allured a substantial extent of attention (Powell and Beall 2015; Sierra et al. 2016; Amir Faiz et al. 2020; Jiang et al. 2020; Liu et al. 2020; Yadav et al. 2020a).

Responsible Editor: George Z. Kyzas

✉ Bonamali Pal
bpal@thapar.edu

[1] School of Chemistry and Biochemistry, TIET-Virginia Tech Center of Excellence in Emerging Materials, Thapar Institute of Engineering and Technology, Patiala 147004, India

[2] Materials Science and Engineering Department, Virginia Tech, Blacksburg, VA 24061-0237, USA

Diamond & Related Materials 143 (2024) 110935

Contents lists available at ScienceDirect

Diamond & Related Materials

journal homepage: www.elsevier.com/locate/diamond

Modified Ag-ZnO coated graphene oxide ternary composite for superior photocatalytic degradation of crystal violet dye under visible light irradiation

Mansimran Kaur, Bonamali Pal, Davinder Kaur *

Department of Chemistry and Biochemistry, Thapar Institute of Engineering & Technology, Patiala 147004, Punjab, India

ARTICLE INFO

Keywords:
Plasmonic photocatalyst
GO@ZnO photocatalyst
Crystal violet degradation
Visible light sensitivity
Surface plasmon resonance

ABSTRACT

The enhancement of advanced nanomaterials into photocatalytic applications has preserved a significant curiosity for its potential to address environmental challenges. To address this concern, a green and eco-friendly catalyst was fabricated. In this study, we examined the enhancement of the photocatalytic activity of various synthesized composites with the modification of graphene oxide (GO) and Ag over the surface of semiconductor zinc oxide (ZnO). The simple wet chemical method was used for the synthesis of ZnO, GO(x)@ZnO, Ag_2@ZnO and GO(*x*)Ag_2-ZnO composites [x = 1,3,5 wt%]. The synthesized samples were characterized by different techniques such as XRD, SEM-EDS, DRS, Raman, and PL. Ternary GO_5@Ag_2-ZnO photocatalyst exhibited superior degradation efficiency up to 97 % in degrading crystal violet (CV) dye, a persistent and environmentally concerning pollutant under visible light irradiation. The significant photocatalytic activity was attributed to the surface plasmon resonance (SPR) phenomenon of Ag, whose broad absorption band was observed in DRS, better electron mobility, and a large surface area of GO facilitates the charge transfer. The highly efficient catalyst was effectively employed for five repeating cycles with only an 11 % decrease in removal rate, demonstrating that it can be easily reused. Kinetic study reveals that the prepared composite follows a pseudo-first-order reaction model with the highest rate constant value of 0.02491 min^{-1} respectively. The possible degradation pathway was determined using the HRMS technique.

1. Introduction

Water pollution has a severe negative influence on water quality and a strong pessimistic impact on aquatic ecology. The discharge of organic dyes through industrial effluent, particularly from manufacturing goods including fabrics, pharmaceuticals and food, is currently causing excessive water contamination [1,2]. Less than 1 mg L^{-1} of dye exposure can significantly impact the water quality as it seriously affects the transparency and quality of water bodies such as rivers, lakes, and others that are harmful to the aquatic environment [3].

CV ($C_{25}N_3H_{30}Cl$) is one such cationic dye that belongs to the triphenylmethane group that is employed in dermatological agents, biological stains, medicine, textile colouring and bacteriostatic agents etc. [4–6]. So far, approaches like adsorption, biological decolouration, photocatalytic degradation, chemical oxidation, and advanced oxidation processes (AOPs) have been used to mineralize injurious CV dye [7]. Among all these methods for the effective removal of toxic pollutants, photocatalytic degradation is the most efficient method for degrading organic dyes. The term "photocatalyst" combines the terms "photo" which denotes light, and "catalyst" which denotes a material that changes the rate of a reaction [8]. Photocatalysis has been shown to have significant potential for the removal of dyes from wastewater as an eco-friendly and sustainable treatment method [9,10].

Significant interest has been shown in semiconductor-based heterogeneous photocatalysts including ZnO, TiO_2, ZnS and Fe_2O_3 for the sustainable and renewable utilizing solar power to solve both energy and environmental issues [11–14]. Among various photocatalysts, ZnO is an outstanding semiconductor with distinct properties, including high electron mobility, good chemical and physical stability, high photosensitivity, band gap tunability and non-toxicity etc. [1,15]. However, ZnO has several drawbacks including photo-corrosion and the rapid recombination of electron-hole pairs and it is only active under UV light [16].

It has been observed that combining semiconductors like ZnO, TiO_2

* Corresponding author.
E-mail address: attandavinder@gmail.com (D. Kaur).

https://doi.org/10.1016/j.diamond.2024.110935
Received 15 December 2023; Received in revised form 6 February 2024; Accepted 19 February 2024
Available online 22 February 2024